Characterization of the Wind Resource in the Upper Midwest

Wind Integration Study – Task 1

Xcel Energy and the Minnesota Department of Commerce

Prepared by

EnerNex Corporation
144-E Market Place Blvd.
Knoxville, Tennessee 37923
tel: (865) 691-5540
fax: (865) 691-5046
www.enernex.com

WindLogics Inc.
1217 Bandana Blvd. N.
St. Paul, Minnesota
tel: (651) 556-4260
fax: (651) 556-4210
www.WindLogics.com

Date:

September 10, 2004

CONTENTS

EXECUTIVE SUMMARY

An abbreviated summary of what has been done learned and produced for this Task:

- Characterization of the Minnesota wind resource has been completed;
- A 1500 MW wind generation scenario was developed in cooperation with the project sponsors;
- Wind speed and wind generation time series for the years 2000, 2002, and 2003 have been developed by WindLogics. The data set consists of 10-minute values for fifty "towers" representing a 5 km x 5 km grid along the Buffalo Ridge from northeastern South Dakota to southeastern Minnesota;
- The wind generation model has been compared with favorable results to measurements from the Buffalo Ridge substation and the Lake Benton II wind;
- Data has been collected to characterize the Xcel-North control are for the study year 2010;
- For the existing wind generation (about 400 MW nameplate), the ELCC is 135 MW, or about 34%;
- Applying MAPP accreditation procedure for variable capacity generation to aggregate wind generation model for the study results in an accreditation of about 19% for the peak months of July and August, based on the three years of data in the WindLogics time series;
- When applied to the historical wind generation data provided by Xcel Energy (primarily concentrated at the Buffalo Ridge substation), the accredited capacity for the peak months of July and August, again based on just three years of data, is 40 MW, or about 13% of nameplate.

TASK 1 – CHARACTERIZE THE NATURE OF WIND POWER VARIABILITY IN THE MIDWEST

Task Description

- Provide an overview and characterization of Midwest wind patterns and resulting wind generation patterns.
- Assess the forecast accuracy of wind generation on a day-ahead basis and assess the implications on the degree of certainty that is included in the forecast.
- Appropriately scale up historical wind data and develop a representative wind plant model, in coordination with the National Renewable Energy Laboratory, for the 1500 MW of wind generation in the study. Evaluate the extent of wind generation variability that the NSP system should experience, including the effects of projected wind turbine technology and projected geographic diversity for the study year of 2010.

1. Wind Resource Characterization

1.1 Controlling Meteorology for the Upper Midwest

The climatology of wind in the Upper Midwest exhibits significant seasonal variability. The essential meteorology driving the wind resource is largely controlled by the position and strength of the upper-level jet stream and disturbances (jet streaks) within the jet stream. As shown in Fig. 1, the jet stream position in the winter season is both farther south and stronger than in the summer. In the transition seasons of spring and fall, the average jet stream position generally lies between these locations. The main factor controlling both the jet stream position and speed is the magnitude and location of the tropospheric meridional (north-south) temperature gradient. A larger (smaller) temperature gradient exists in the winter (summer) and corresponds to a stronger (weaker) jet stream. Note that although Fig. 1 indicates a mean ridge axis over western North American and trough axis over eastern North American, at any particular time (e.g., day, week, or even several week period), the jet stream orientation and strength could be very different from that indicated in Fig. 1.

The jet stream position can be thought of as the current "storm track". In this context, "storm track" means the track of mid-latitude cyclones and anticyclones (i.e., low and high pressure systems of one to several thousand kilometer horizontal dimension) seen on a meteorological pressure and geopotential height analysis maps. Weather phenomena of this size are called *synoptic* scale systems. In general, the stronger the jet stream and jet streaks, the more intense the lower-tropospheric pressure systems due to the dynamic link between the upper and lower troposphere. The key factor driving the wind resource in the lowest 100 m of the atmosphere is the horizontal pressure gradient. Large pressure gradients are associated with the transient cyclones and anticyclones, thus, if a region is co-located near the storm track, that region will realize higher wind speed than a region farther away from the storm track. Figure 2 provides a schematic of typical cyclone tracks that influence the Upper Midwest. The northwest-southeast track represents a common storm track in all seasons. The southwest-northeast track, although less common and usually relegated to transition and winter seasons,

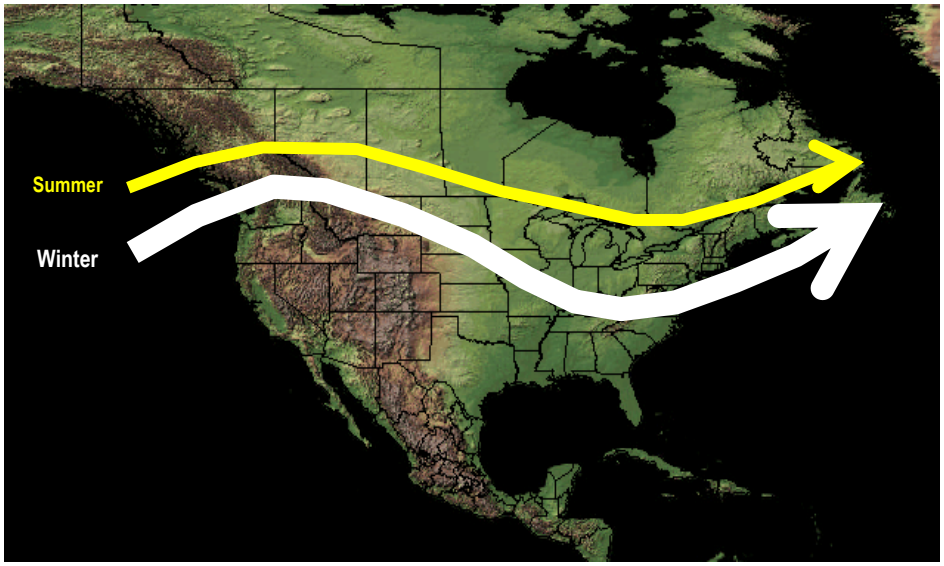

Figure 1: Mean winter and summer positions of the upper-tropospheric jet stream. Line width is indicative of jet stream wind speed

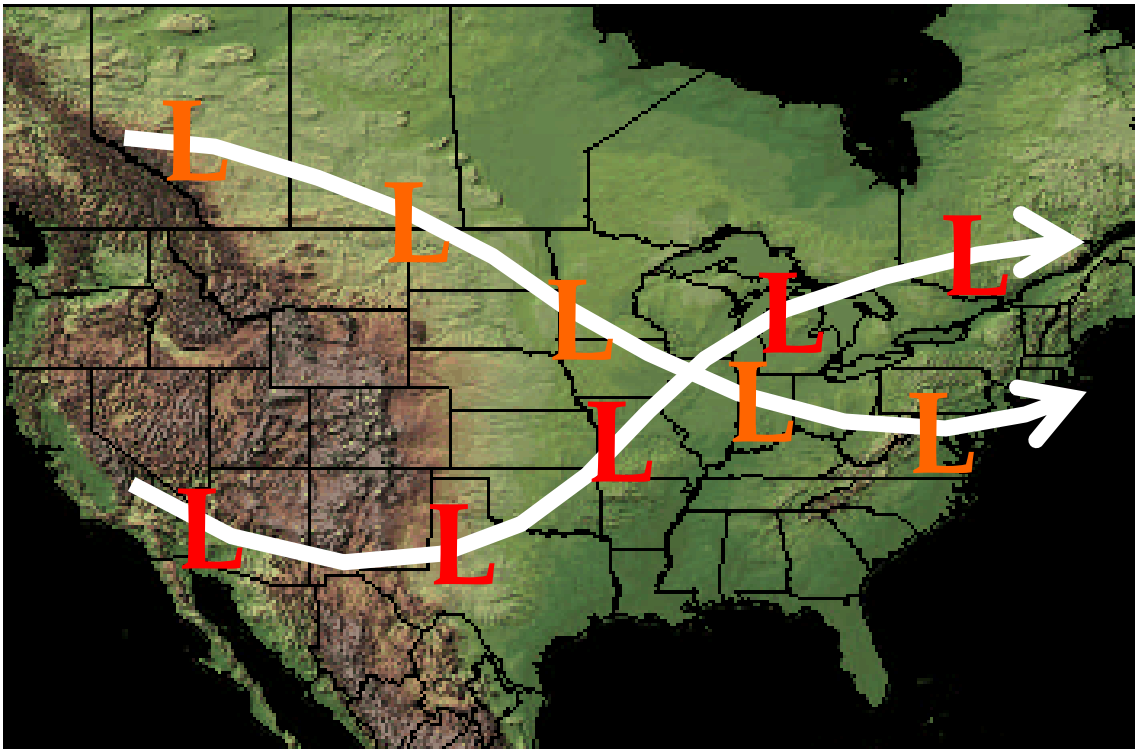

Figure 2: Typical "storm tracks" that influence the wind resource of the Upper Midwest. The bold Ls represent surface cyclone positions as they move along the track.

can correspond to large and intense cyclones. On the time scale of a several hours to approximately one day, fronts attendant to the transient cyclones have a large influence on wind variability. In summary, the seasonal wind resource is largely controlled by the jet stream position and frequency of associated cyclone and anticyclone passages over the region. The best wind resource for the Upper Midwest is expected with the stronger low-

level pressure gradients of the winter and transition seasons while the weaker pressure systems of summer yield a reduced wind resource.

Superposed on the background low-level meteorological pattern of high and low pressure systems are the diurnal effects of the solar insulation cycle and their influence on thermal stability and boundary layer evolution. On this diurnal time scale, low-level wind speed variability is highly influenced by the vertical transport of momentum. An important feature in the Upper Midwest (and other Plains and near-Plains geographical locations) is the nocturnal low-level jet (Bonner 1968) that develops when low-momentum near-surface air no longer mixes vertically due to the development of the shallow nocturnal inversion. So while the lowest levels may experience their weakest wind speeds of the day, in the layers just above the surface layer (> ~30-40 m) this results in dramatically reduced surface-based drag and acceleration to speeds frequently greater than those seen during the daytime.

On the shorter time scale of tens of minutes to several hours, wind variability is frequently influenced by thunderstorm outflow boundaries during the convective season (late spring through early fall). These outflow boundaries can range in size from only a few kilometers to hundreds of kilometers in horizontal extent. Outflow strength and size are usually dependent on the degree of organization of the convective system and the thermodynamic environment the thunderstorms develop in. Note that in all environmental conditions, the very small time scale wind speed variability (seconds to 10s of seconds) is controlled by boundary layer turbulence.

1.2 Modeling Methodology and Utilization of Weather Archives

To evaluate the historic wind resource and variability (over several time scales) of southern Minnesota and eastern South Dakota, the MM5 mesoscale atmospheric model (Grell et al. 1995) was utilized. This prognostic regional atmospheric model is capable of resolving meteorological features that are not well represented in coarser-grid simulations from the standard weather prediction models run by the National Center for Environmental Prediction (NCEP). The MM5 was run in a configuration utilizing 3 grids with finer internal nests as shown in Fig. 3. This "telescoping" 2-way nested grid configuration allowed for the greatest resolution in the area of interest with coarser grid spacing employed where the resolution of small mesoscale meteorological phenomena was not as important. This methodology was computationally efficient while still providing the necessary resolution for accurate representation of the meteorological phenomena of interest in the innermost grid. More specifically, the 5 km innermost grid spacing was deemed necessary to capture terrain influences on boundary layer flow and resolve mesoscale meteorological phenomena such as thunderstorm systems. The 45, 15 and 5 km grid spacing utilized in grids 1, 2, and 3, respectively, yield the physical grid sizes of: 2700 x 2700 km for grid 1, 1050 x 1050 km for grid 2, and 560 x 380 km for grid 3.

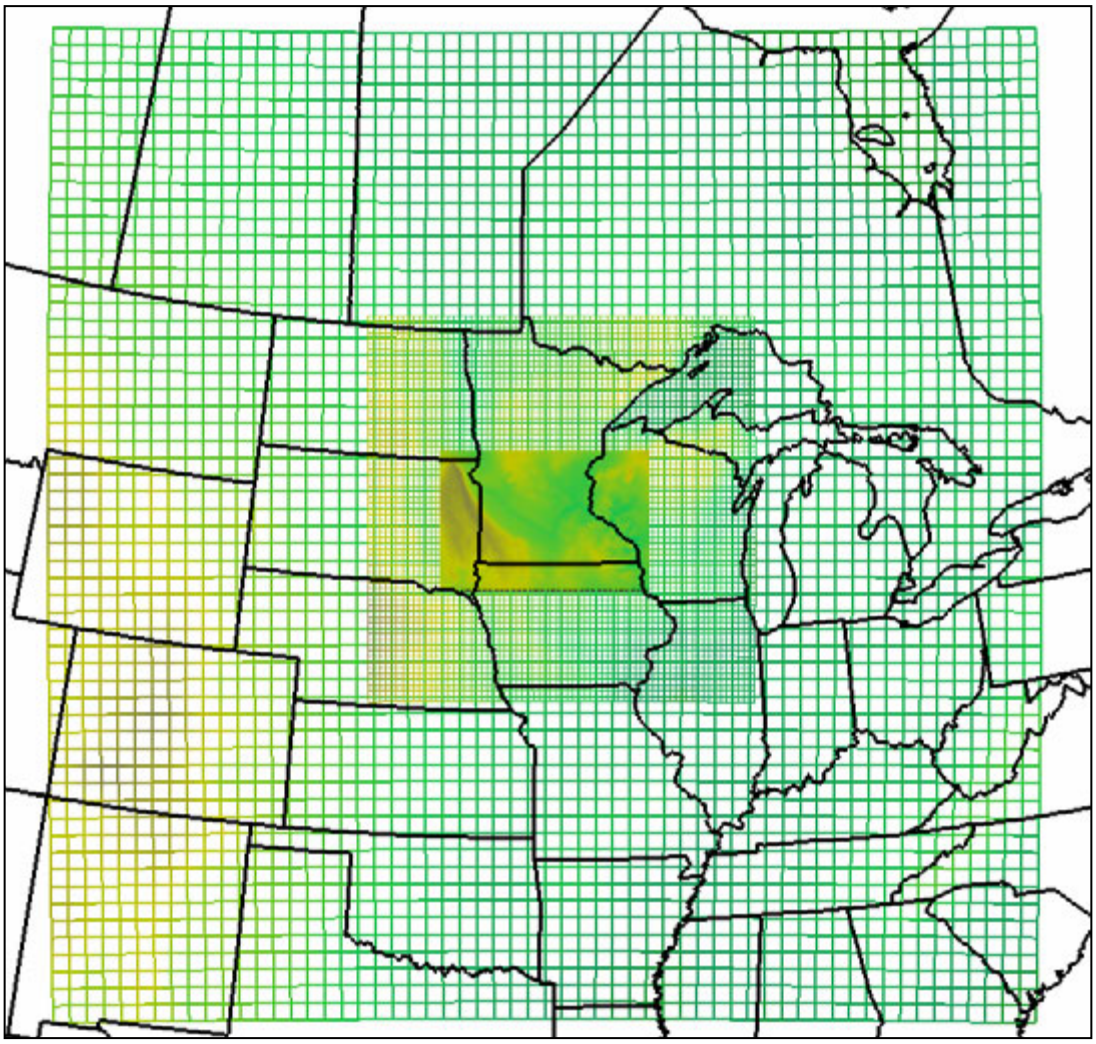

Figure 3: MM5 nested grid configuration utilized for study area. The 3 grid run includes 2 inner nested grids to optimize the simulation resolution in the area of greatest interest. The grid spacing is 45, 15 and 5 km for the outer, middle and innermost nests, respectively. The colors represent the surface elevation respective to each grid.

To provide an accurate simulation of the character and variability of the wind resource for eastern South Dakota and southern Minnesota, 3 full years of MM5 model simulations were completed. To initialize the model, the WindLogics archive of NCEP's Rapid Update Cycle (RUC) model analysis data was employed. The years selected for simulation were 2000, 2002 and 2003. The RUC analysis data was used both for model initialization and for updating the model boundary conditions every 3 hr. This RUC data had a horizontal grid spacing of 40 km for 2000 and 20 km for 2002 and 2003. To ensure that the model was properly representing the larger scale meteorological systems and to avoid model drift, the MM5 simulations were restarted every day with a new initialization.

To support the development of the system integrated wind model, data at 50 grid points (proxy towers) in the innermost model nest were extracted every 10 min as the simulation progressed. This process ensured that an analysis of the character and variability of the wind resource over several time scales could be performed at geographically disperse but favored locations. Fig. 4 depicts the MM5 innermost grid and the locations selected for high time resolution data extraction. The locations were

selected to 1) correspond to existing wind farm locations such as the Lake Benton I and II wind farms, 2) to represent a more geographically disperse Buffalo Ridge distribution while also including the greater geographical dispersion provided with Mower County sites. In particular, 5 sites were located in each of 10 counties where, *a priori*, the wind resource was expected to be good. Data extracted at each site included wind direction and speed, temperature and pressure at an 80 m hub height. The non-wind variables were extracted to calculate air density that is subsequently used along with the wind speed in turbine power calculations.

1.3 Normalization of Model Wind Data with Long-Term Reanalysis Database

To more accurately characterize the historic wind resource over the Xcel wind integration study area, the MM5 wind speed data was normalized with the WindLogics archive of the National Center for Atmospheric Research (NCAR)/NCEP Reanalysis Database (RNL). This RNL database represents 55 years of atmospheric data that is processed through a modeling assimilation cycle to ensure dynamic consistency. This RNL database is the best objective long- term dataset available and was created for purposes such as climate research investigations. By comparing applicable RNL grid points for a given month and year to the long-term average at those points, ratios are created that are applied to the MM5 wind data (including all proxy tower extractions). This process normalizes the model data to better represent the historic character of the wind resource.

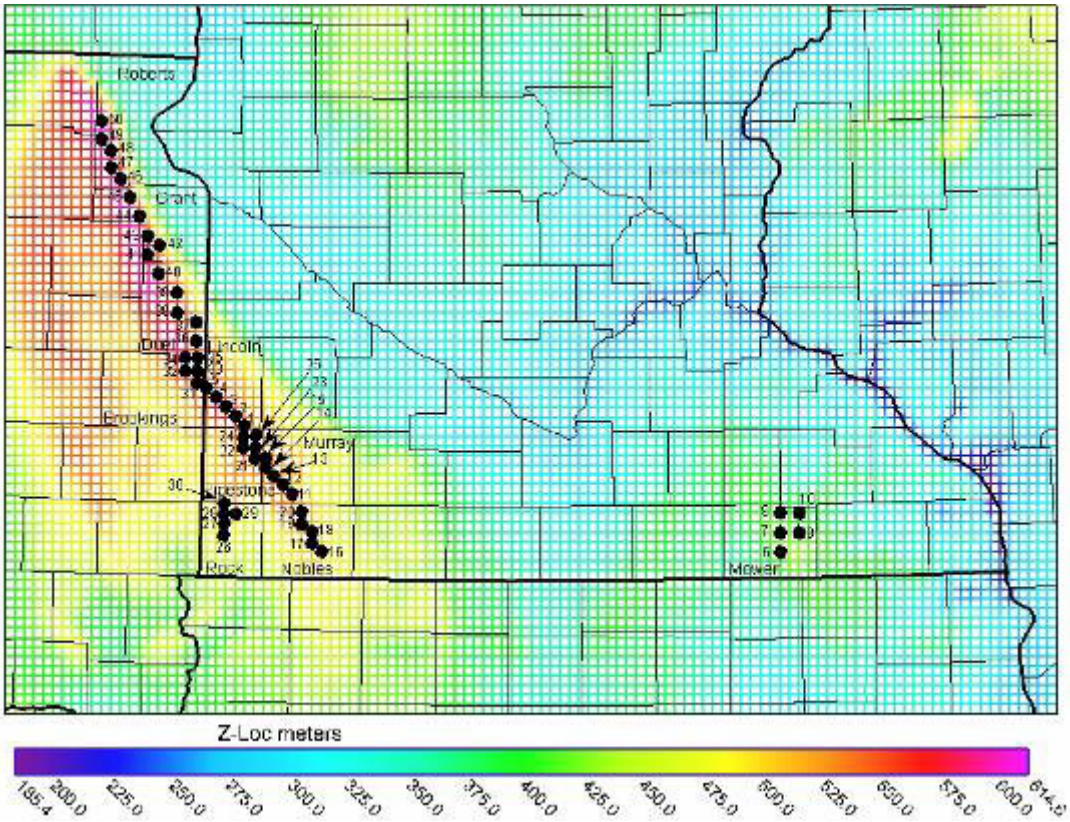

Figure 4: Innermost model grid with proxy MM5 tower (data extraction) locations. The color spectrum represents surface elevation.

1.4 Mapping of Mean Resource Quantities

In this section, a series of 3 year averages of annual and monthly parameters are mapped including wind speed, air density, power density, and energy production. In all

cases, the wind data was normalized to the long term RNL dataset and the analysis uses atmospheric data at an 80 m hub height. Each parameter map series is followed by a summary analysis.

Mean annual and monthly wind speed

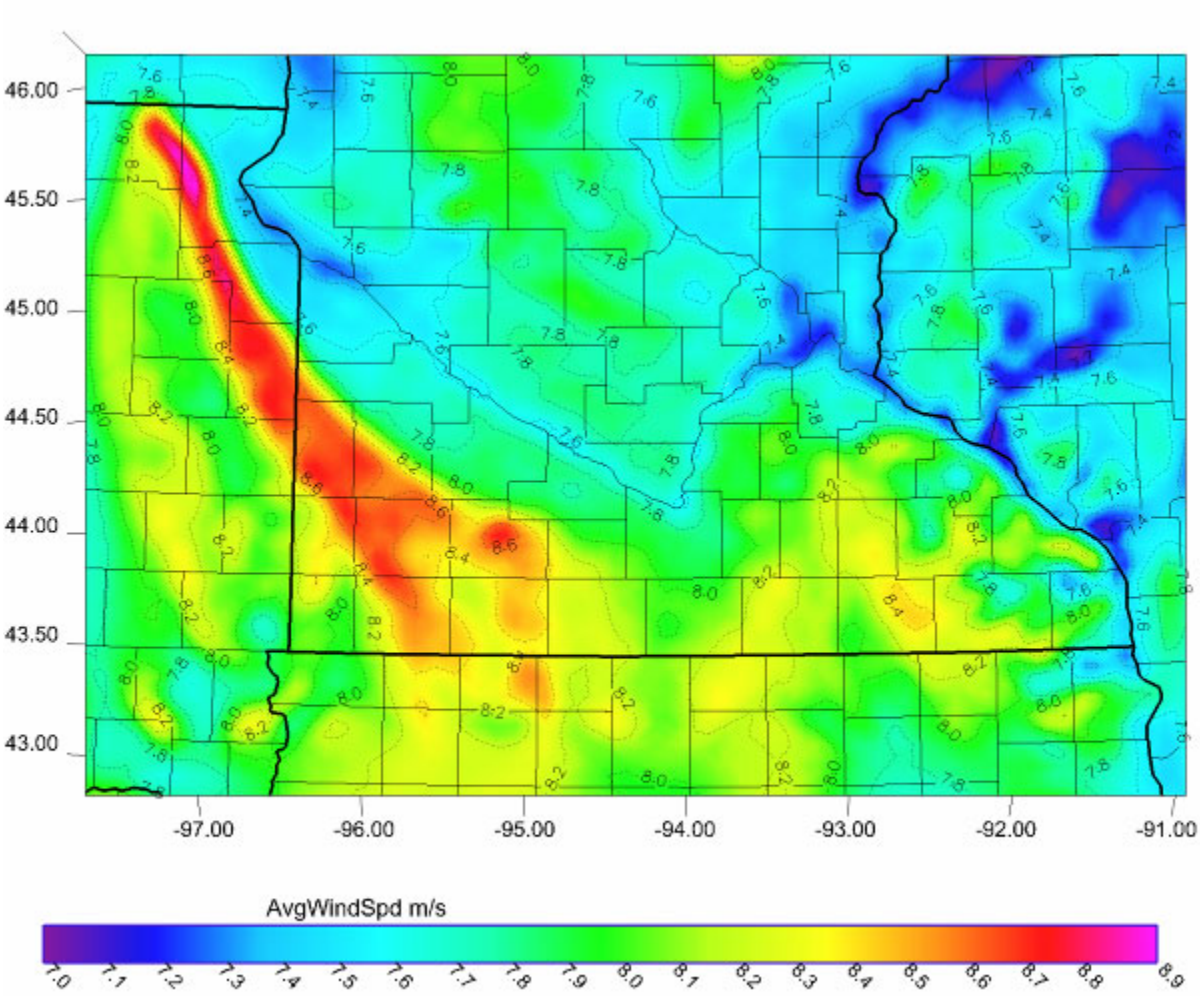

Figure 5: Mean annual average wind speed in m s^{-1}.

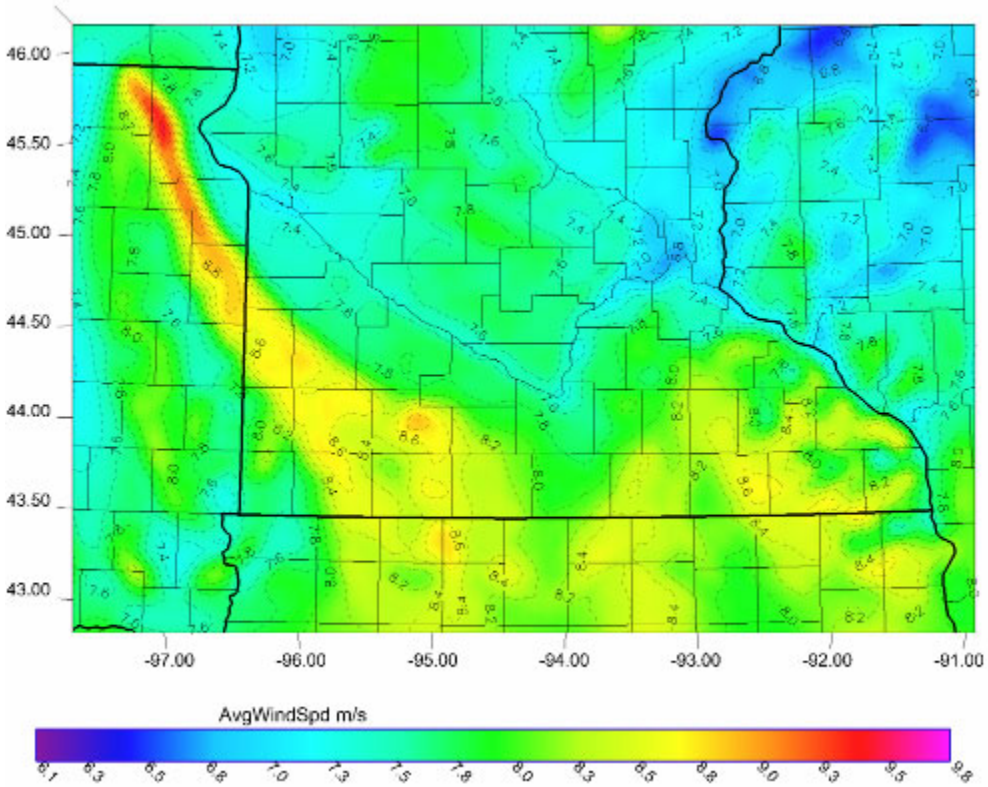

Figure 6: Mean wind speed (m s^{-1}) for January.

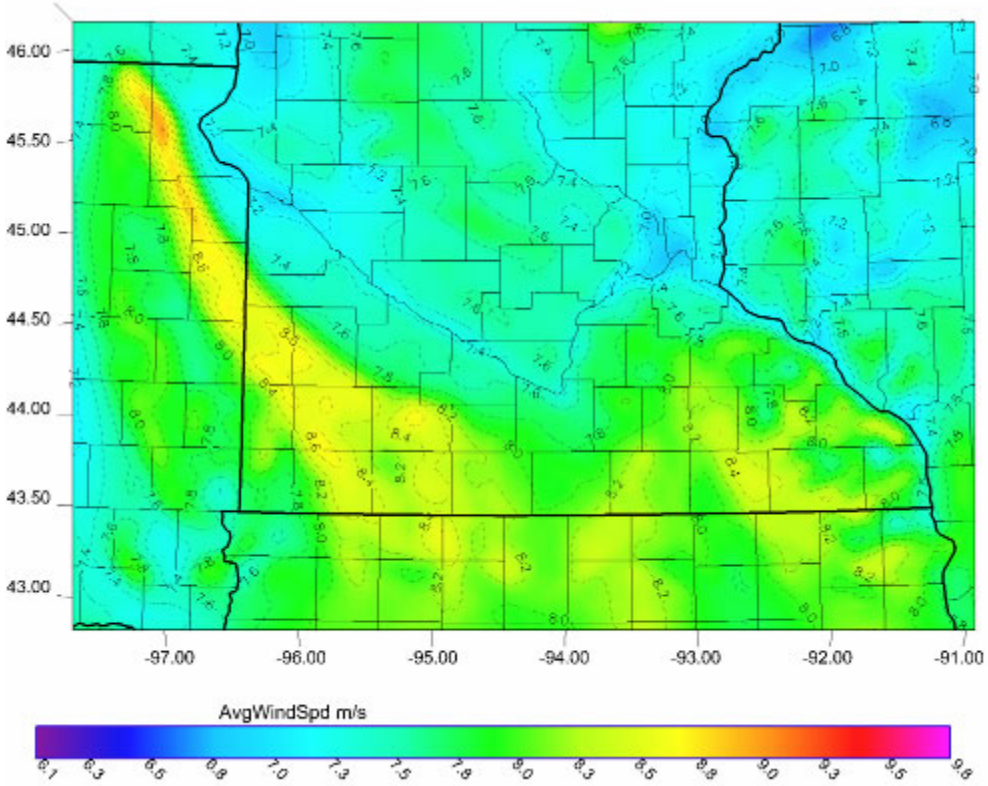

Figure 7: Mean wind speed (m s^{-1}) for February.

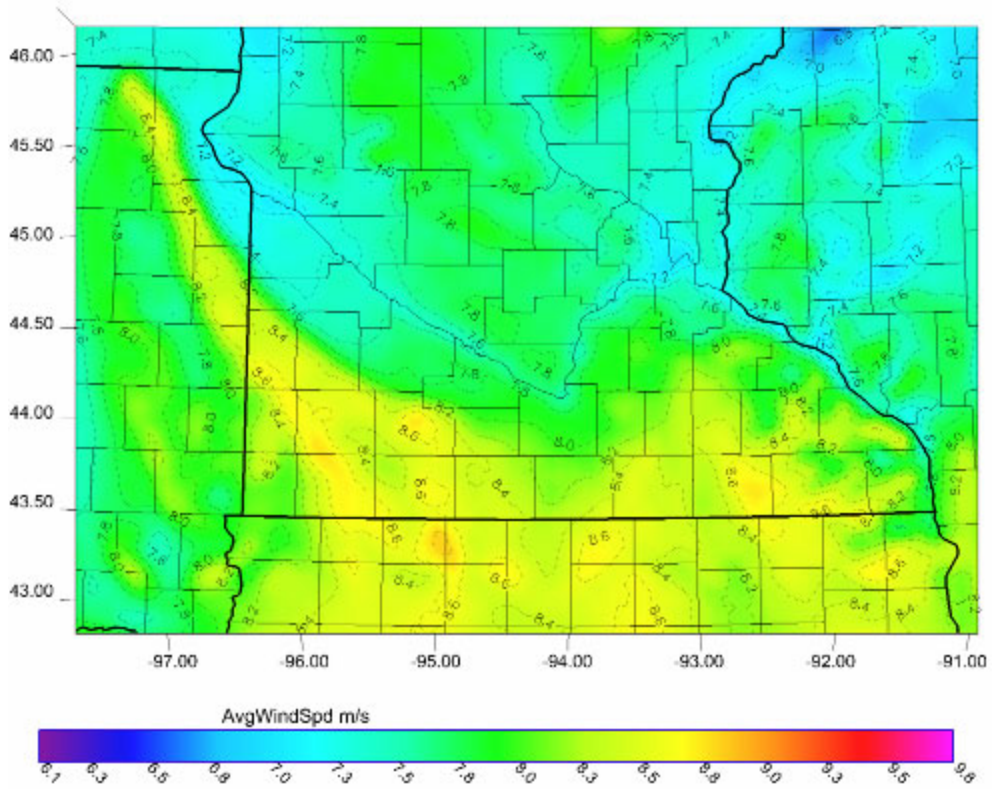

Figure 8: Mean wind speed (m s^{-1}) for March

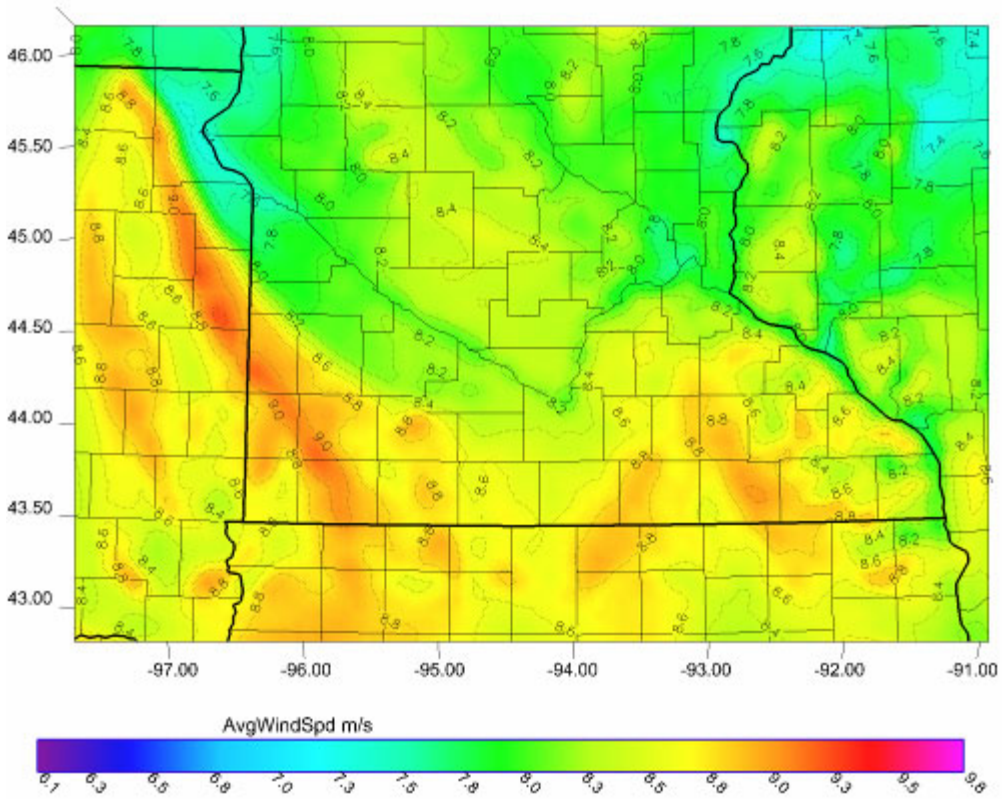

Figure 9: Mean wind speed (m s^{-1}) for April.

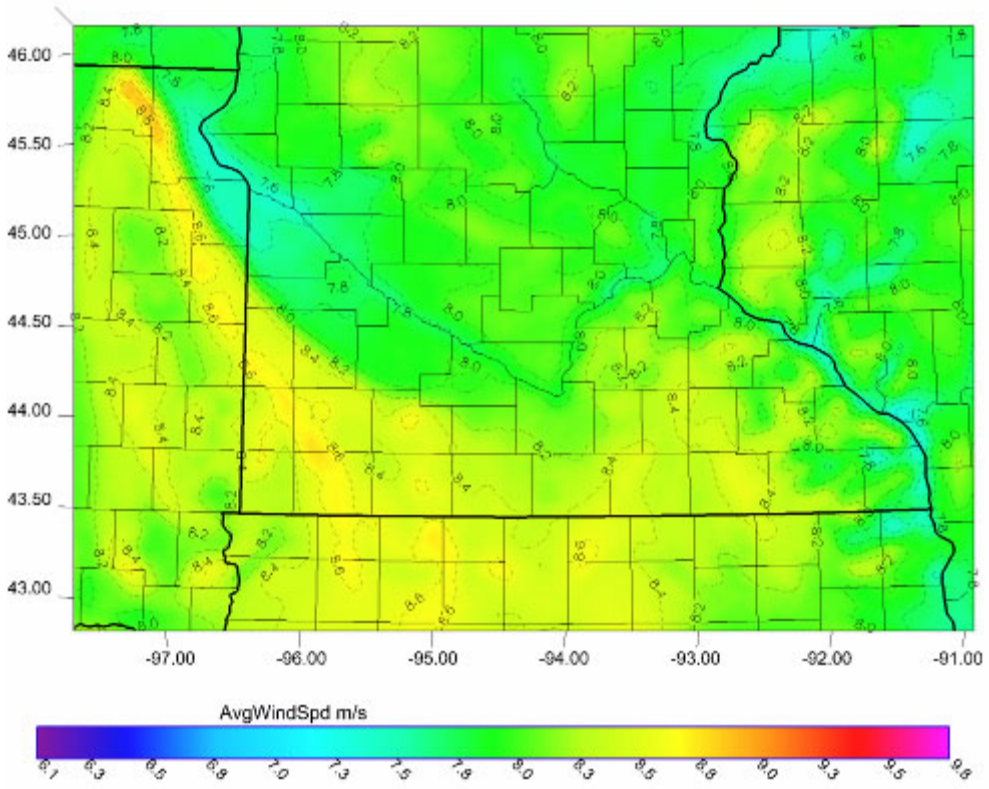

Figure 10: Mean wind speed (m s^{-1}) for May.

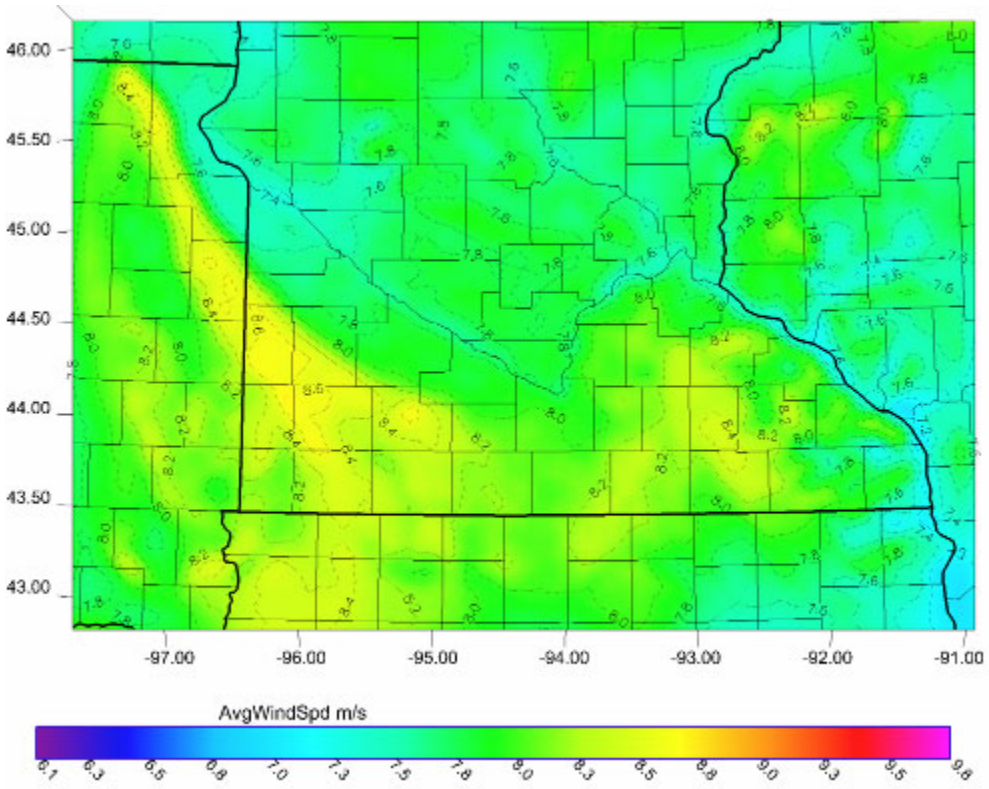

Figure 11: Mean wind speed (m s^{-1}) for June.

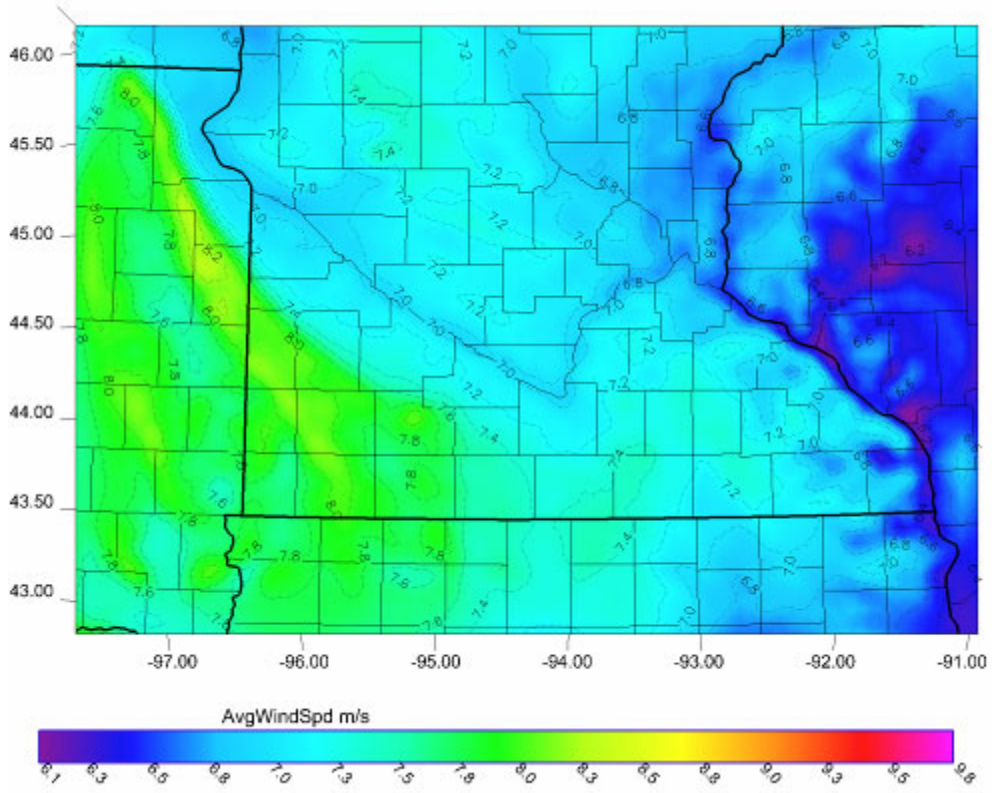

Figure 12: Mean annual wind speed (m s^{-1}) for July.

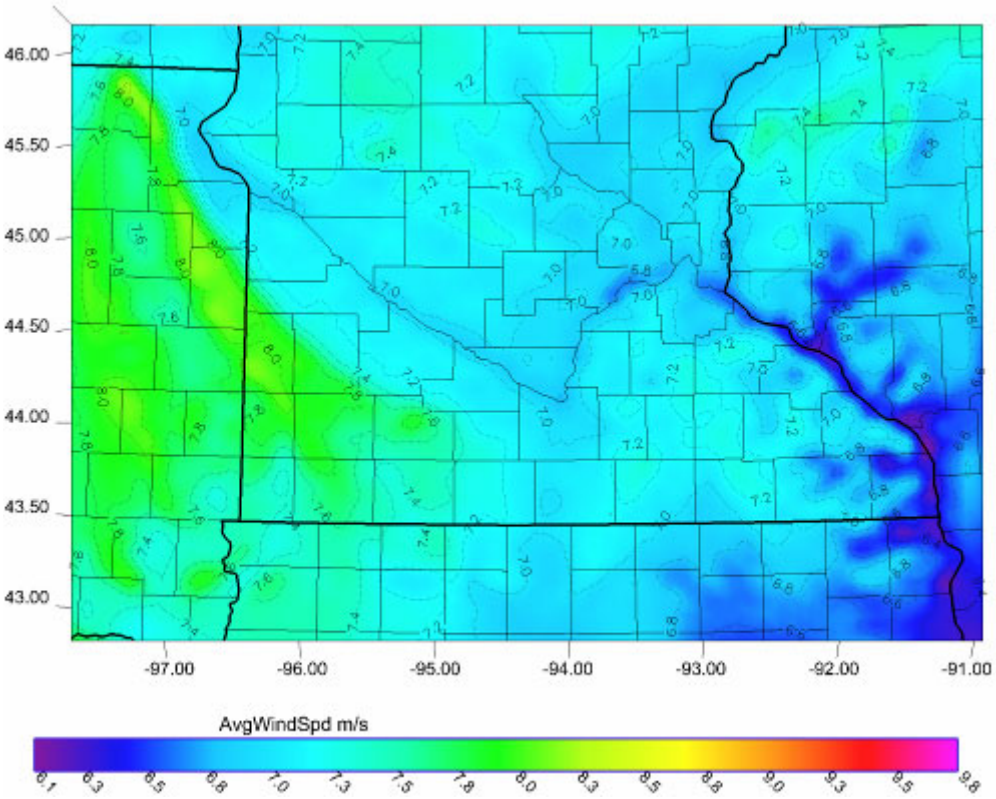

Figure 13: Mean wind speed (m s^{-1}) for August.

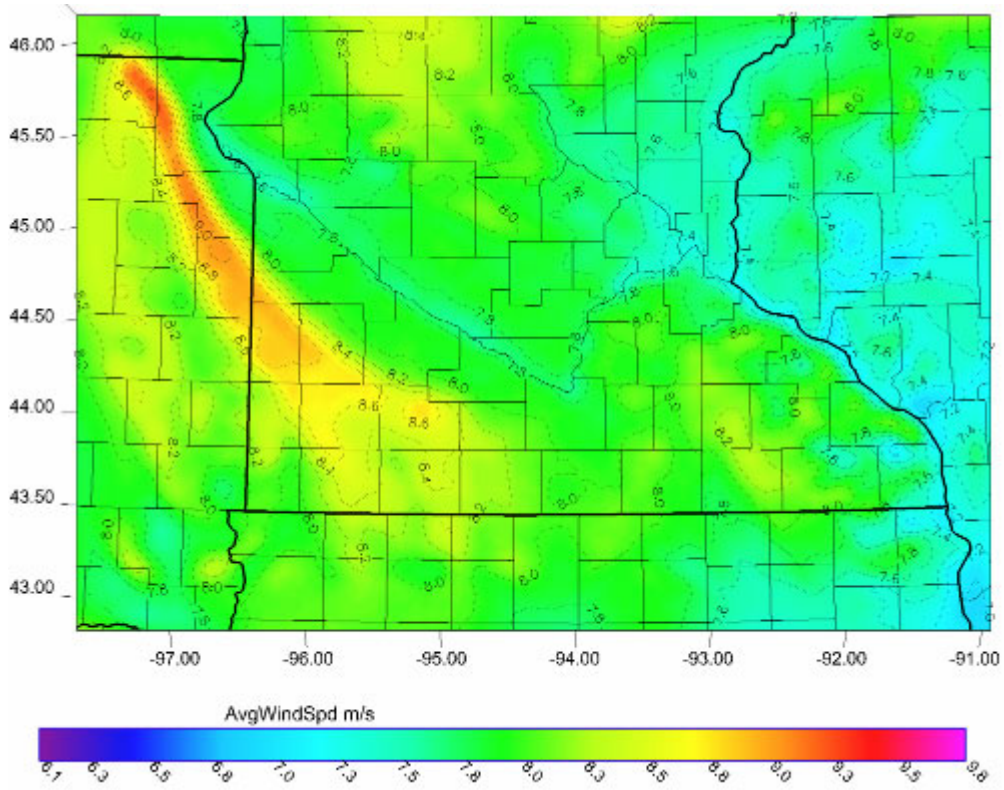

Figure 14: Mean wind speed (m s^{-1}) for September.

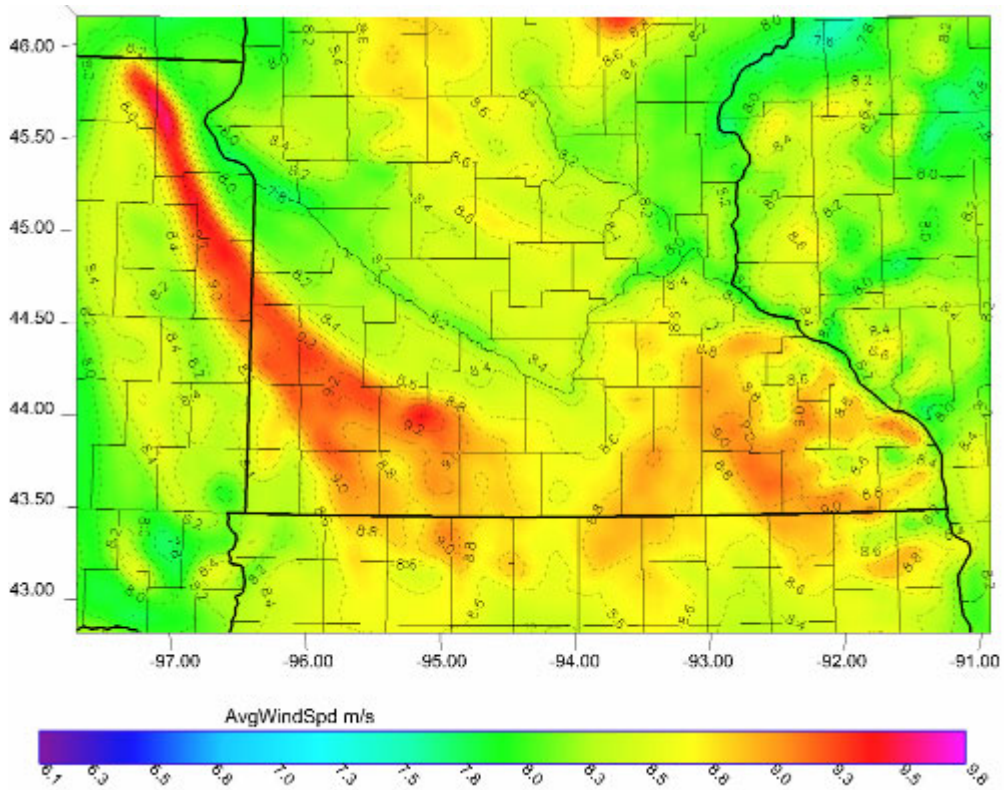

Figure 15: Mean wind speed (m s^{-1}) for October.

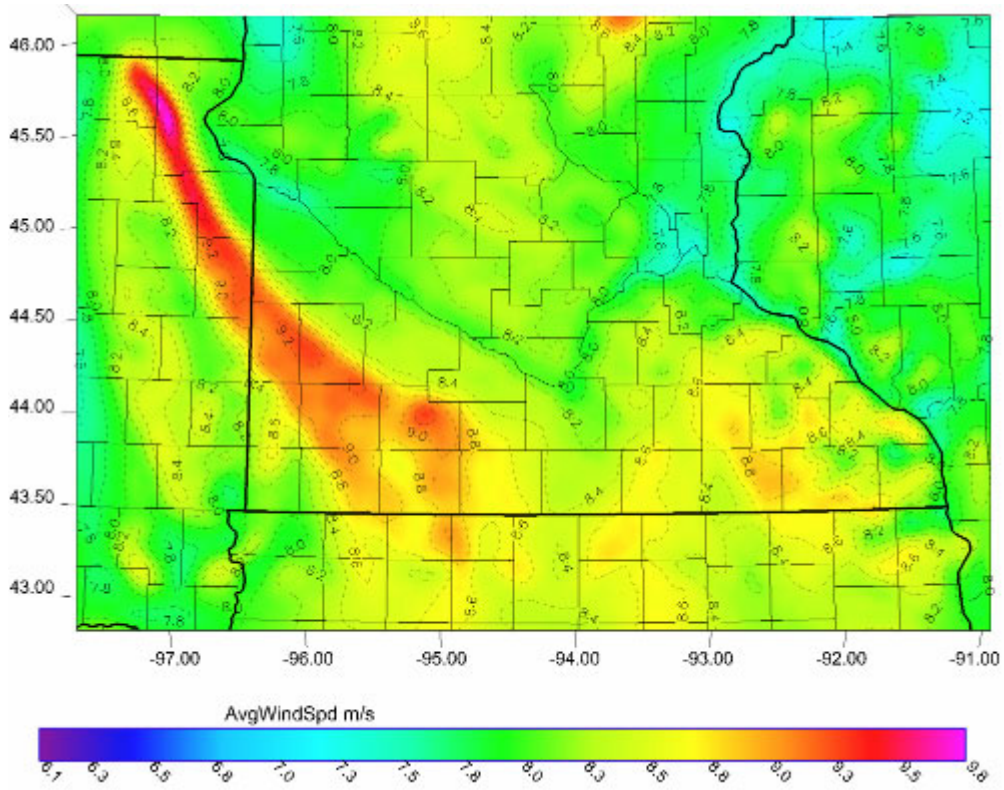

Figure 16: Mean wind speed (m s^{-1}) for November.

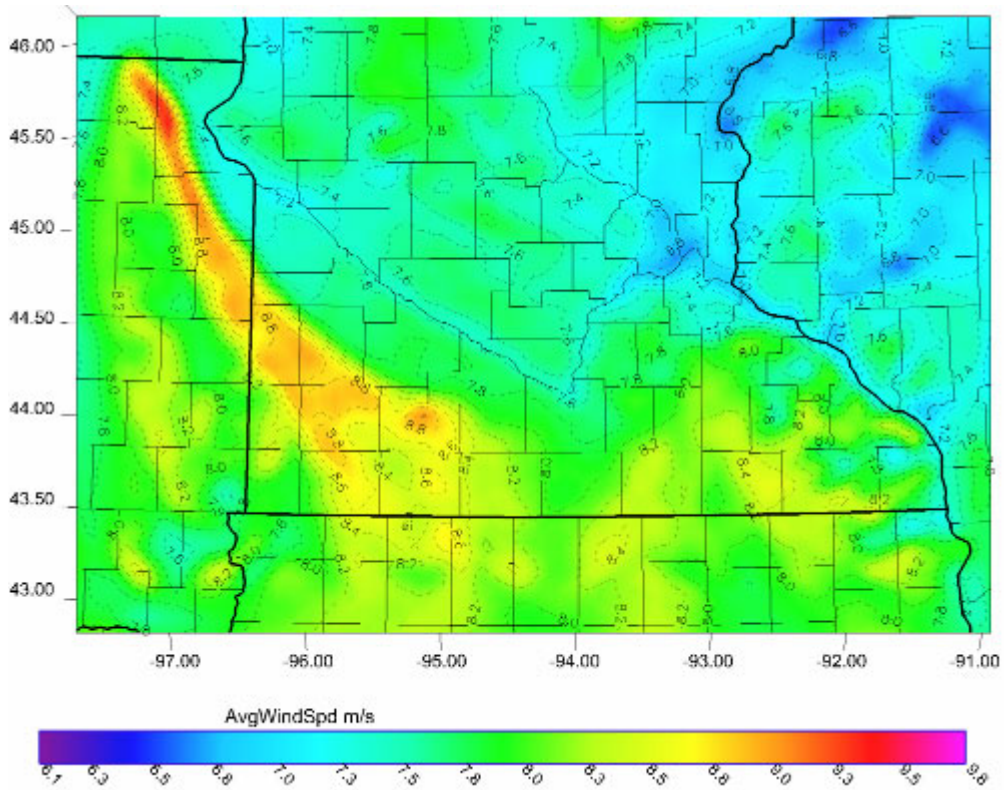

Figure 17: Mean wind speed (m s^{-1}) for December.

Summary of 3 year averages of annual and monthly wind speed.

The 3 year annual and monthly wind speed averages portray marked geographic and seasonal signals. As shown in Fig. 5 through 17, the wind resource of the Buffalo Ridge of Minnesota and eastern South Dakota is a very prominent feature of the wind speed mapping on an annual and monthly basis. Another region, roughly centered on Mower County in southeast Minnesota, exhibits a clear secondary wind resource maxima. Over the study region, the best wind resource exists in the climatologic transition and winter seasons. This meteorological characteristic of more vigorous flow in the transition and winter seasons is fundamentally related to the jet stream position and corresponding synoptic weather system pattern as described in section 1.1. The weaker pressure gradient in the summer months is responsible for the slower mean wind speeds. Interestingly, Mille Lacs Lake in central Minnesota (top of map to the center right), with its low-friction surface characteristic, exhibits is a marked local maximum in wind speed.

Mean annual air density

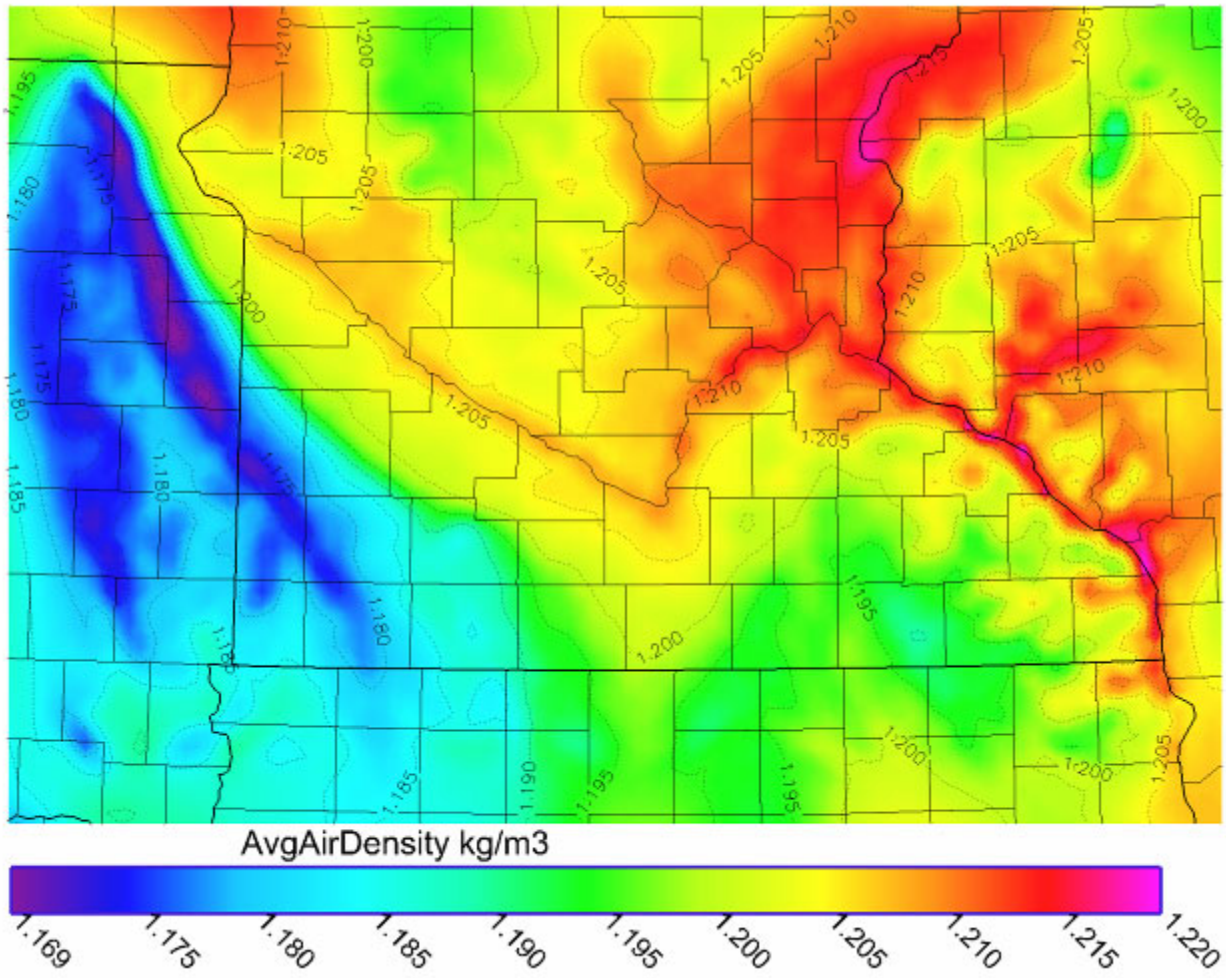

Figure 18: Mean annual air density (kg m^{-3}).

Summary of mean annual air density

The annual distribution of air density is largely controlled by elevation with the Buffalo Ridge clearly evident as a region of lower density. On a seasonal basis, the highest local densities are experienced in the coldest months and lowest densities in the warmest months.

Mean annual and monthly power density

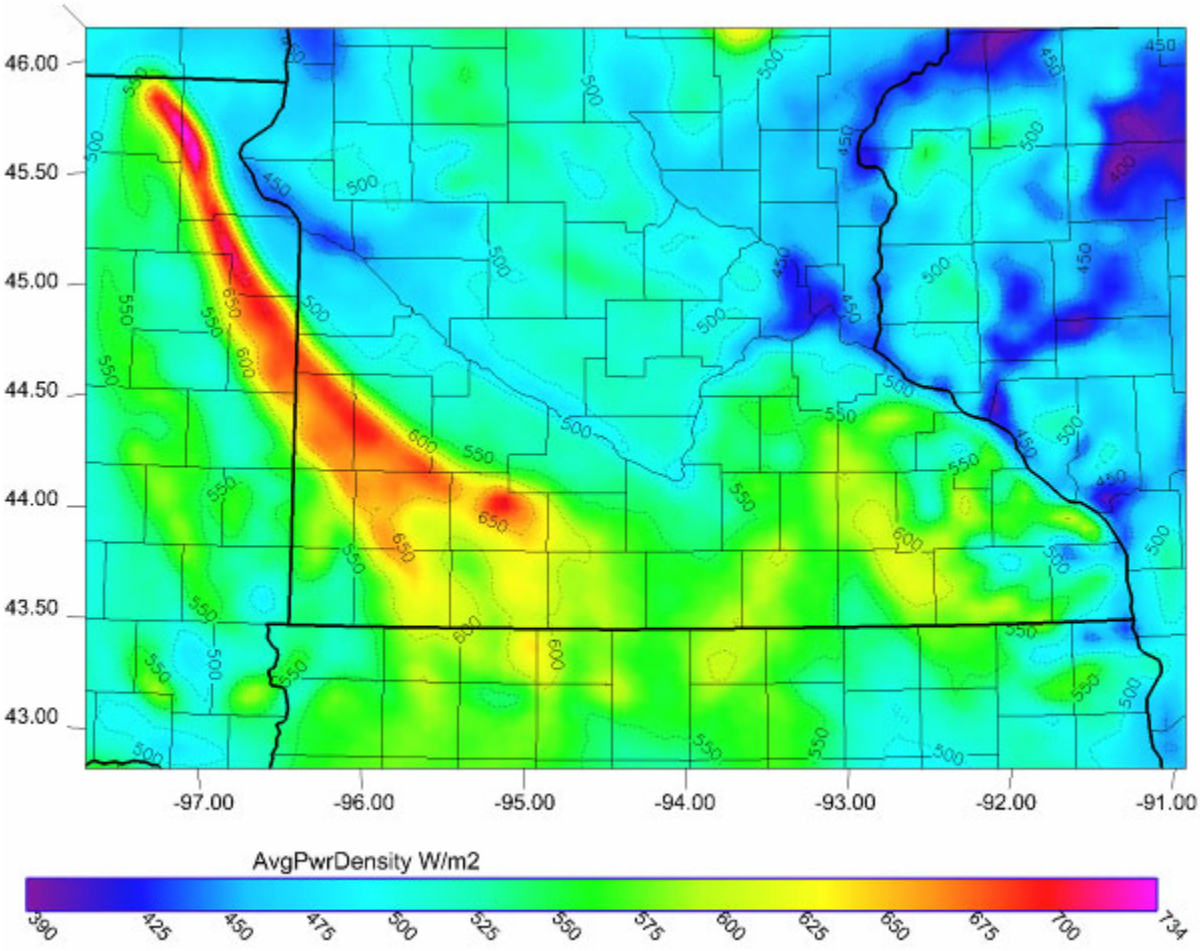

Figure 19: Mean annual power density in W m^{-2}.

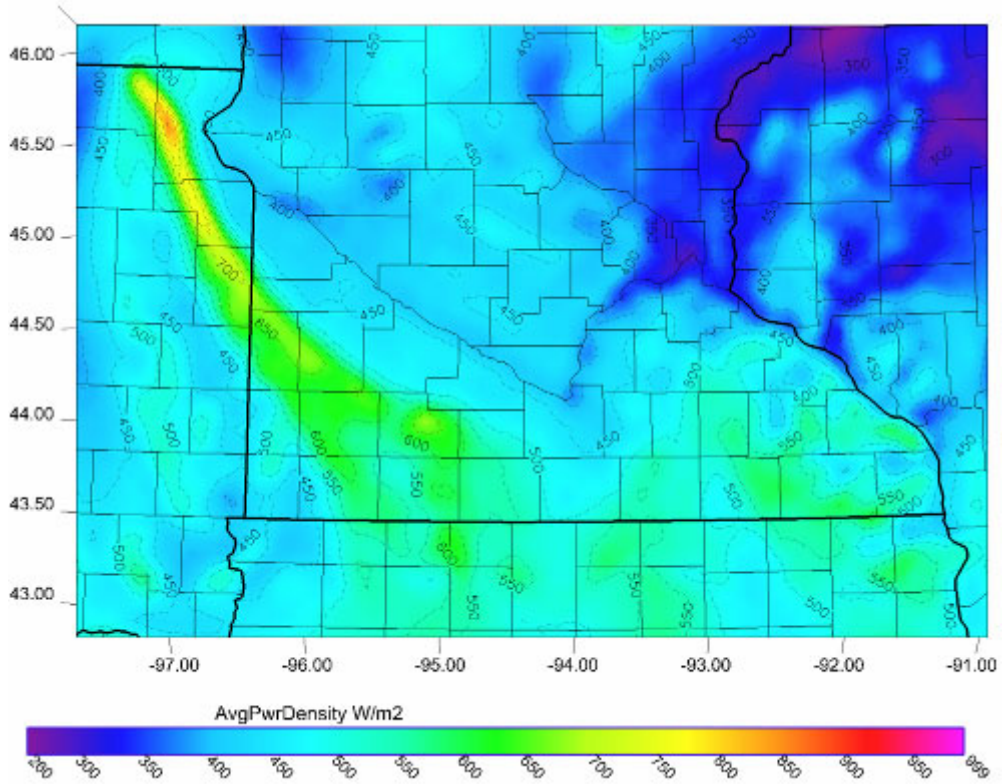

Figure 20: Mean January power density in W m^{-2}.

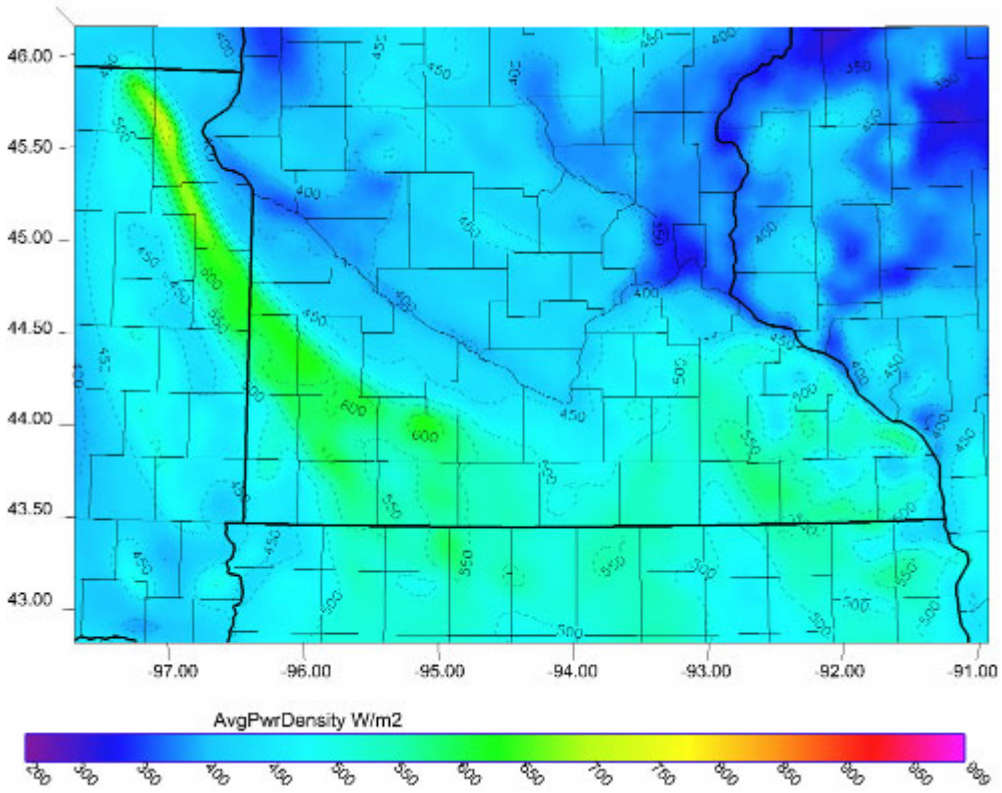

Figure 21: Mean February power density in W m^{-2}.

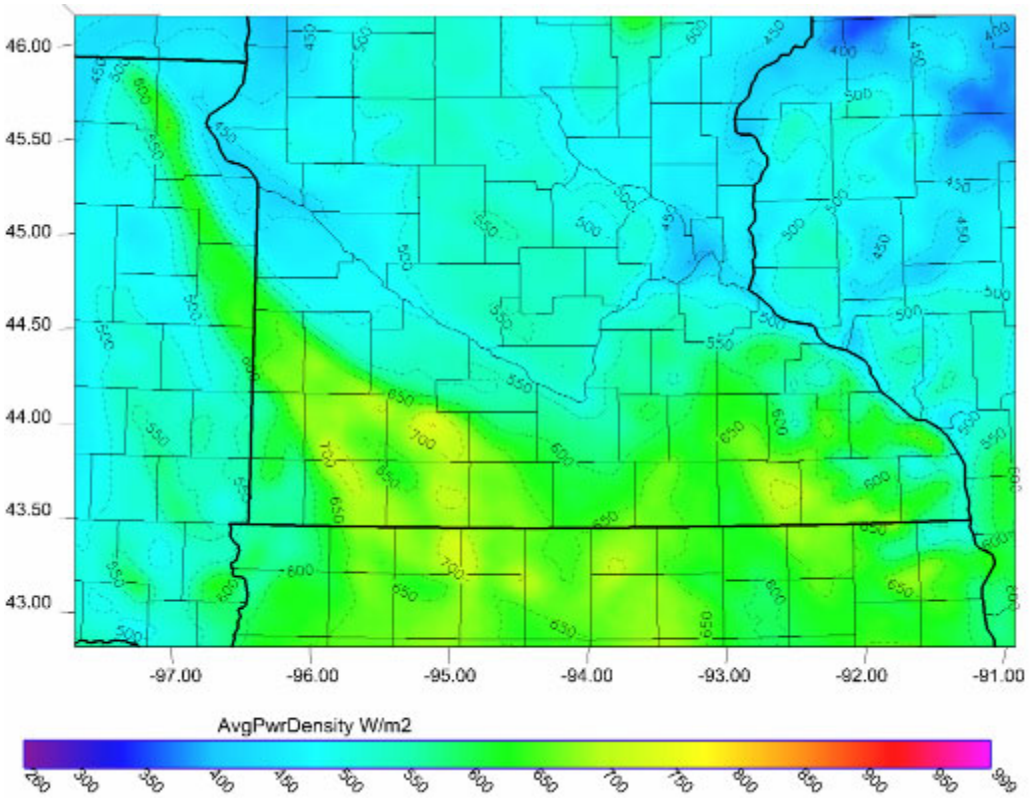

Figure 22: Mean March power density in W m^{-2}.

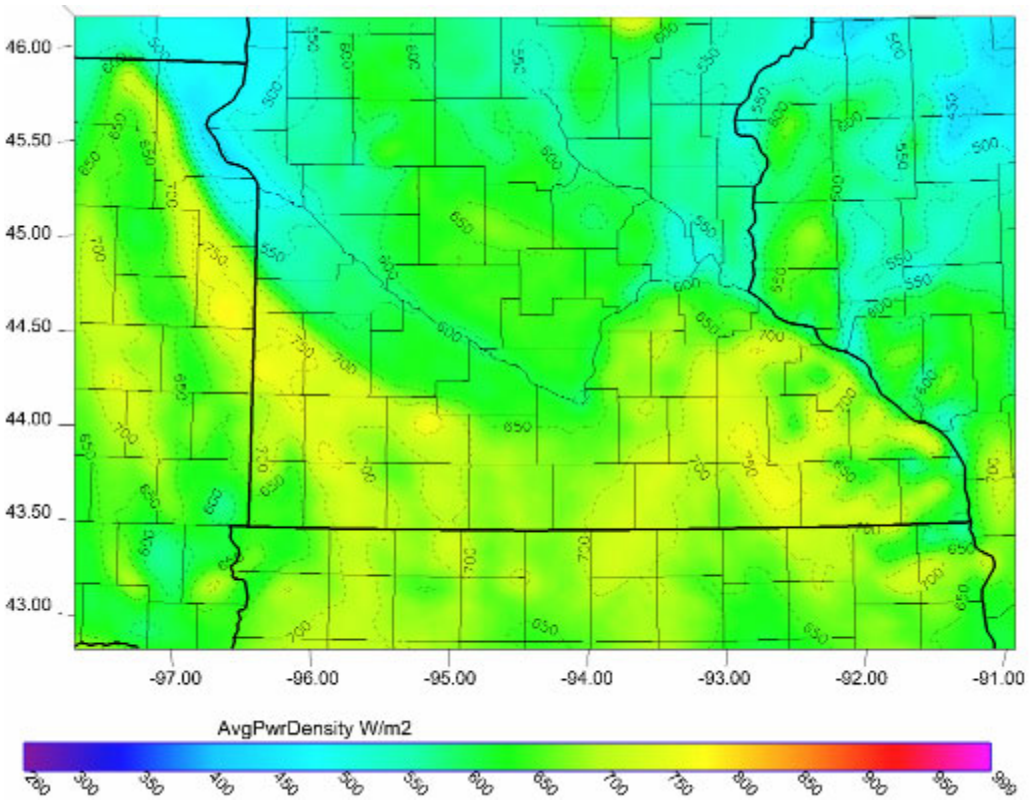

Figure 23: Mean April power density in W m^{-2}.

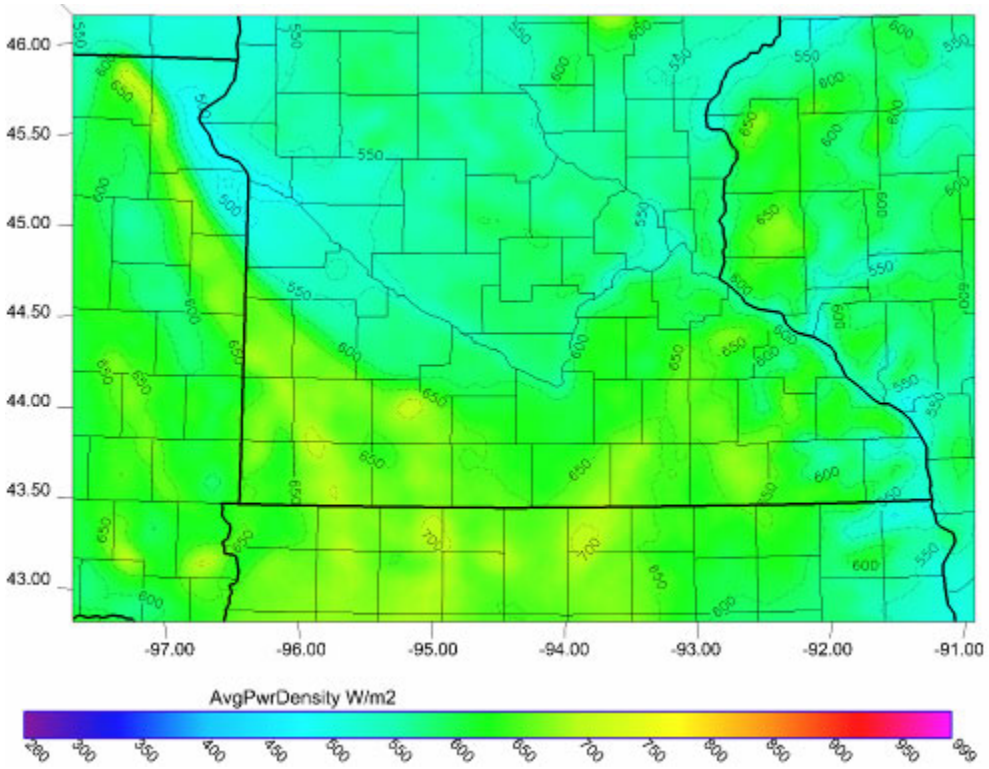

Figure 24: Mean May power density in W m^{-2}.

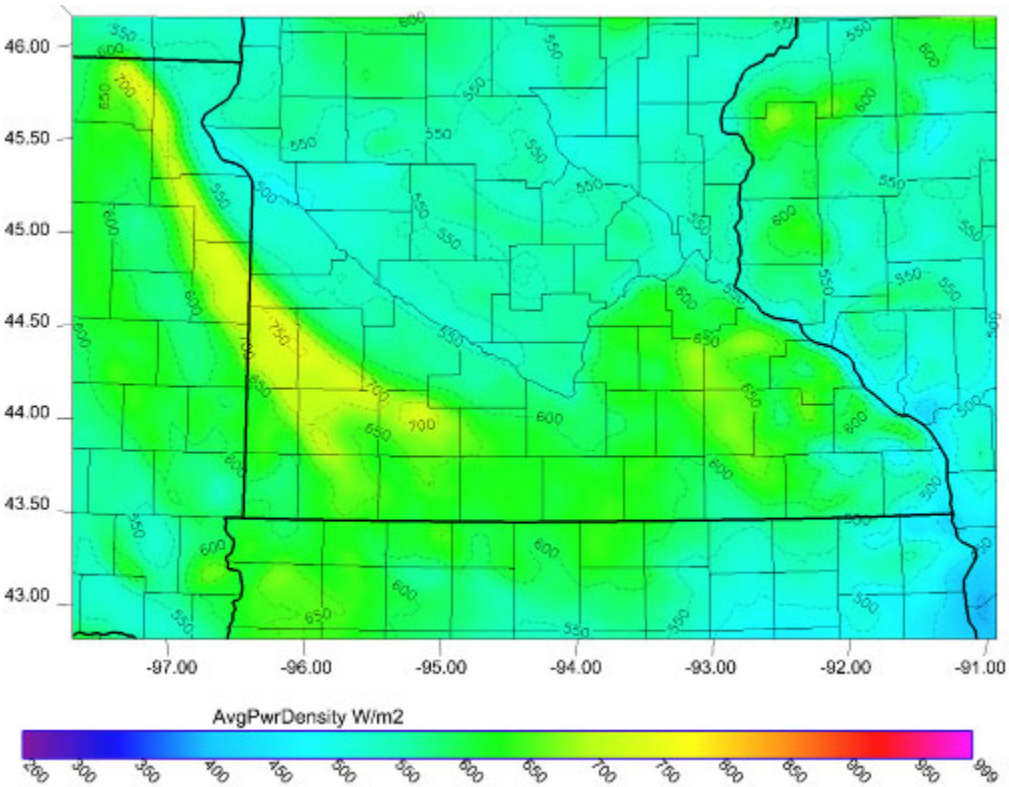

Figure 25: Mean June power density in W m^{-2}.

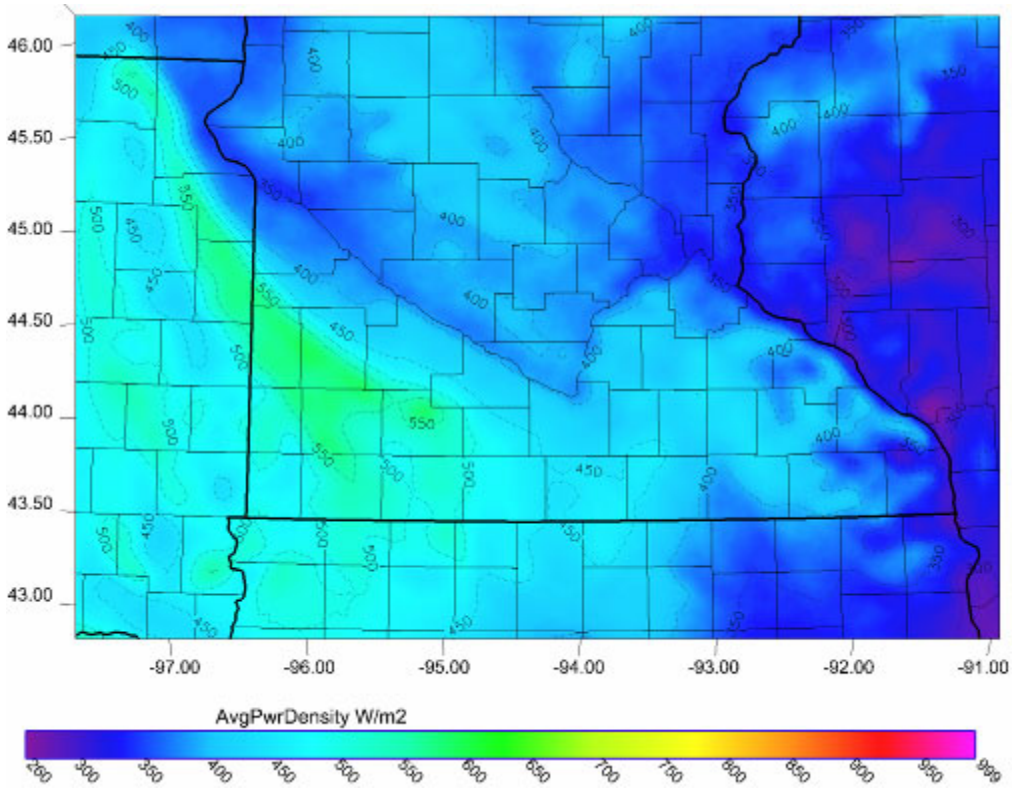

Figure 26: Mean July power density in W m^{-2}.

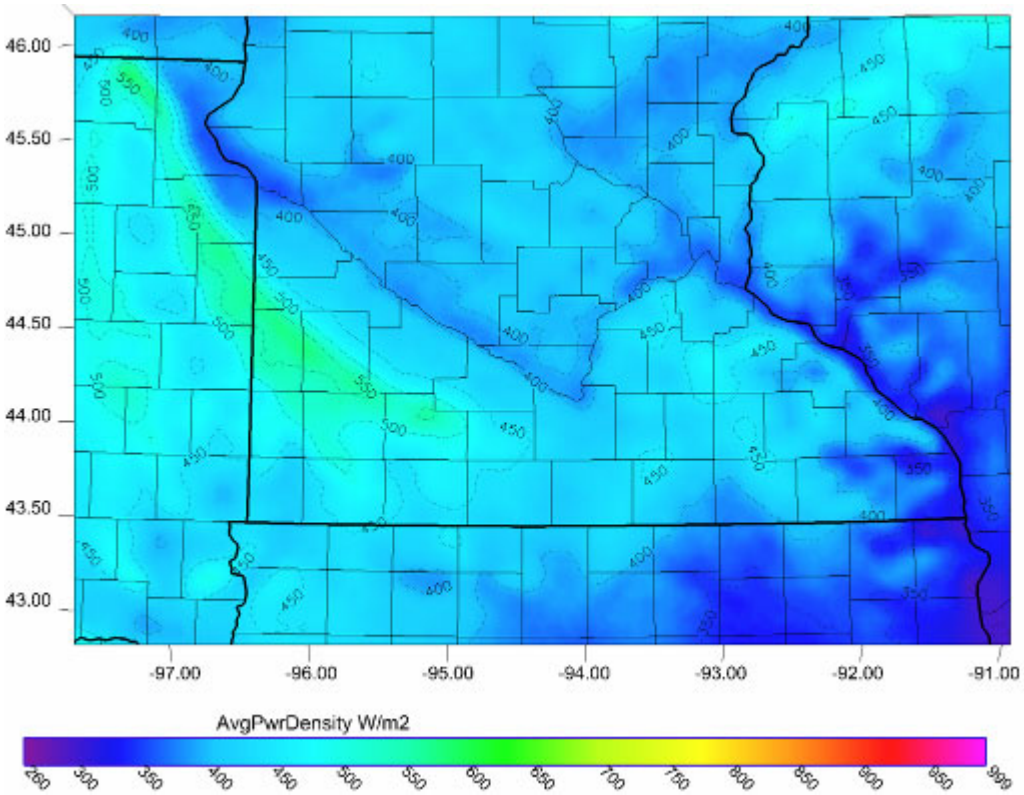

Figure 27: Mean August power density in W m^{-2}.

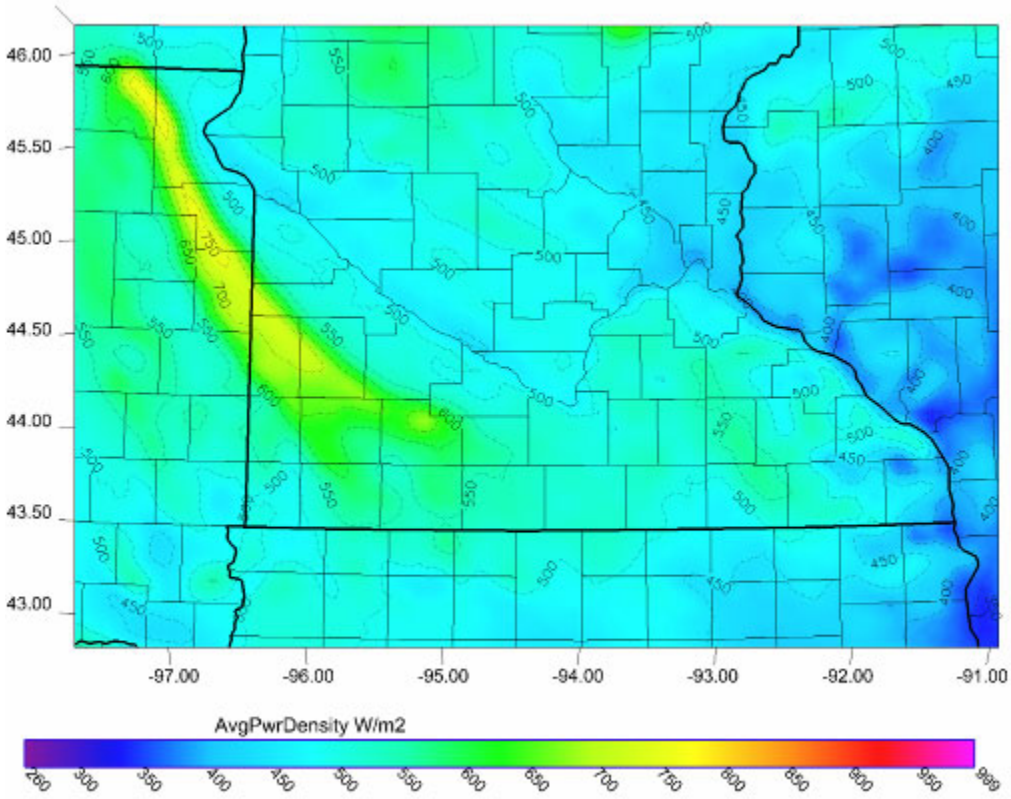

Figure 28: Mean September power density in W m^{-2}.

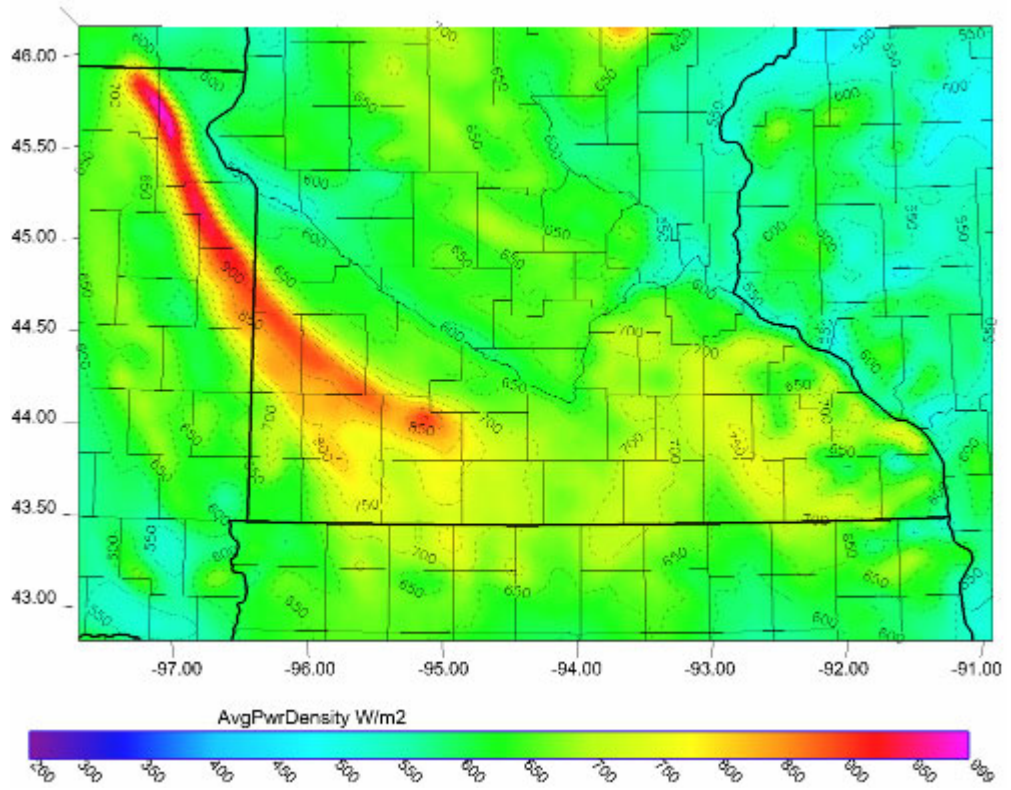

Figure 29: Mean October power density in W m^{-2}.

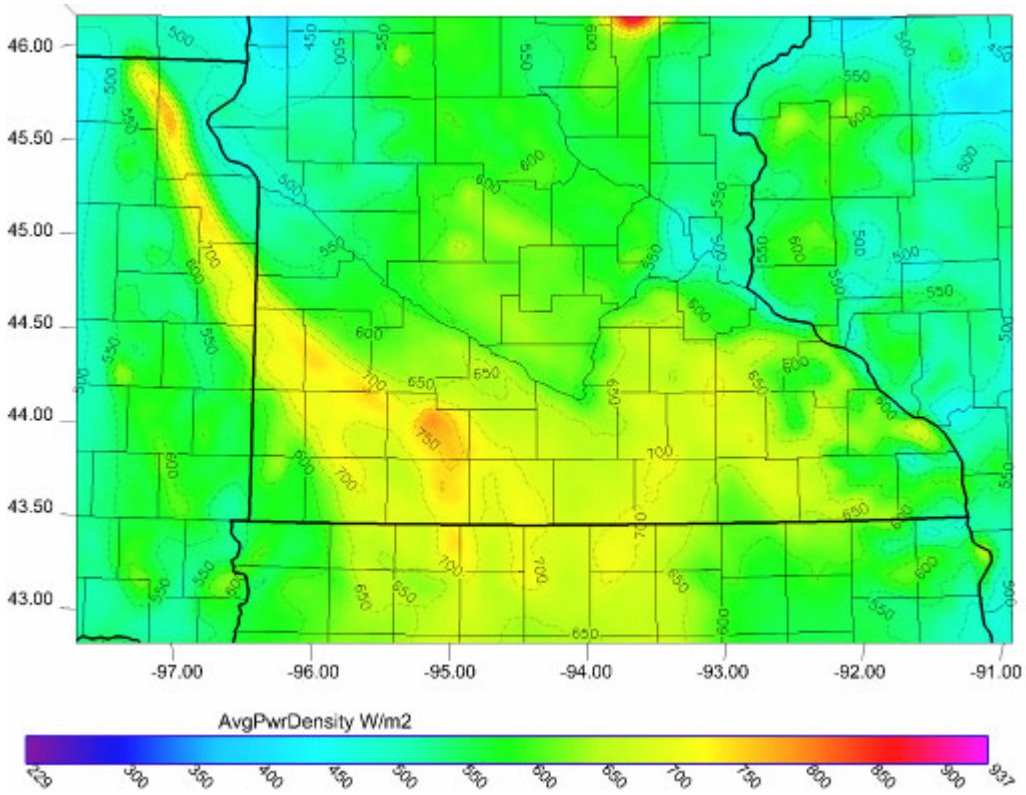

Figure 30: Mean November power density in W m^{-2}.

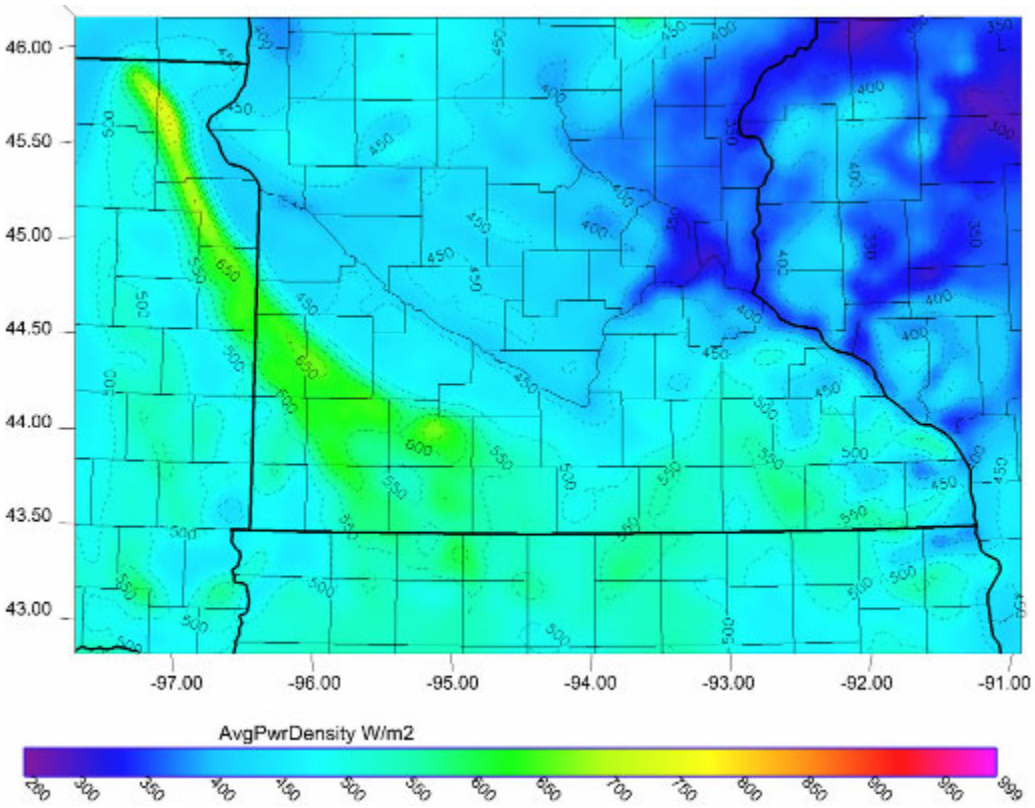

Figure 31: Mean December power density in W m^{-2}.

Summary of 3 year averages of annual and monthly power density

The mean annual geographic distribution of power density is dominated by the annual distribution of wind speed (note the pattern correspondence with Fig. 5). As shown in Figs. 19 - 31, the Buffalo Ridge exhibits a maximum in power density throughout the year. Even though the highest elevation portion of the Buffalo Ridge in northeast South Dakota has the lowest annual air density, the greater wind speeds occurring in this area dominate the power density calculation. The secondary Mower County wind resource may also be seen; however, this feature is less distinguishable in the summer months. The monthly power density variations closely correspond to the monthly wind climatology.

1.4.4 Mean annual energy production for 2 turbine types

Mean annual energy calculations have been completed using power curves for 2 wind turbine types: 1) a 1.5 MW turbine characterizing contemporary installations, and a 1.5 MW turbine optimized for lower wind speeds (designated 1.5 MW L).

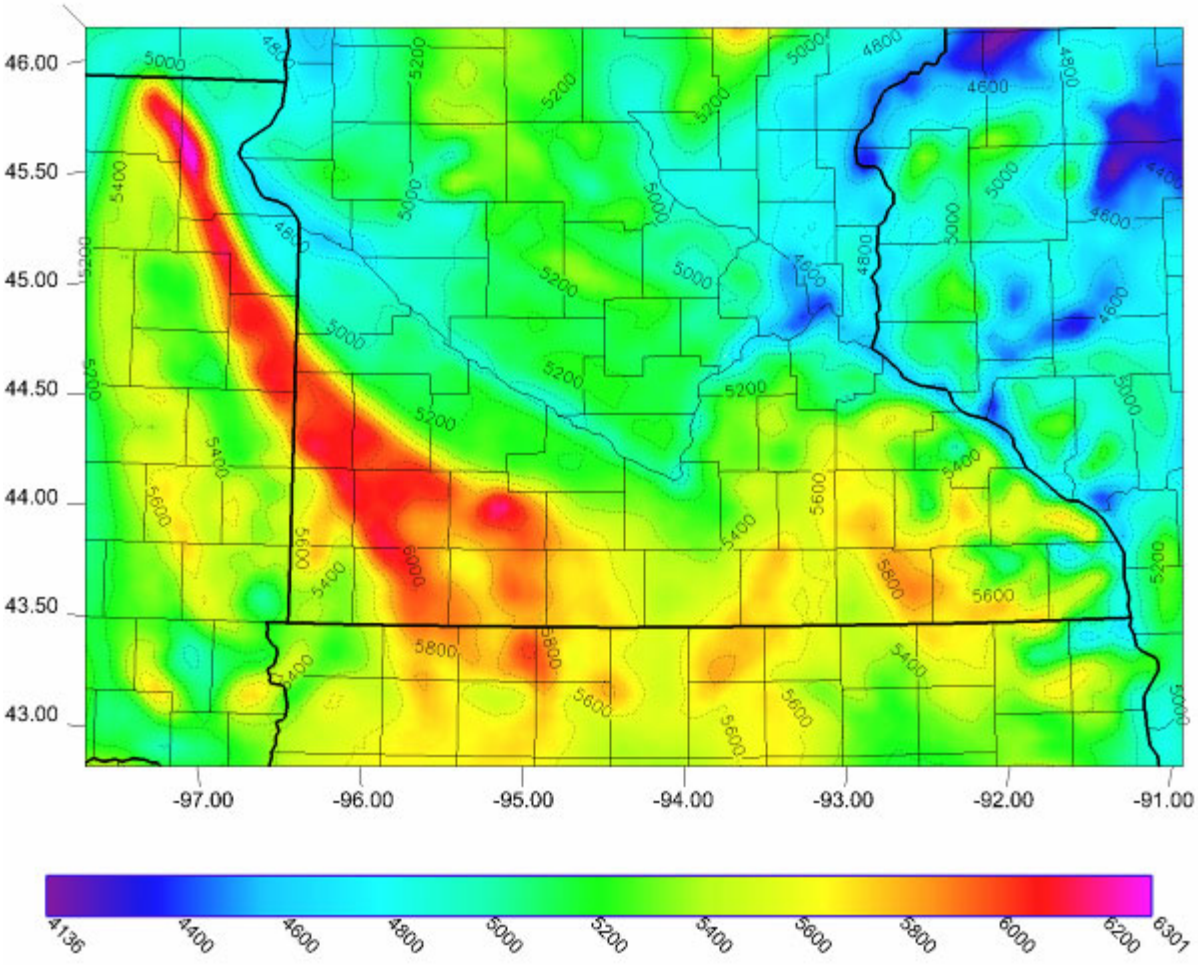

Figure 32: Mean annual energy production (MWh) for the 1.5 MW turbine.

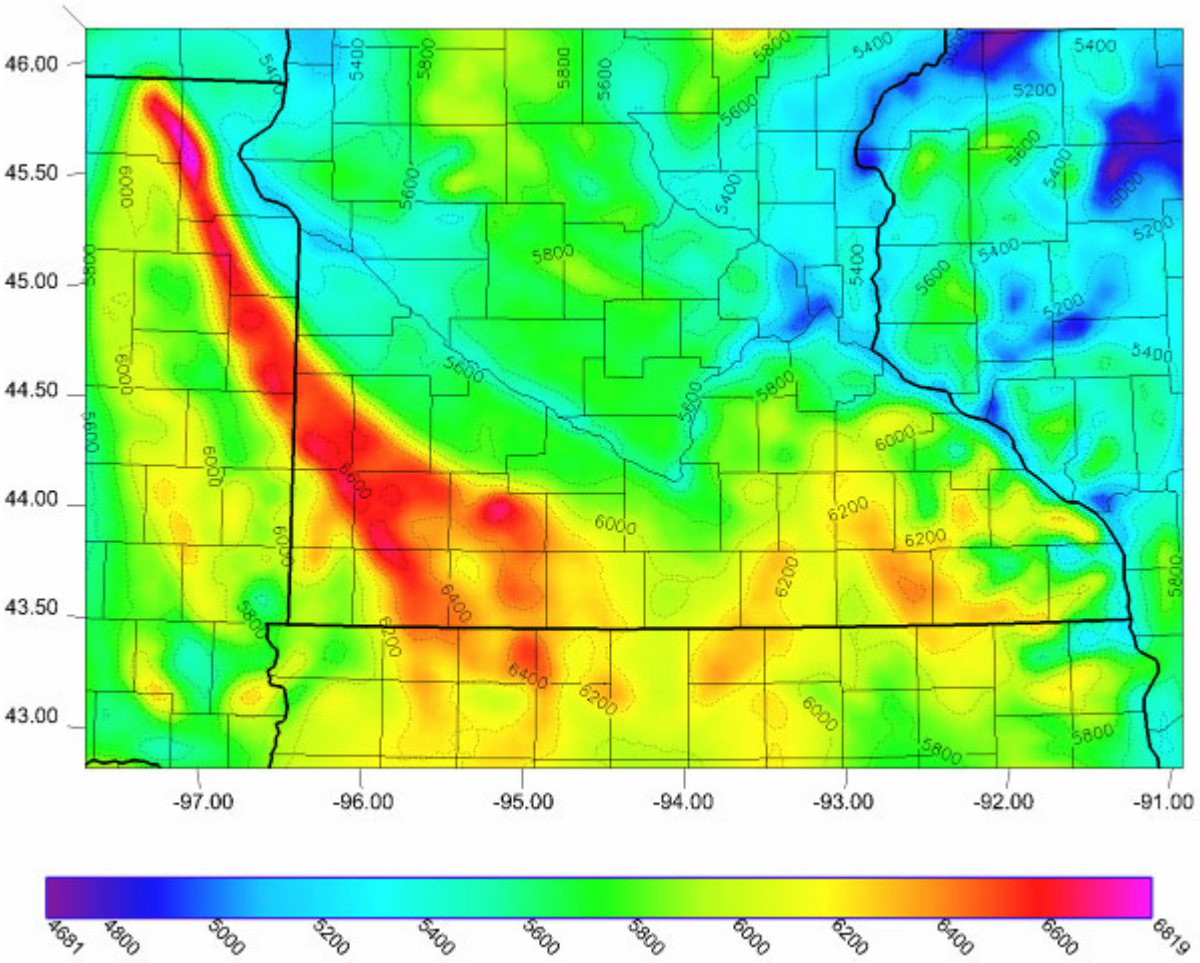

Figure 33: Mean annual energy production (MWh) for the 1.5 MW L turbine. Note that the reference color scaling is optimized for this map and is different from that used in Fig. 32.

Summary of 3 year average of annual energy production

The unambiguous region of maximum energy production corresponds to the Buffalo Ridge. More specifically, the areas near the ridge crest and just east of the ridge crest exhibit an enhanced wind energy production resource. The region within and near Mower County represents a secondary maxima of wind energy production. A comparison of the standard 1.5 MW turbine energy production with the values for the 1.5 MW L turbine reveal marked differences over the entire study area. Energy production differences in the 7-10 % range are common in many areas with the 1.5 MW L turbine clearly superior for the wind regime of eastern South Dakota and southern Minnesota.

1.5 Wind resource temporal variability and geographic dispersion

Temporal variability of the wind resource at MM5 Tower 24

An essential objective of this study is the characterization of the temporal variability of the wind resource. To accomplish this assessment, hourly data from MM5 proxy Tower 24 was utilized for all 3 modeling years. This tower site geographically corresponds to the Delta Sector of the Lake Benton II Wind Facility where power production data has been collected and archived by the National Renewable Energy Laboratory (NREL). A validation exercise comparing MM5 model output (converted to power) with actual power production

values from the NREL database is presented in section 2. RNL normalized model wind speed data for a hub height of 52 m was corrected for air density and applied to the power curve for the Zond-750 turbine (750 kW peak capacity) to produce hour-of-day power production statistics for each month of the year. Note that the Zond-750 is the currently installed turbine at Lake Benton I and II. Multiple years of specific months were combined (e.g., January of 2000, 2002, 2003) to assemble a time-dependent monthly dataset of power production. To better reflect "in the field" power production for a given wind speed, losses due to array, transmission, collection, and other sources were estimated to be 14 % (applied to all hourly power calculations), based on initial recommendations from the Technical Review Committee (TRC) . At a subsequent TRC meeting, the general consensus indicated that the 14 % loss figure could be somewhat lower. A definitive study of losses would be of substantial benefit in wind farm planning studies.

To characterize the temporal variability of the MM5 derived power production at proxy Tower 24, probability distributions and frequency of production histograms have been created. Probability plots indicate that at a certain hour of the day for a specific month, there exists a 50, 75, or 90 % probability of producing a particular power value from a single Zond-750 turbine. The histograms are divided up into bins for evaluating the frequency of power production exceeding incremented multiples of 20 % of turbine capacity (i.e., 150 kW increments). These monthly quantities are presented in Figs. 34-45. The combined analyses reveal a wind resource with a significant diurnal dependence all months of the year. The monthly analysis shows that the length of the period of lowest power production is directly associated with the duration of solar insolation. The magnitude of diurnal variability in power production is magnified in the summer season with its much longer period of solar insolation. The late summer to early fall period is known for the frequent occurrence of nocturnal low-level jets over the central United States (Bonner 1968). The mid-late summer months show a strong signal of this low-level jet, although all months show some indication of a nocturnal wind maximum. In months that show a strong low-level jet signal like July and August, the peak wind resource exists just before dawn. Although July and August are among the weakest months for mean wind speed and power density (see section 1.4), the predawn period exhibits a wind resource approximately equivalent to the peak resource period of some of the best wind resource months (October and November). Clearly, boundary layer thermal stability and its control on the vertical transport of momentum to turbine hub height has a dominant influence on the diurnal character of the wind resource. During nighttime hours, there is reduced vertical mixing of low-momentum near-surface air to hub height due to the large thermal stability in an often shallow layer just above the surface (i.e., the nocturnal inversion). The result is a wind resource increase in the nocturnal hours. This nocturnal increase is enhanced in climatologically favored periods of frequent low-level jet occurrence (Bonner 1968). The opposite is true during the daytime with enhanced mixing of near-surface low-momentum air parcels with those at higher levels within the boundary layer under the influence of low thermal stability. Reduced thermal stability is indicative of small resistance to vertical motions, and indeed the formation of surface heating-driven thermals within the boundary layer. The net result is an enhanced nocturnal wind resource and a reduced wind resource during daylight hours at hub height. Note that for wind near the surface (e.g., 10 m) the trend is reversed with a wind speed maximum occurring during the afternoon.

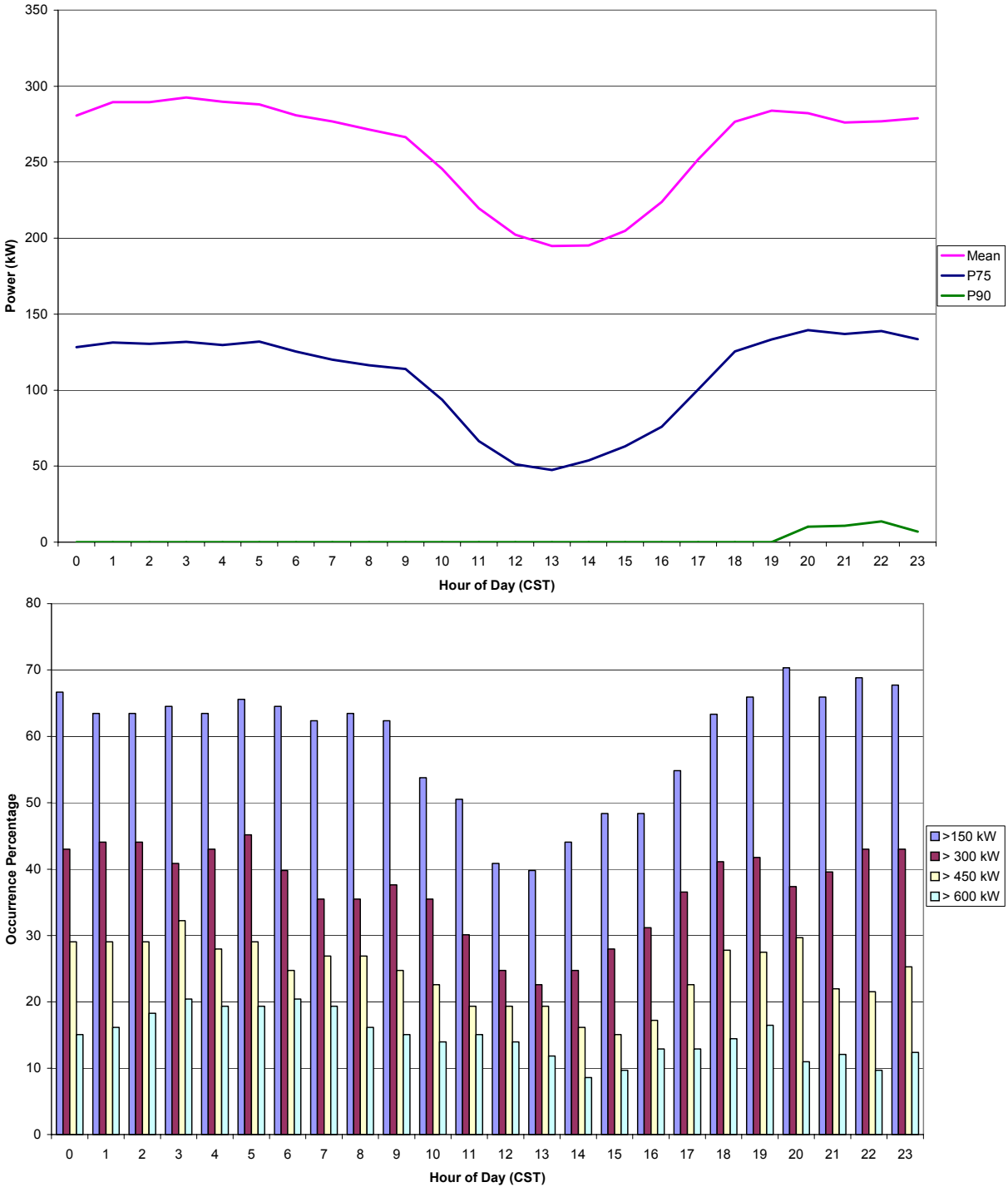

Figure 34: Probability distribution and frequency histogram for January power production (Z-750).

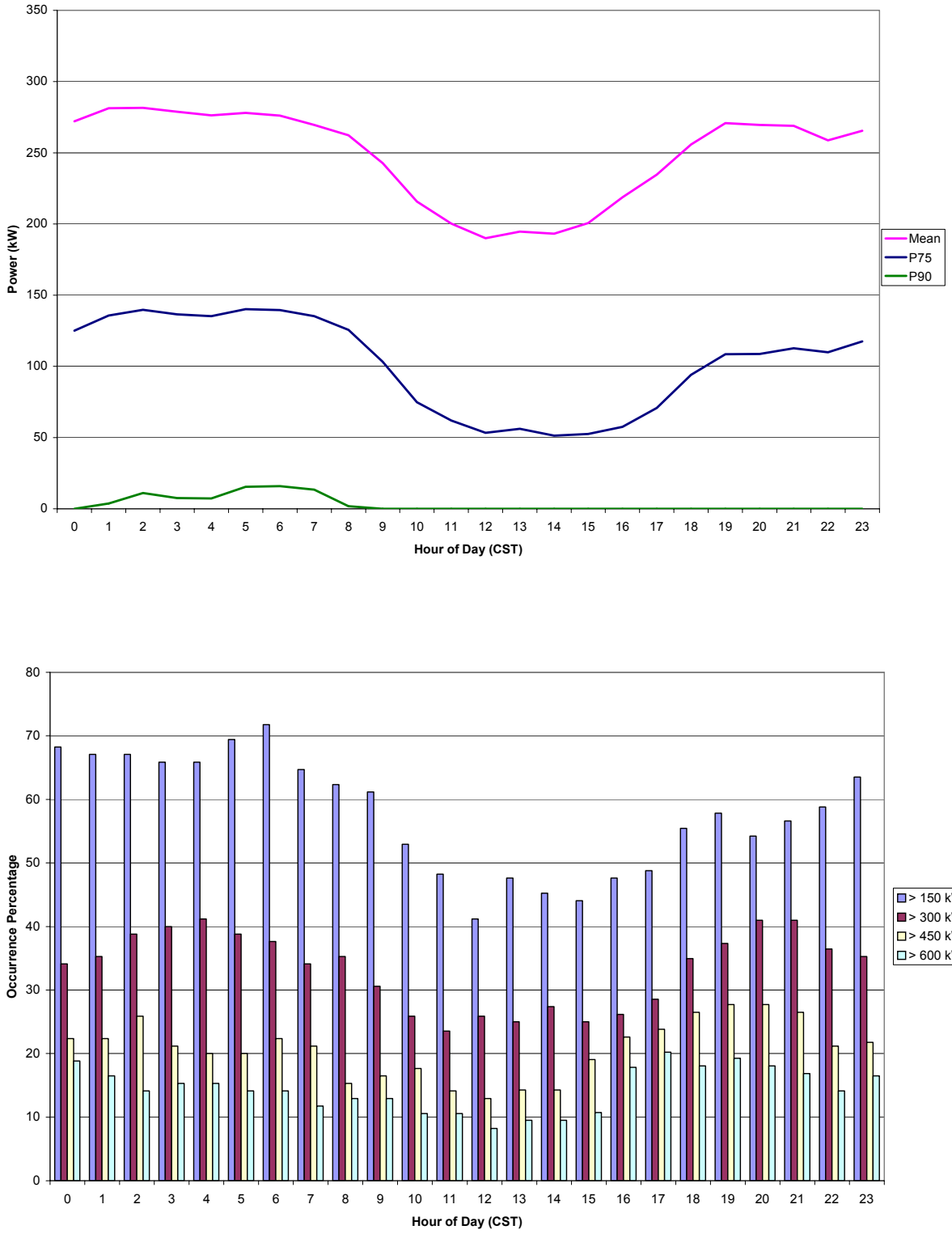

Figure 35: Probability distribution and frequency histogram for February power production (Z-750).

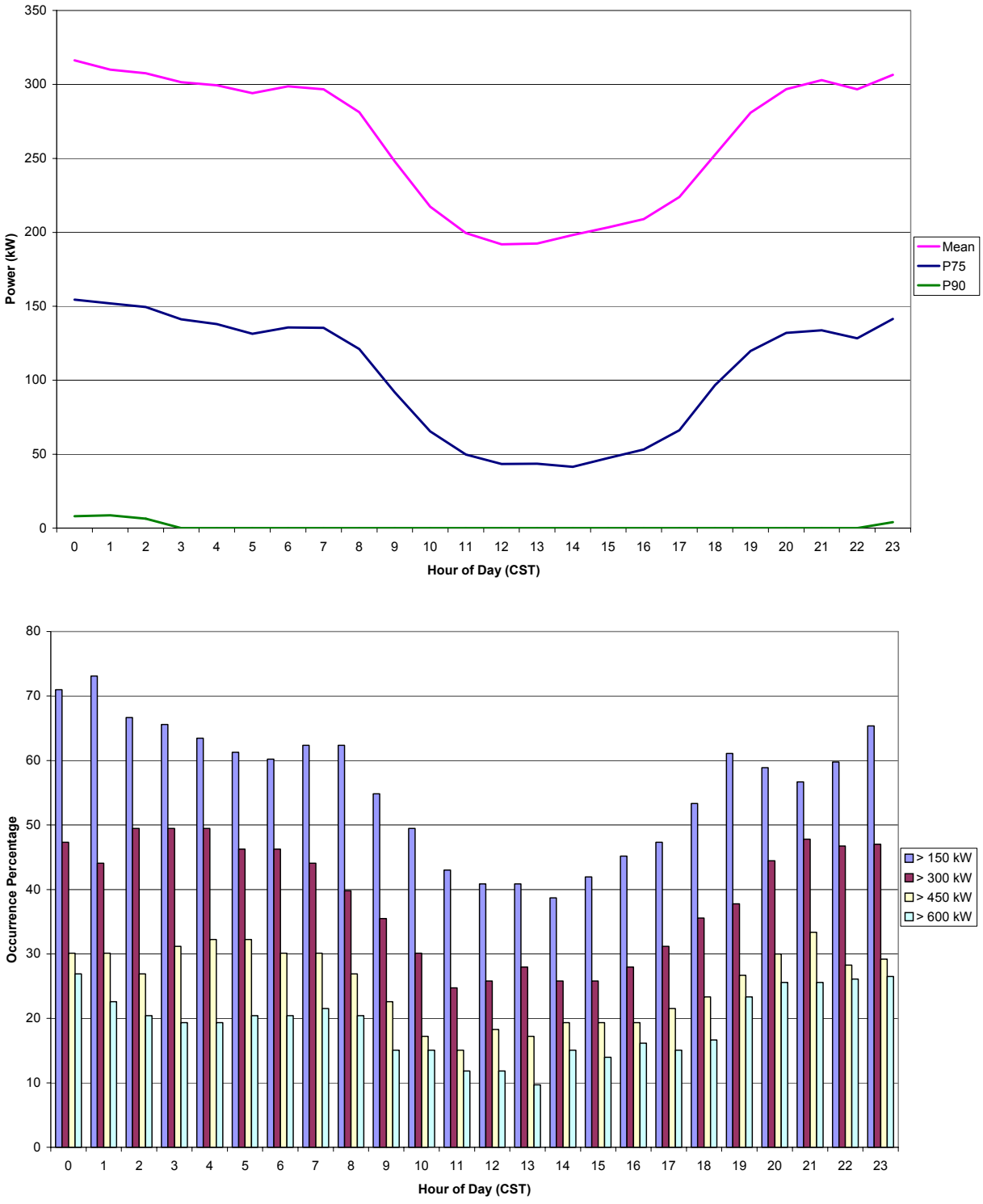

Figure 36: Probability distribution and frequency histogram for March power production (Z-750).

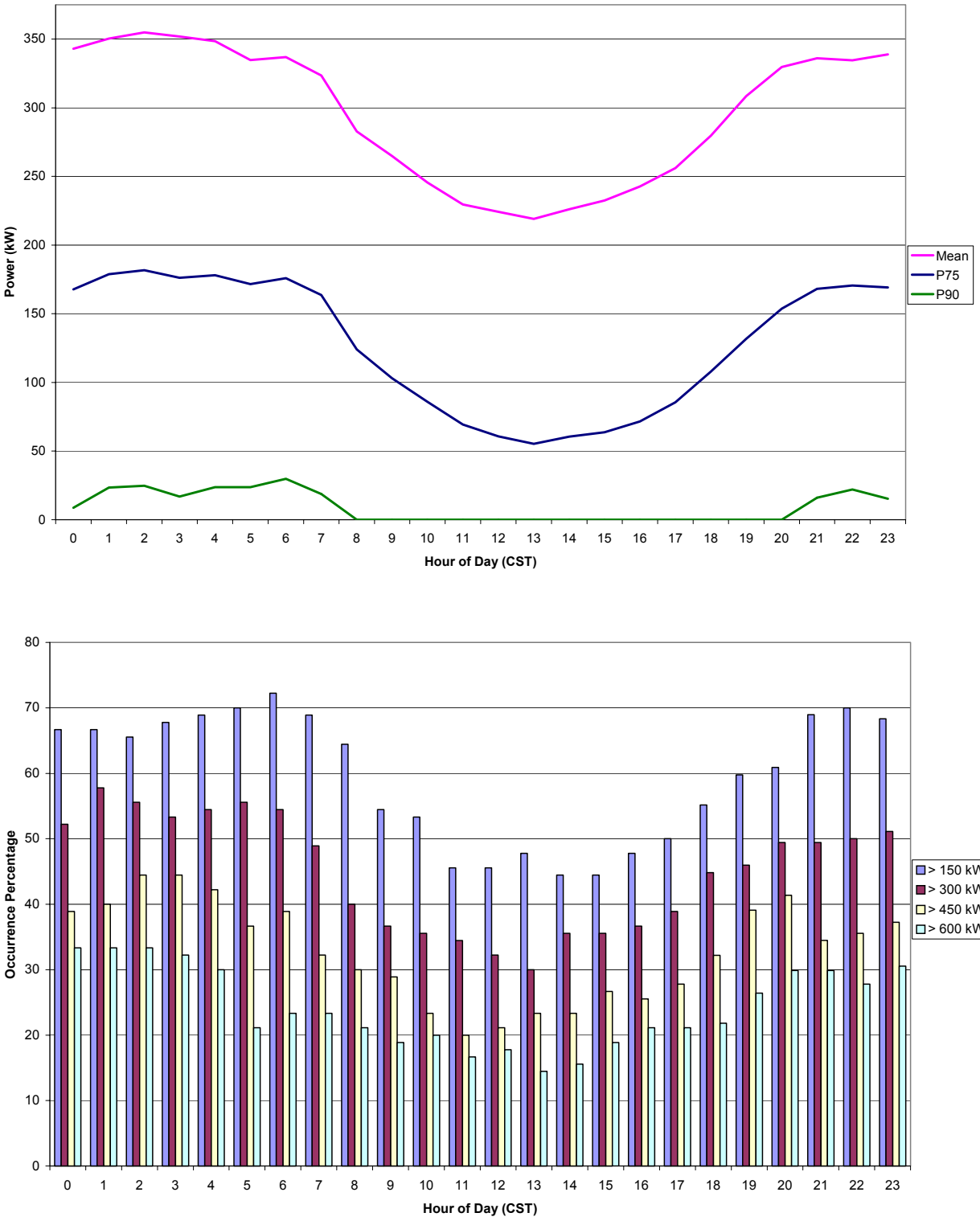

Figure 37: Probability distribution and frequency histogram for April power production (Z-750).

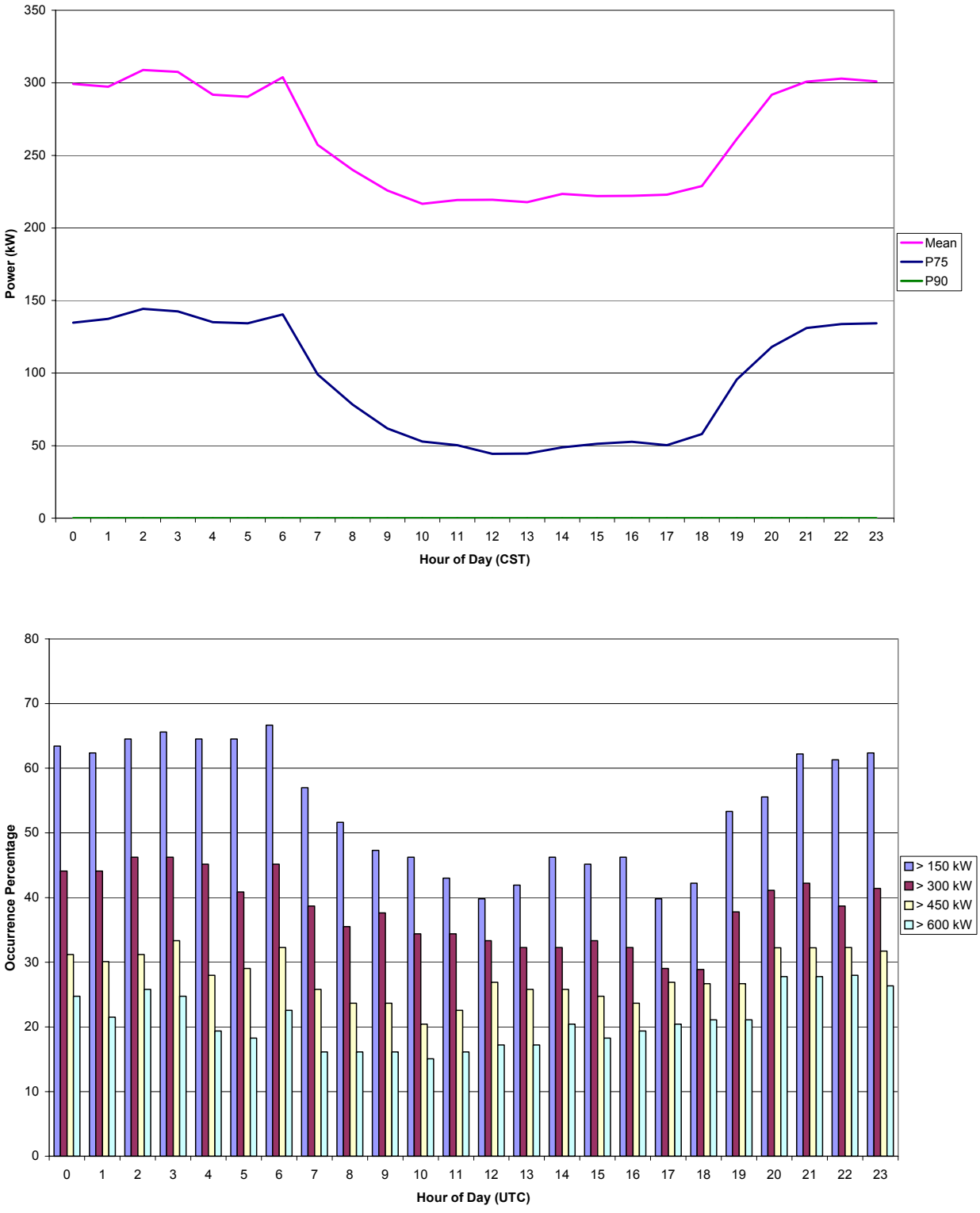

Figure 38: Probability distribution and frequency histogram for May power production (Z-750).

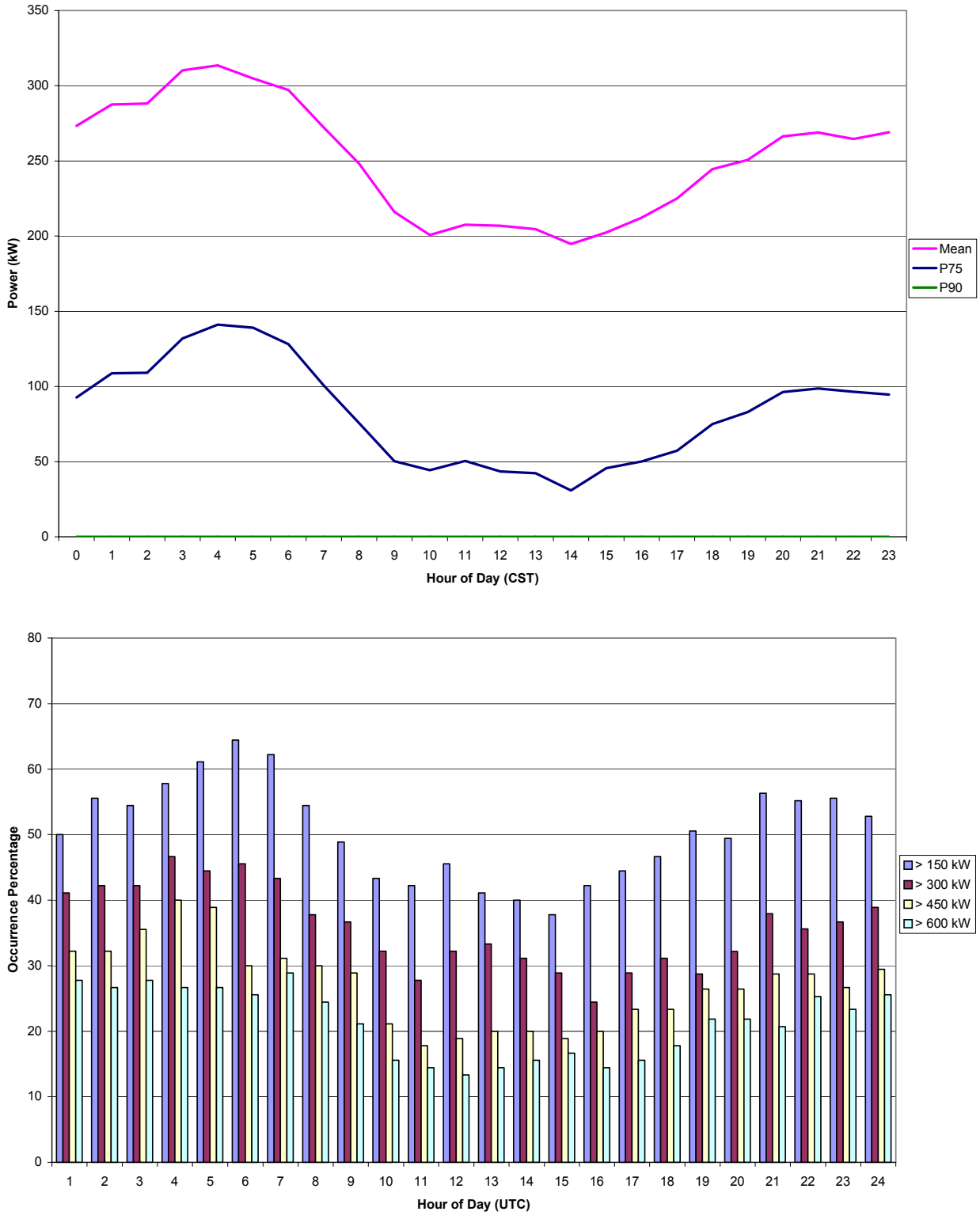

Figure 39: Probability distribution and frequency histogram for June power production (Z-750).

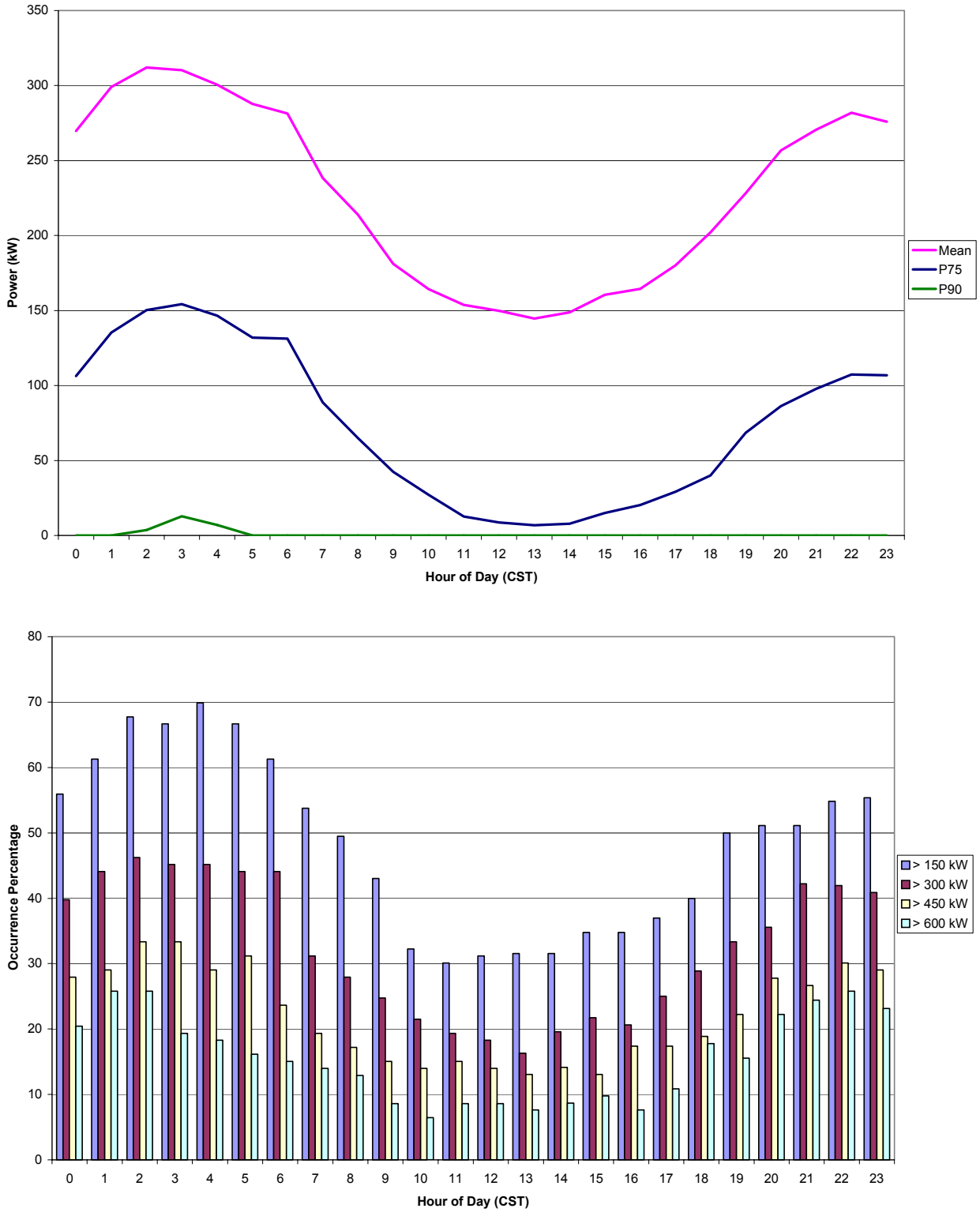

Figure 40: Probability distribution and frequency histogram for July power production (Z-750).

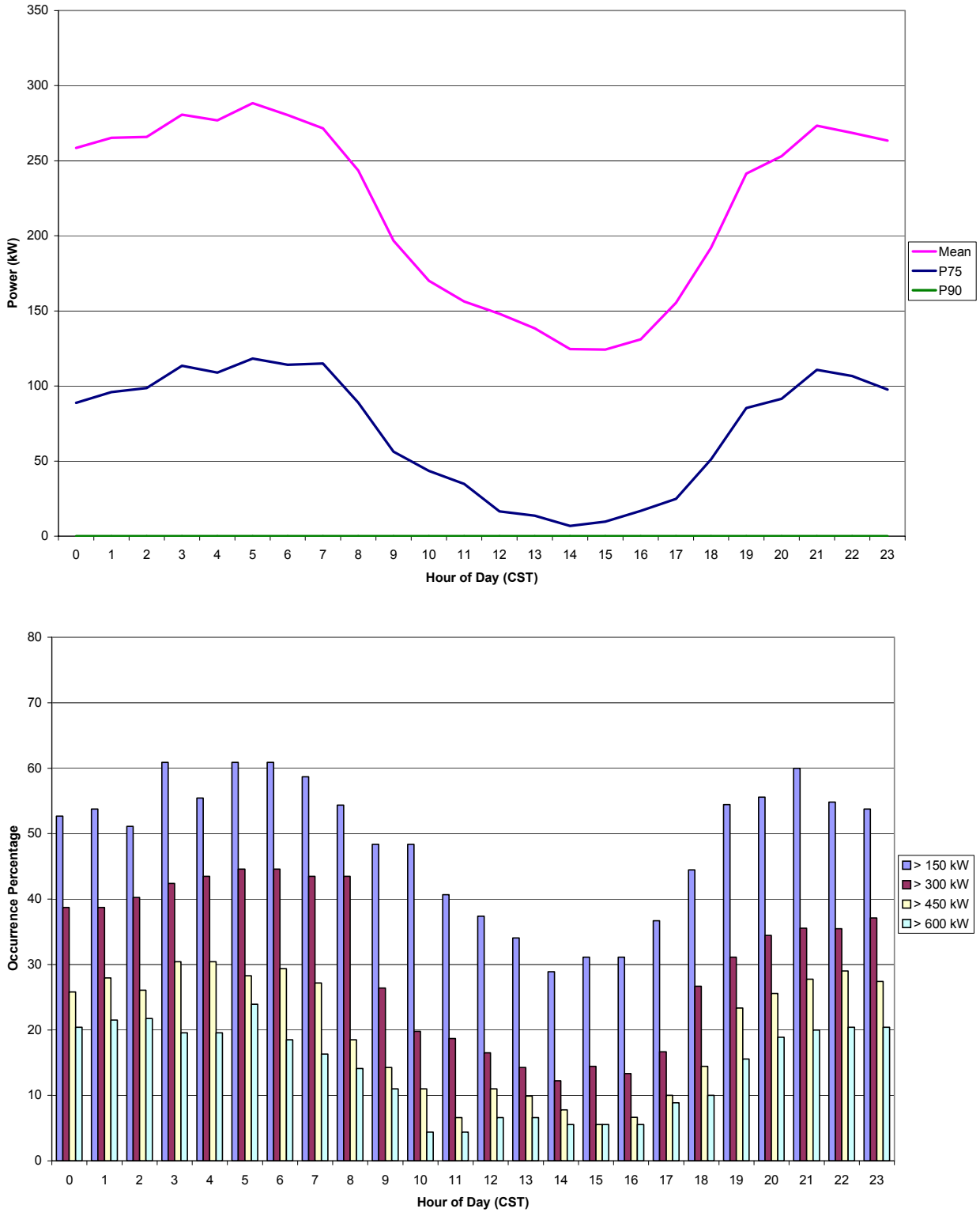

Figure 41: Probability distribution and frequency histogram for August power production (Z-750).

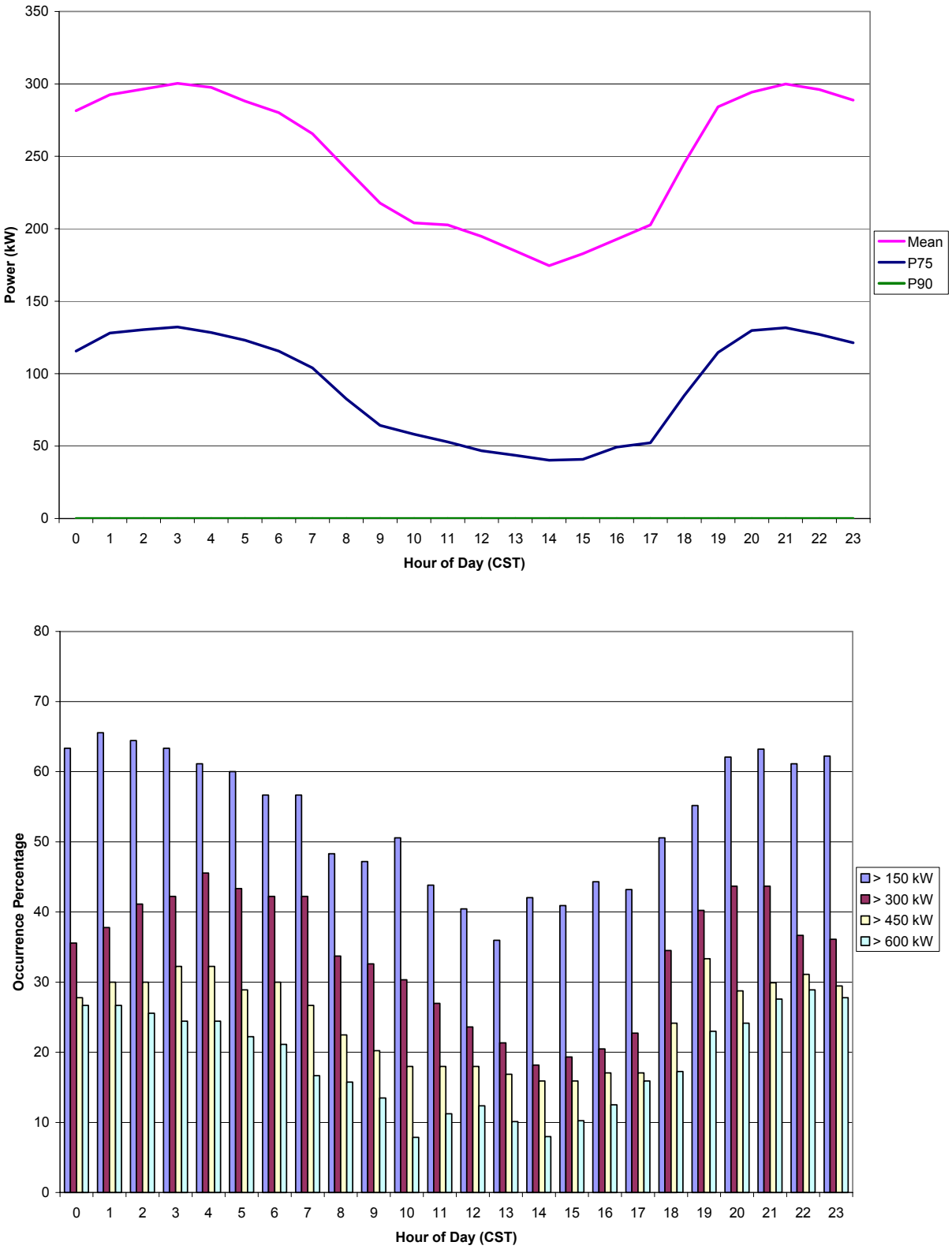

Figure 42: Probability distribution and frequency histogram for September power production (Z-750).

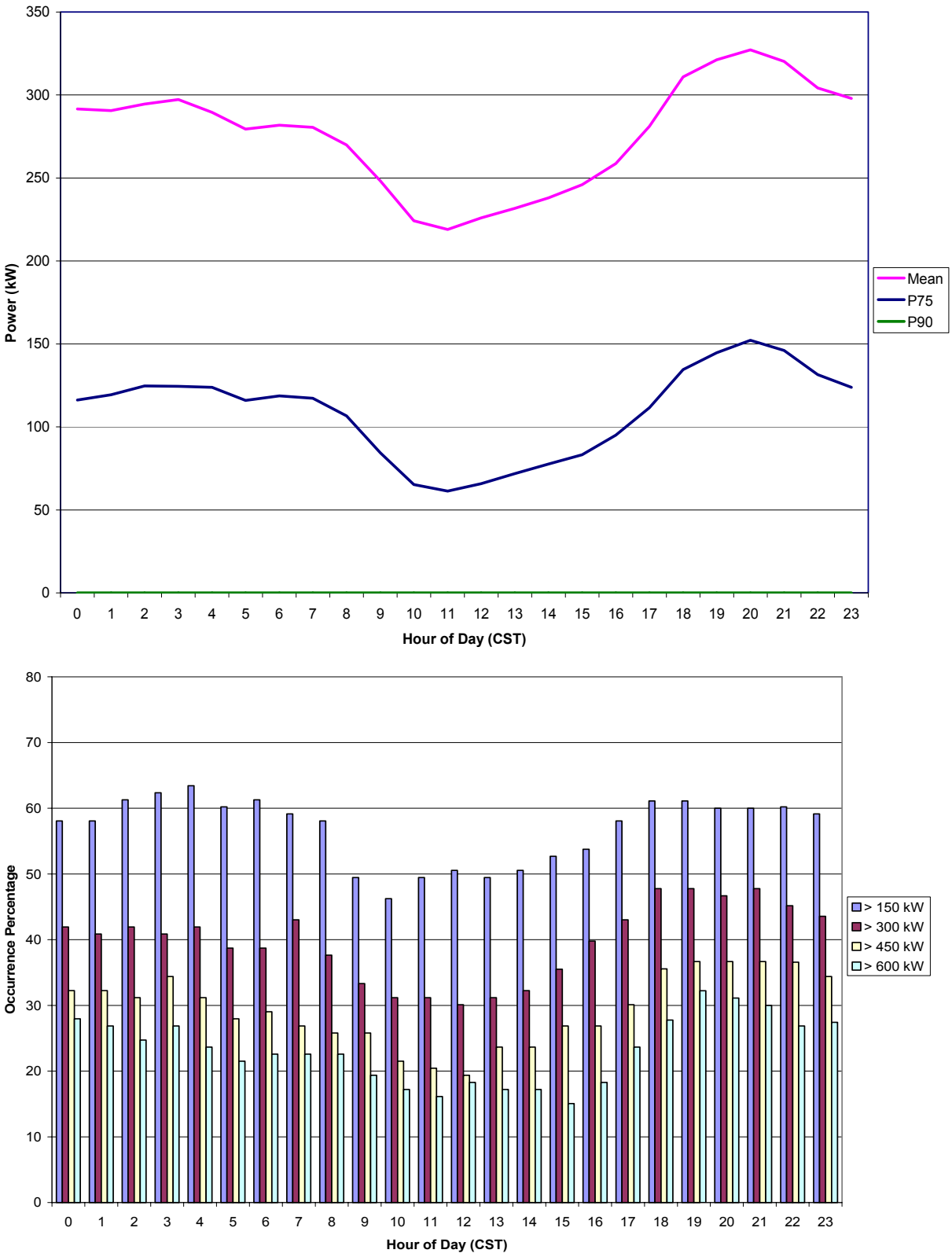

Figure 43: Probability distribution and frequency histogram for October power production (Z-750).

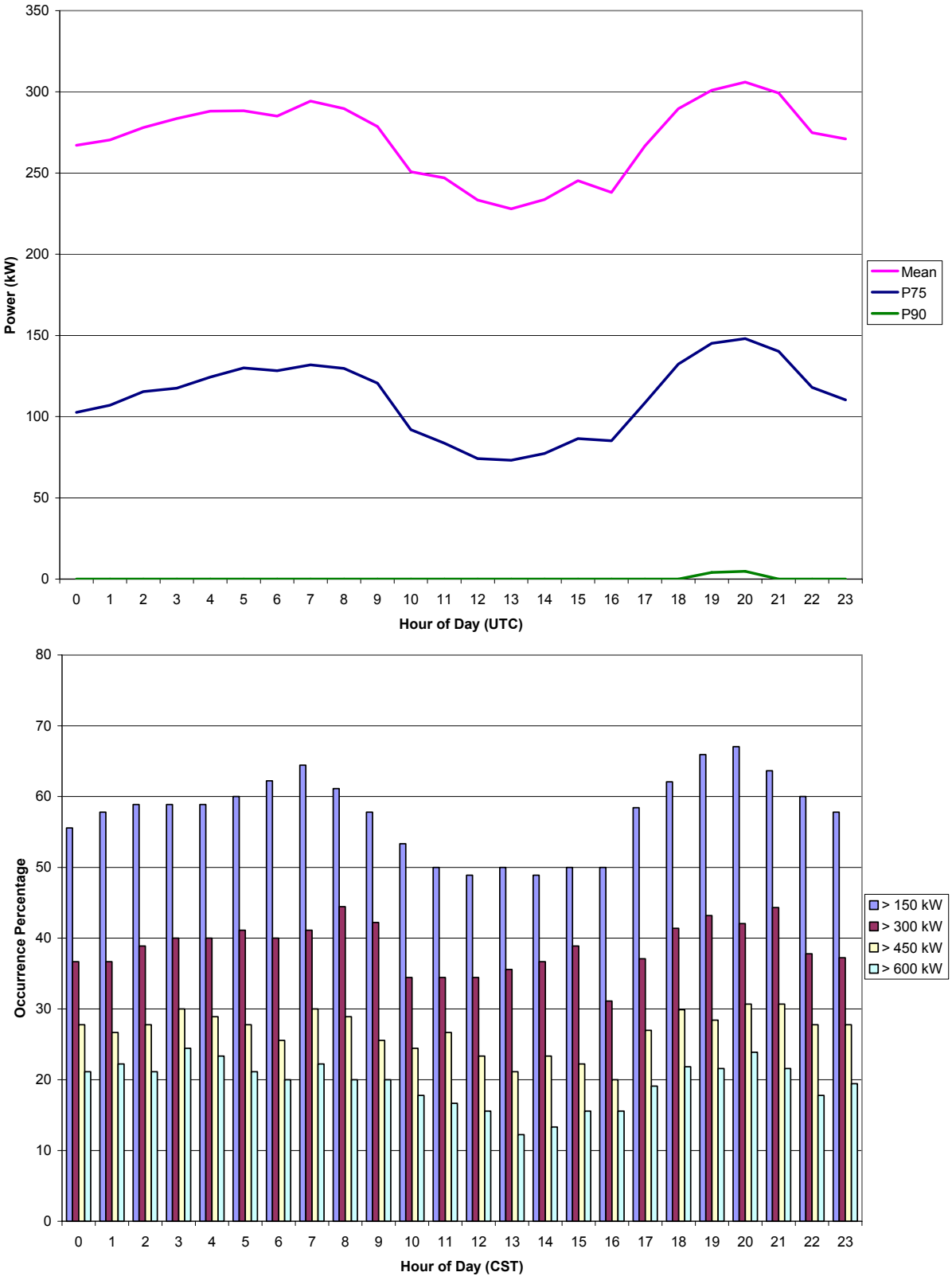

Figure 44: Probability distribution and frequency histogram for November power production (Z-750).

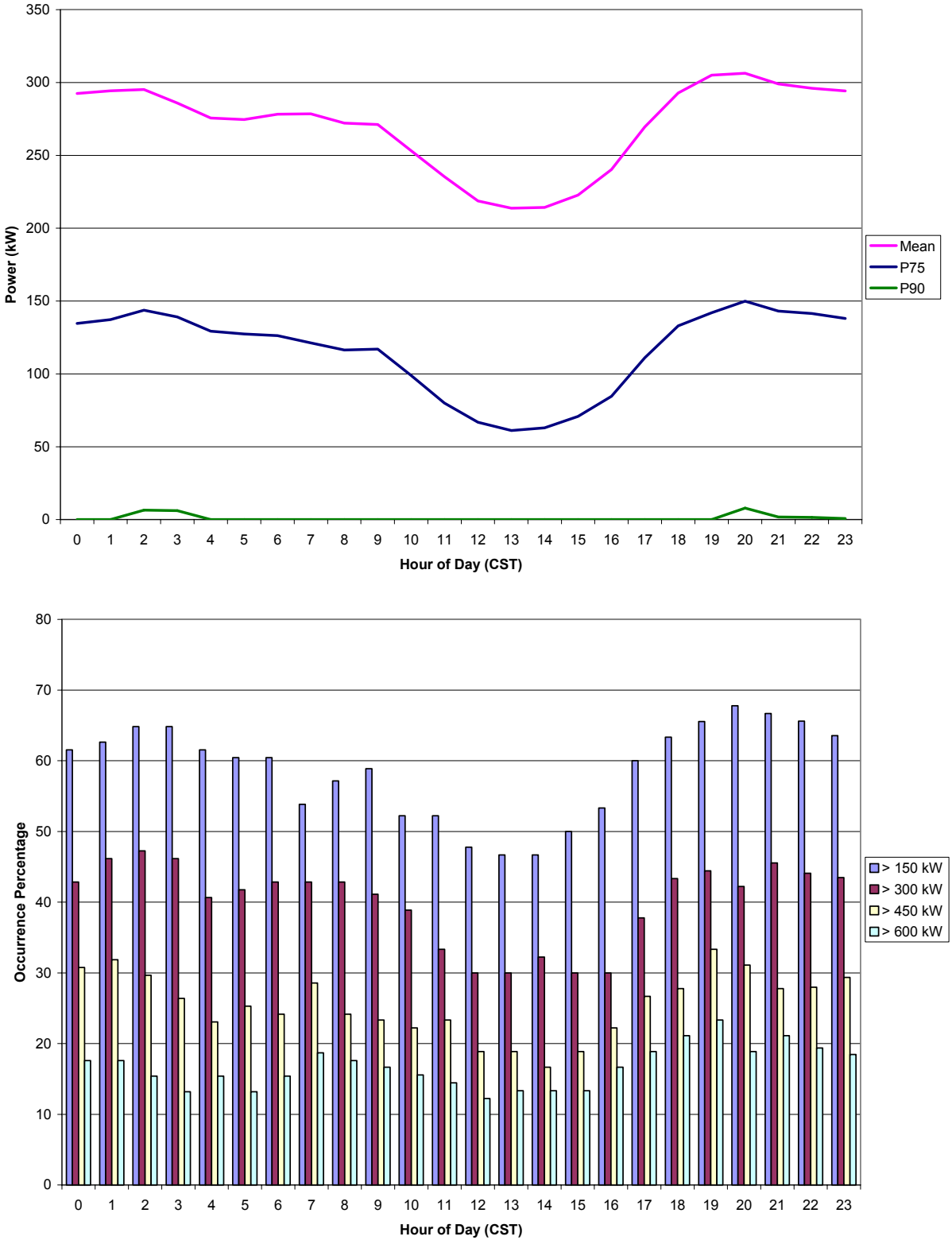

Figure 45: Probability distribution and frequency histogram for December power production (Z-750).

Wind resource geographic dispersion

Two levels of wind farm geographic dispersion are assessed to investigate the potential benefits for reducing the temporal variability of the wind resource. Both levels of geographic dispersion are contrasted with a single wind farm designated as Tower 24. Tower 24 is coincident with the location of the Delta Sector of the Lake Benton 2 Wind Facility. The first level of geographic dispersion includes an analysis of 3 wind farms distributed along the northwest-southeast extent of the Buffalo Ridge entirely within Minnesota. This experiment is designated as SW_MN and represents production distributed over a 104 km distance. The MM5 proxy towers utilized were Towers 5, 16 and 24 (see Fig. 4). In the second level of geographic dispersion, a six tower ensemble is utilized that includes 3 proxy towers from Mower County in southeastern Minnesota (Towers 6, 8, 9) in addition to the proxy towers of SW_MN. This experiment is designated SW_MN+SE_MN and represents production spread out over a 321 km distance. A similar probability analysis to that described for a single tower in the previous section was completed for both levels of geographic dispersion and is shown in Figs. 46 – 51. To understand the relationship between geographic dispersion of production and levels of power generation, plots of the frequency distribution of the occurrence percentage of power production (as a percent of capacity) are shown in Fig. 52-57. Note that in these plots, maximum production is 86 % of capacity due to the application of a 14 % loss factor to the modeled proxy wind farm production data. In another analysis of geographic dispersion, an investigation of the effects of production spatial dispersion on the hourly power change frequency (as a percent of capacity) is shown in Figs. 58 – 63. All the analyses were based on power production for the Z-750 turbine.

The probability plots for each month can generally be separated into 3 groupings: the mean power production traces at the top of the graphs, the more centrally-positioned P75 traces, and, if present, the P90 traces. The understanding of these plots is facilitated by recognizing that the mean traces for the various geographic dispersion experiments provide an awareness of the locationally averaged background resource. For example, for the months of July and August (Fig. 49) the wind resource in SE_MN is substantially weaker than the Buffalo Ridge area of southwestern Minnesota (SW_MN), thus, the combined mean production is lower throughout the day. In contrast, in the cold and transition seasons, the wind resource of SE_MN can be comparable to the Buffalo Ridge, thus all the mean lines (Tower 24, SW_MN and SW_MN+SE_MN) track with a more grossly similar magnitude. The relative advantage of geographically spreading out the wind power production is best assessed at the P75 and P90 levels. In general, on an hourly basis, there appears to be benefit derived from just the geographical dispersion provided by the SW_MN wind farm distribution when compared to the single Tower 24, but this benefit is quantitatively minor. It is quite probable, on the intra-hour time scales of just minutes or tens of minutes, that the geographical advantage of distributed wind farms along the Minnesota Buffalo Ridge would be considerable. This advantage might be most evident in the convective season when mesoscale weather phenomena such as thunderstorm outflows may be influencing one region of the Minnesota Buffalo Ridge but not the full extent of the Ridge. The advantage of greater geographical dispersion is quite apparent in the plots, whether comparing SW_MN+SE_MN to just Tower 24 or to SW_MN. This advantage is most evident in the winter and transition seasons, and is maximized in the non-daylight hours (e.g., see October in Fig. 50). At the P90 level, the plots for the SW_MN+SE_MN production scenario provides the only considerable area under the curve for 8 of the 12 months. In the

summer months (e.g., July and August in Fig. 49) at the P75 level, the advantage provided by the significant geographical dispersion of SW_MN+SE_MN is roughly balanced by the deleterious effect of the weaker wind resource of the Mower County portion of this wind farm ensemble. One caveat worthy of consideration is the deployment of more optimal wind turbines that better match the wind resource of southeast Minnesota. This production scenario would have a beneficial effect on the SW_MN+SE_MN P75 and P90 probability curves, especially in the months of the year and/or time of day where the SE_MN portion of the SW_MN+SE_MN geographic production mix is retarding the resource (as seen in the mean SW_MN+SE_MN probability curves).

The analysis of power generation frequency distributions for the geographical dispersion production scenarios (Figs. 52-57) reveals grossly similar qualitative characteristics throughout the year. In general, the smaller the geographic dispersion, the higher the occurrence percentage of either, negligible production (< 5 % of capacity) or near/at maximum production (> 85 %). Note that maximum production is 86 % of capacity due to the application of a 14 % loss factor to the modeled power production. At production levels between these extremes, in most cases, the greater the geographic dispersion of wind power production, the higher the percentage occurrence. Figures 52-57 also reflect the monthly wind climatology of the Upper Midwest, with the most frequent occurrence of weak winds and reduced power production in the summer months and the most frequent occurrence of strong winds and high power production in the transition and winter months.

The frequency distributions of hourly power change show similar monthly profiles throughout the year. While it is advantageous to have a high frequency of very small hourly power changes, a much more important attribute of wind power production variability lies in the overall narrowness of the distribution. An advantageous generation scenario would involve a reduction in the occurrence of very large hourly power changes in the wings of the distributions shown in Figs. 58-63. A close inspection of the wings of the monthly hourly power change frequency distributions shows this advantage of geographic dispersion of wind power production. In general, beyond approximately 2 standard deviations from the center point of the distributions (an hourly power change of approximately 10 percent of capacity), the SW_MN+SE_MN scenario had the least occurrence of these significant hourly changes. As a measure of the narrowness of the distributions for all scenarios, standard deviations were calculated for each month and are shown in Figs. 58-63. In every month, the standard deviation was reduced for each level of increased geographic dispersion. Overall, the annual standard deviations of hourly power change were 5.47, 5.15, and 4.86 percent for Tower 24, SW_MN, and SW_MN+SE_MN, respectively. While not shown on the hourly power change graphics, the percentage incidence of very large hourly power changes above 30 percent of capacity were 2.10, 0.87 and 0.35 for Tower 24, SW_MN, and SW_MN+SE_MN, respectively. Put another way, the probability of seeing a 30% or greater hourly change in the SW_MN+SE_MN configuration is 1/6th that for Tower 24, and roughly 2.5 times smaller than for SW_MN. These statistics for the very significant hourly power change occurrence percentages reflect the advantage of geographic wind power production dispersion. Another notable statistic with regard to these large (above 30 percent) hourly power production changes involves the seasonality of the wind variability driving these large hourly power changes. For the summer months the incidence percentage for these large hourly power changes is 4.05, 1.35, and 0.70 for Tower 24, SW_MN and SW_MN+SE_MN, respectively. In contrast, the respective winter incidence percentage was 0.75, 0.49, and 0.14. A clear meteorological reason for this

seasonal contrast lies in the larger synoptic scale dominance for the atmospheric wind forcing over the Upper Midwest in the winter season. During the summer months, mesoscale meteorological phenomena (e.g., convective systems) provide a significant contribution to the wind forcing related to large variability.

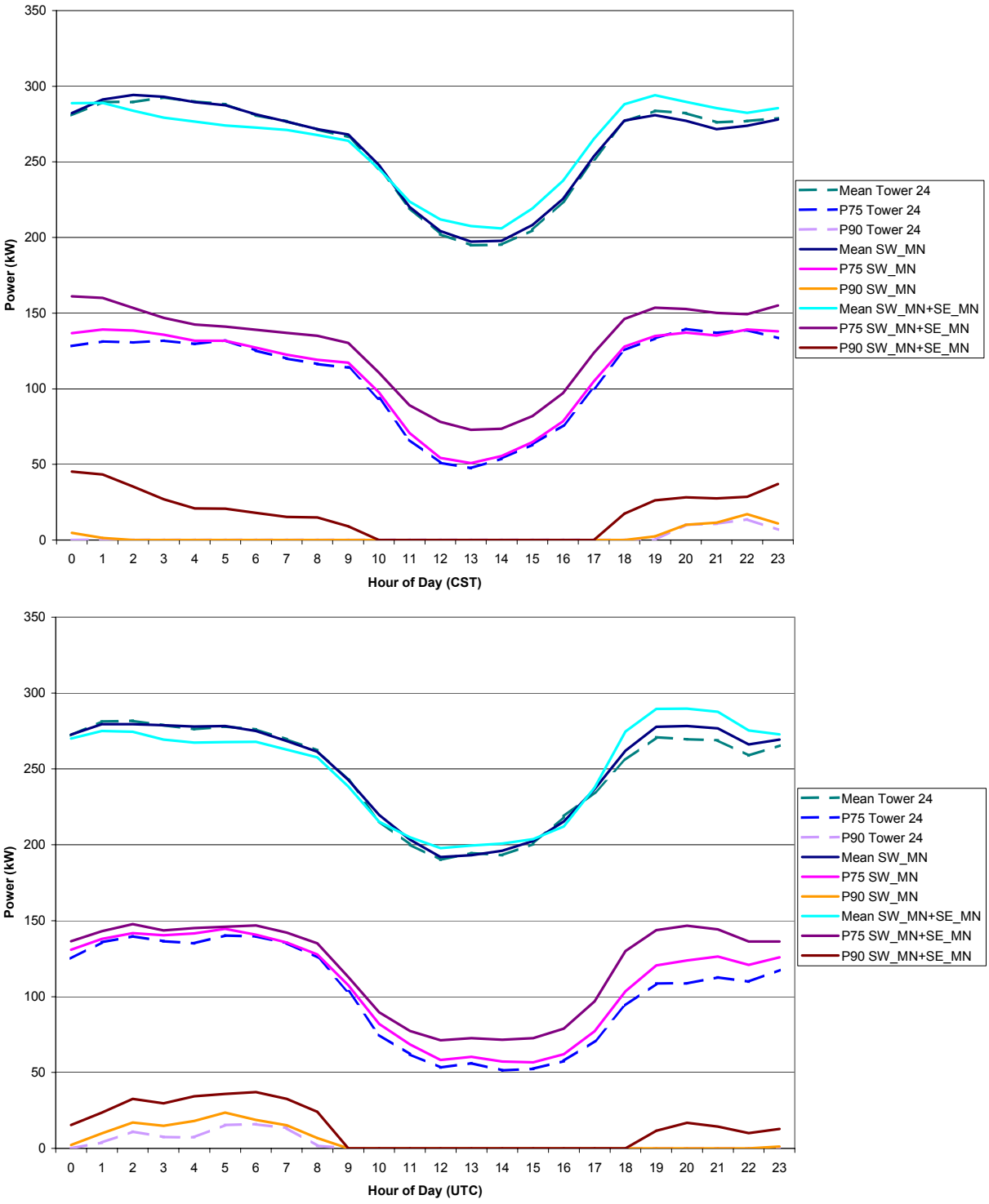

Figure 46: January and February probability analysis for the SW_MN and SW_MN+SE_MN geographical dispersion experiments (Z-750).

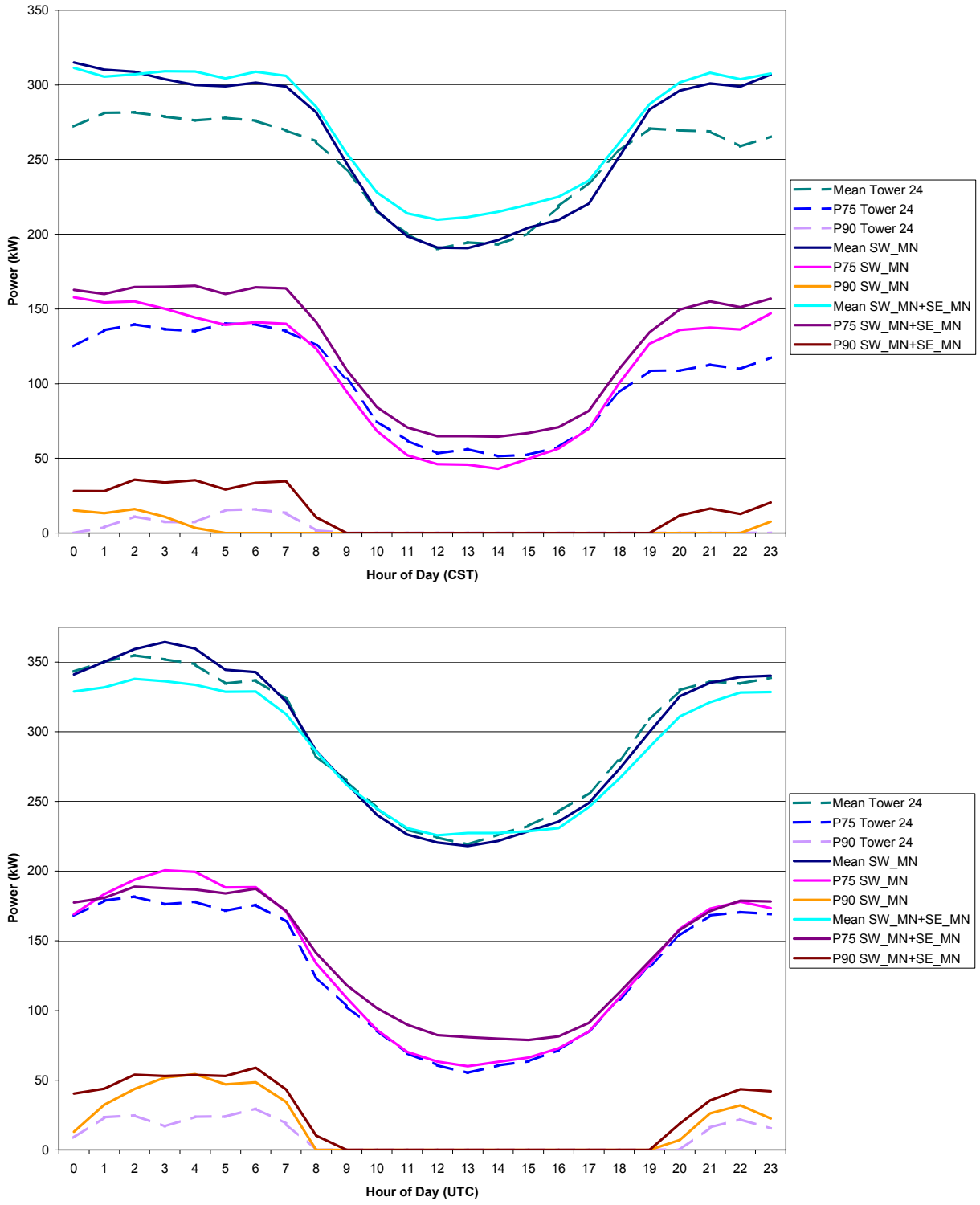

Figure 47: March and April probability analysis for SW_MN and SW_MN+SE_MN geographical dispersion experiments (Z-750).

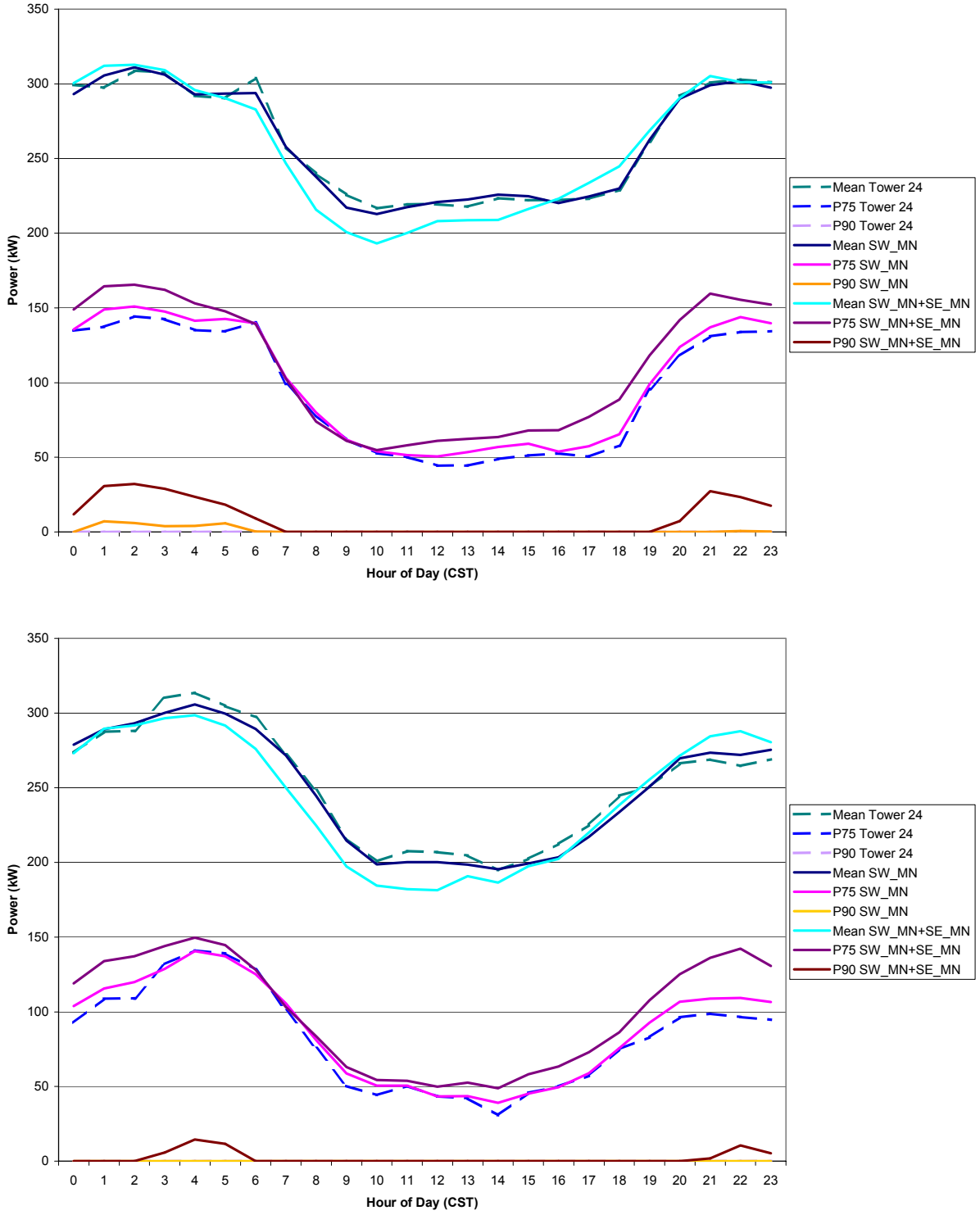

Figure 48: May and June probability analysis for the SW_MN and SW_MN+SE_MN geographical dispersion experiments (Z-750).

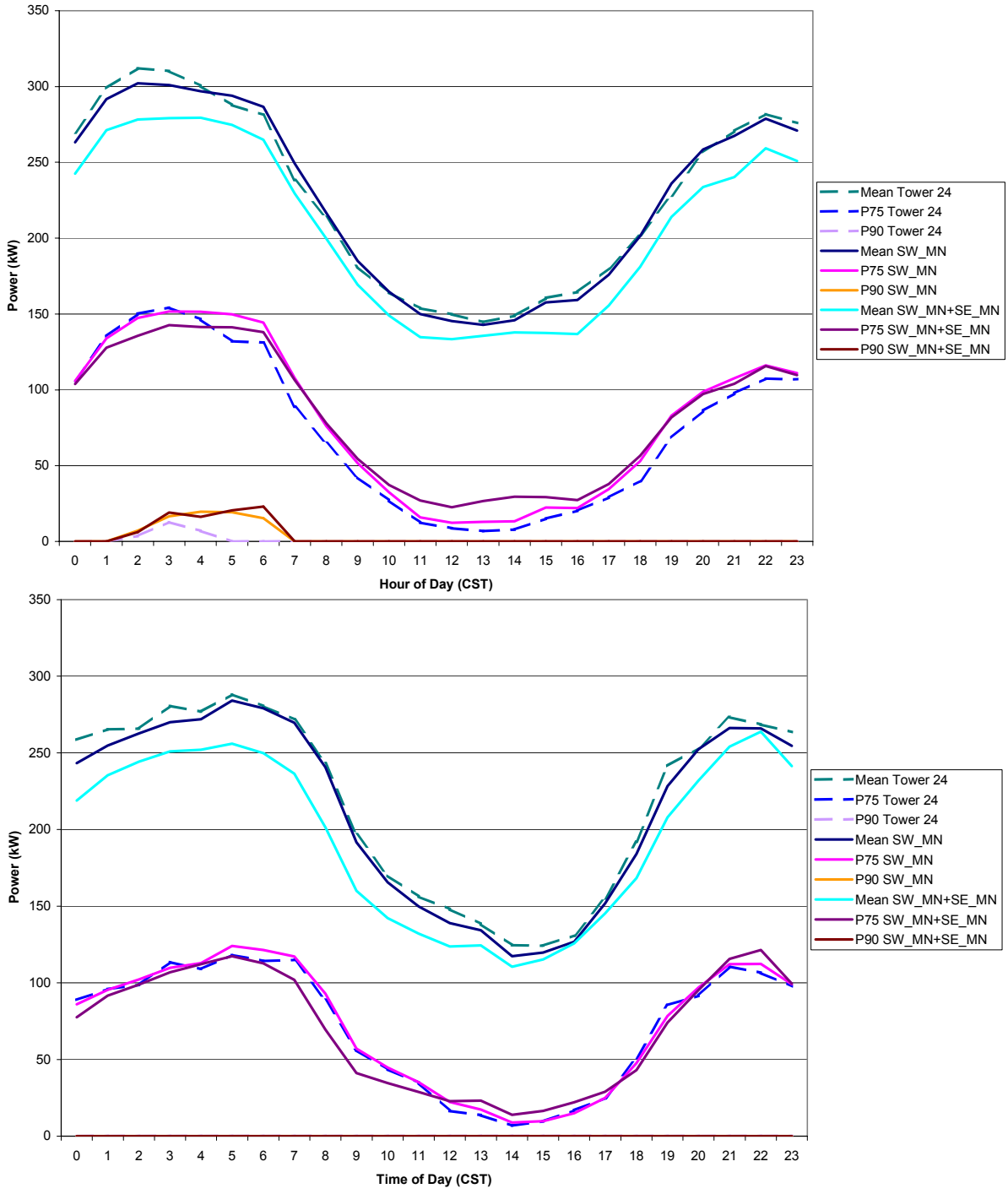

Figure 49: July and August probability analysis for SW_MN and SW_MN+SE_MN geographical dispersion experiments (Z-750).

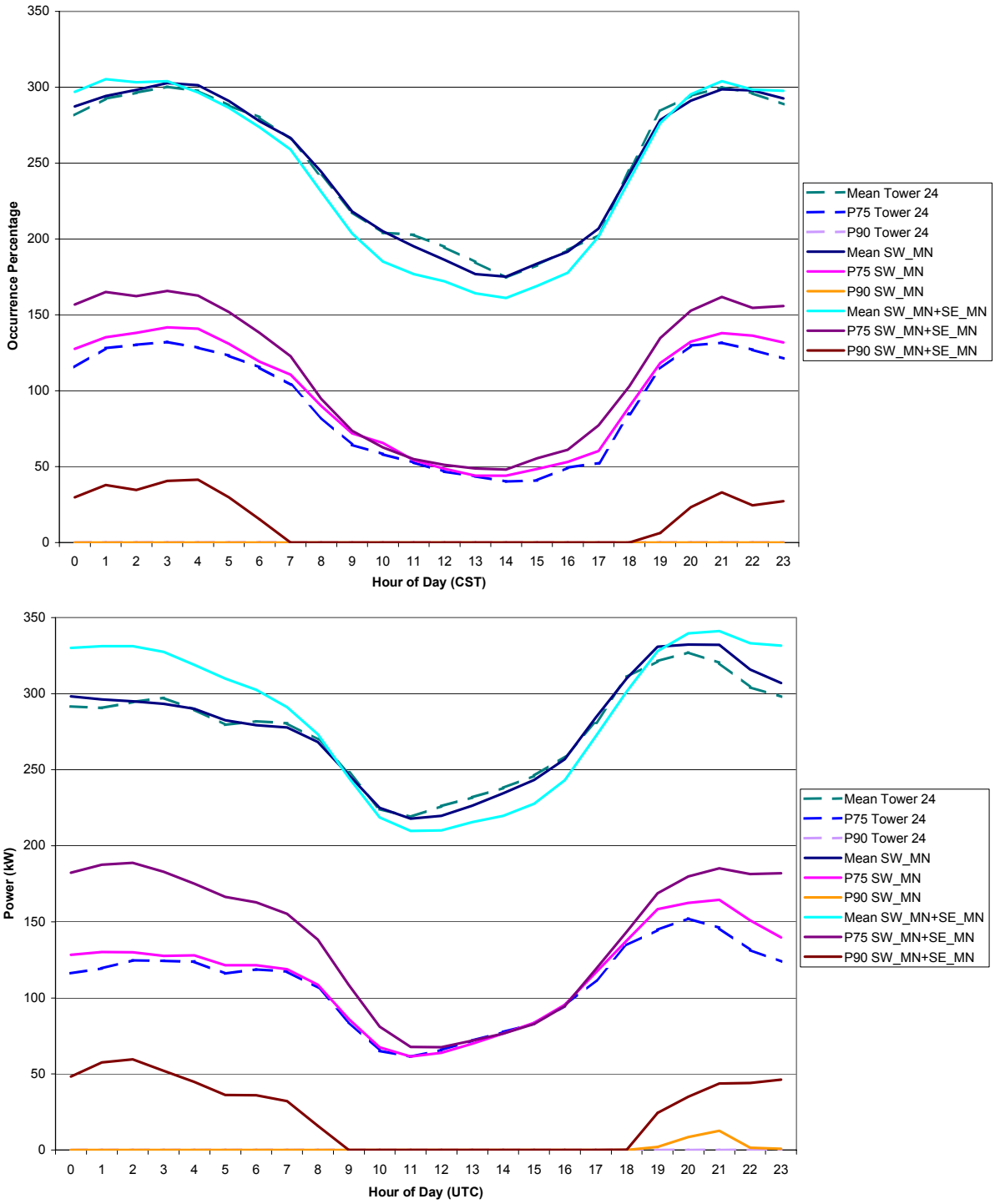

Figure 50: September and October probability analysis for the SW_MN and SW_MN+SE_MN geographical dispersion experiments (Z-750).

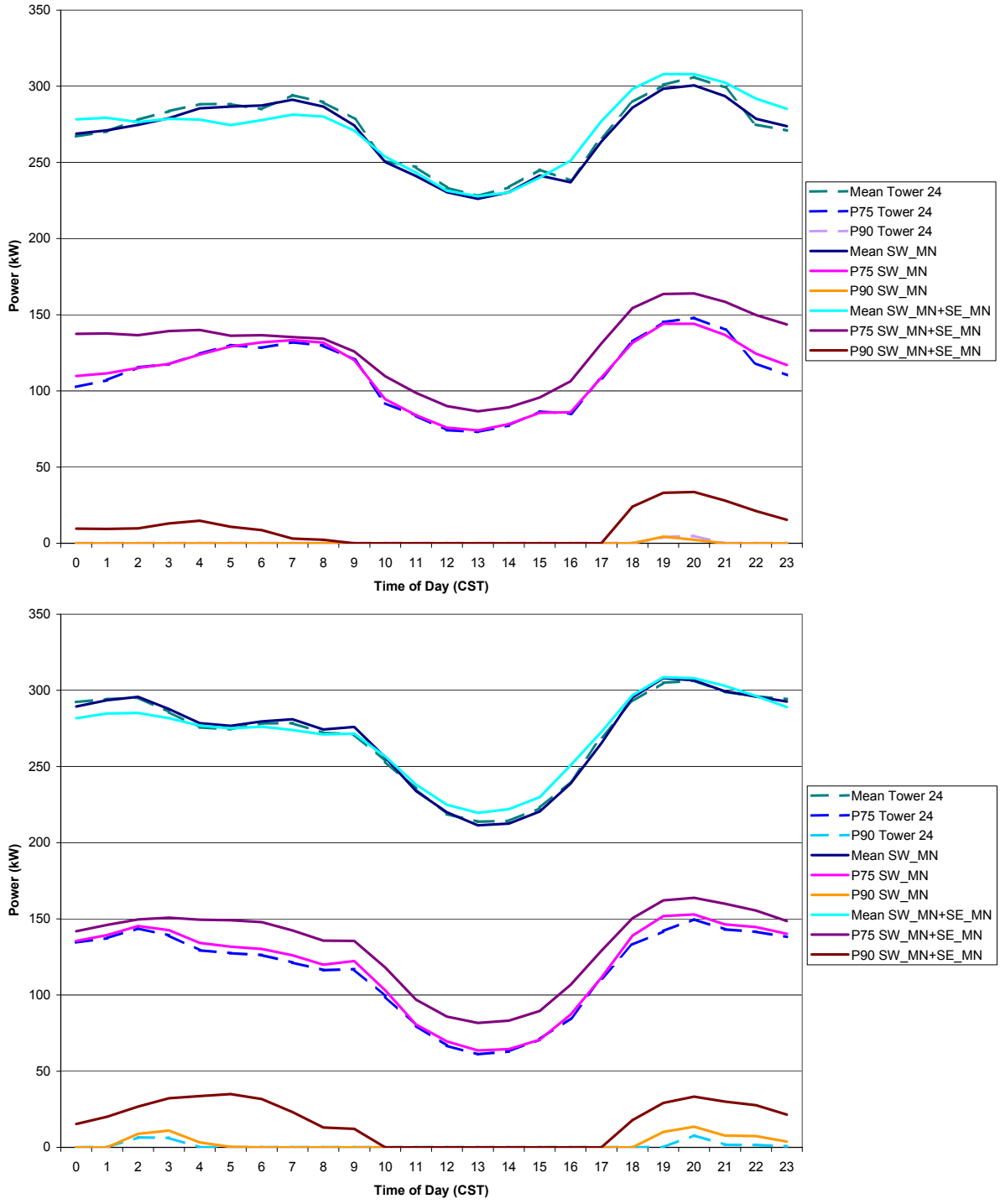

Figure 51: November and December probability analysis for SW_MN and SW_MN+SE_MN geographical dispersion experiments (Z-750).

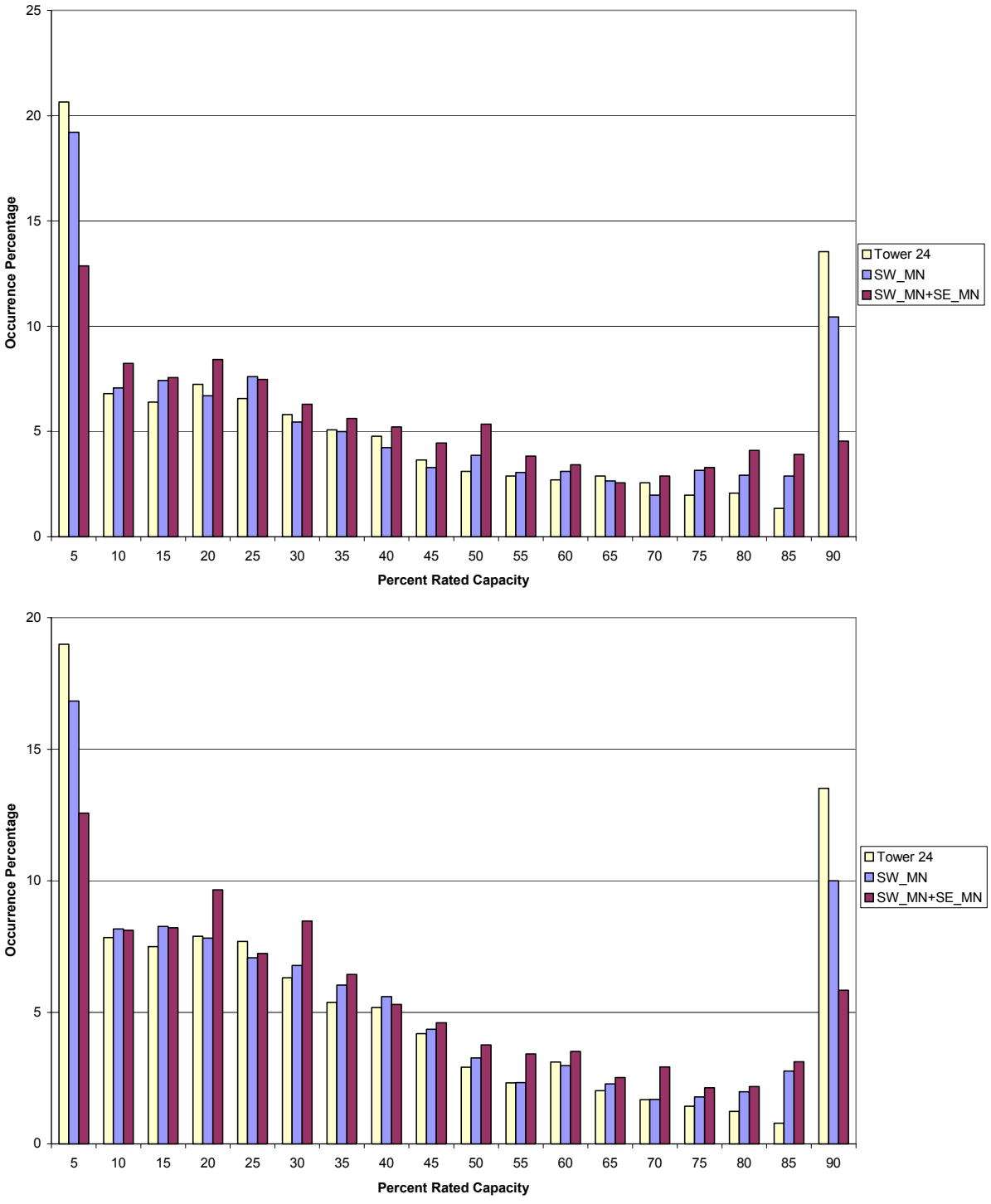

Figure 52: January and February frequency distributions of the occurrence percentage of power production (as a percent of capacity) for the SW_MN and SW_MN+SE_MN geographical dispersion experiments (Z-750).

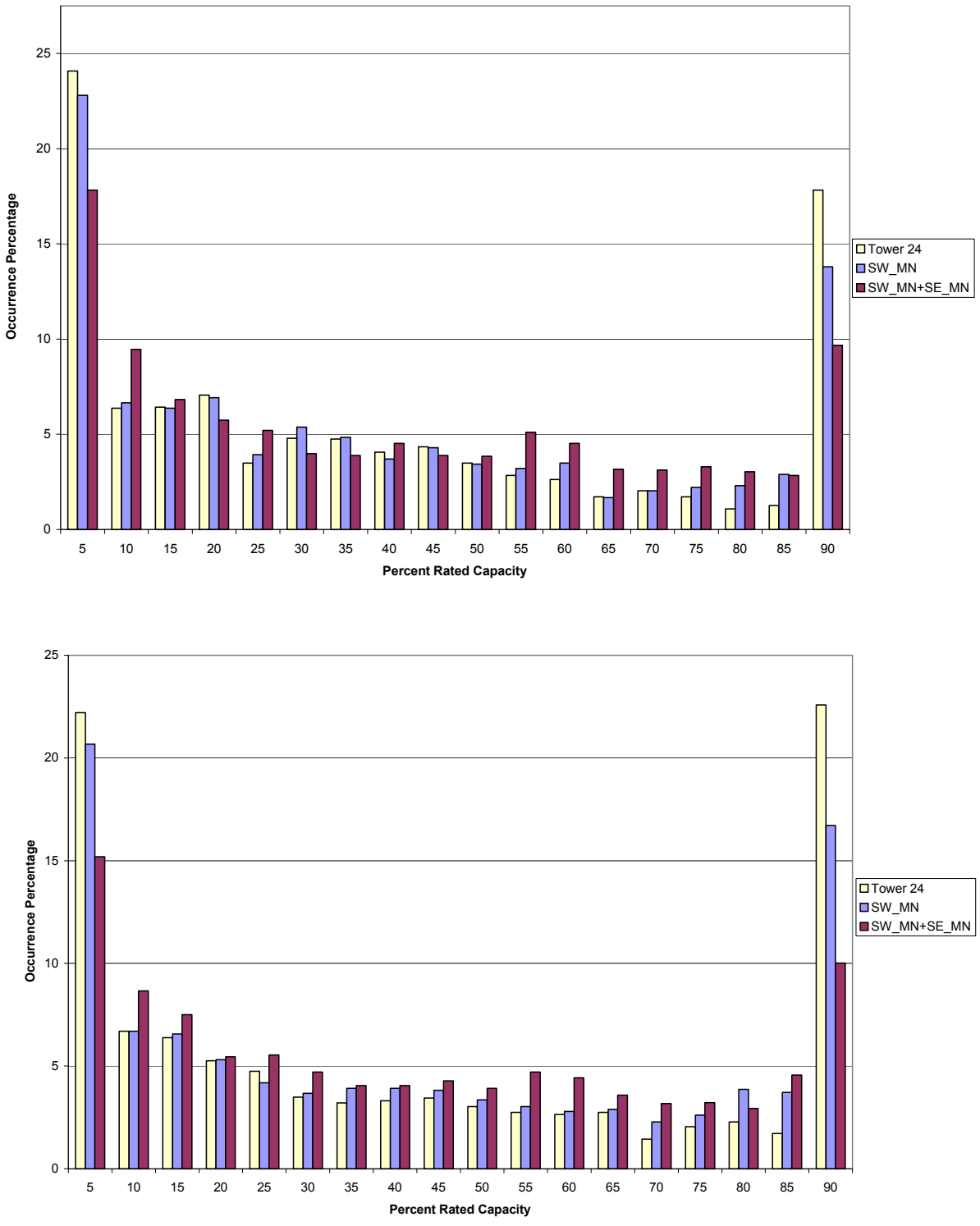

Figure 53: March and April frequency distributions of the occurrence percentage of power production (as a percent of capacity) for the SW_MN and SW_MN+SE_MN geographical dispersion experiments (Z-750).

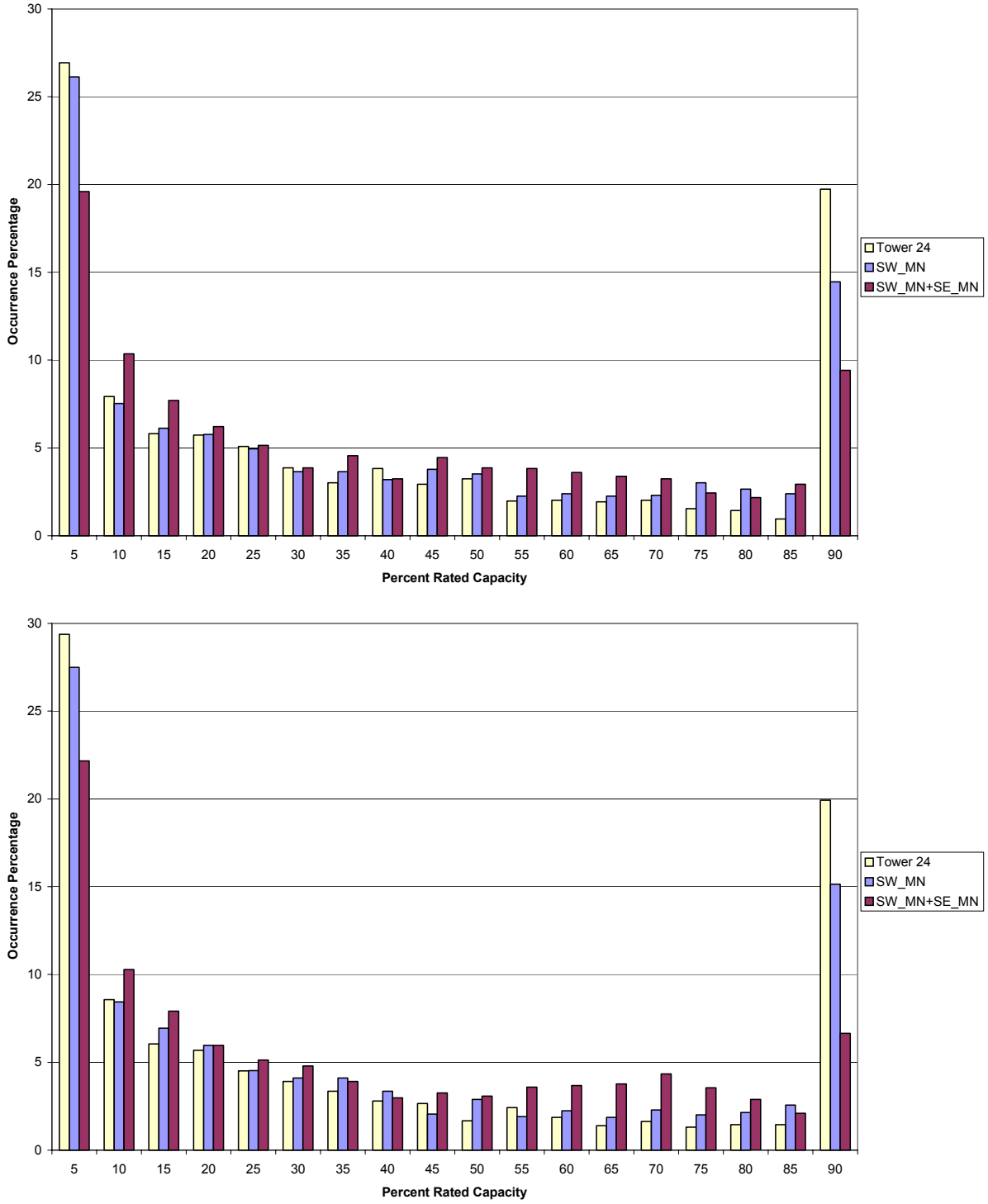

Figure 54: May and June frequency distributions of the occurrence percentage of power production (as a percent of capacity) for the SW_MN and SW_MN+SE_MN geographical dispersion experiments (Z-750).

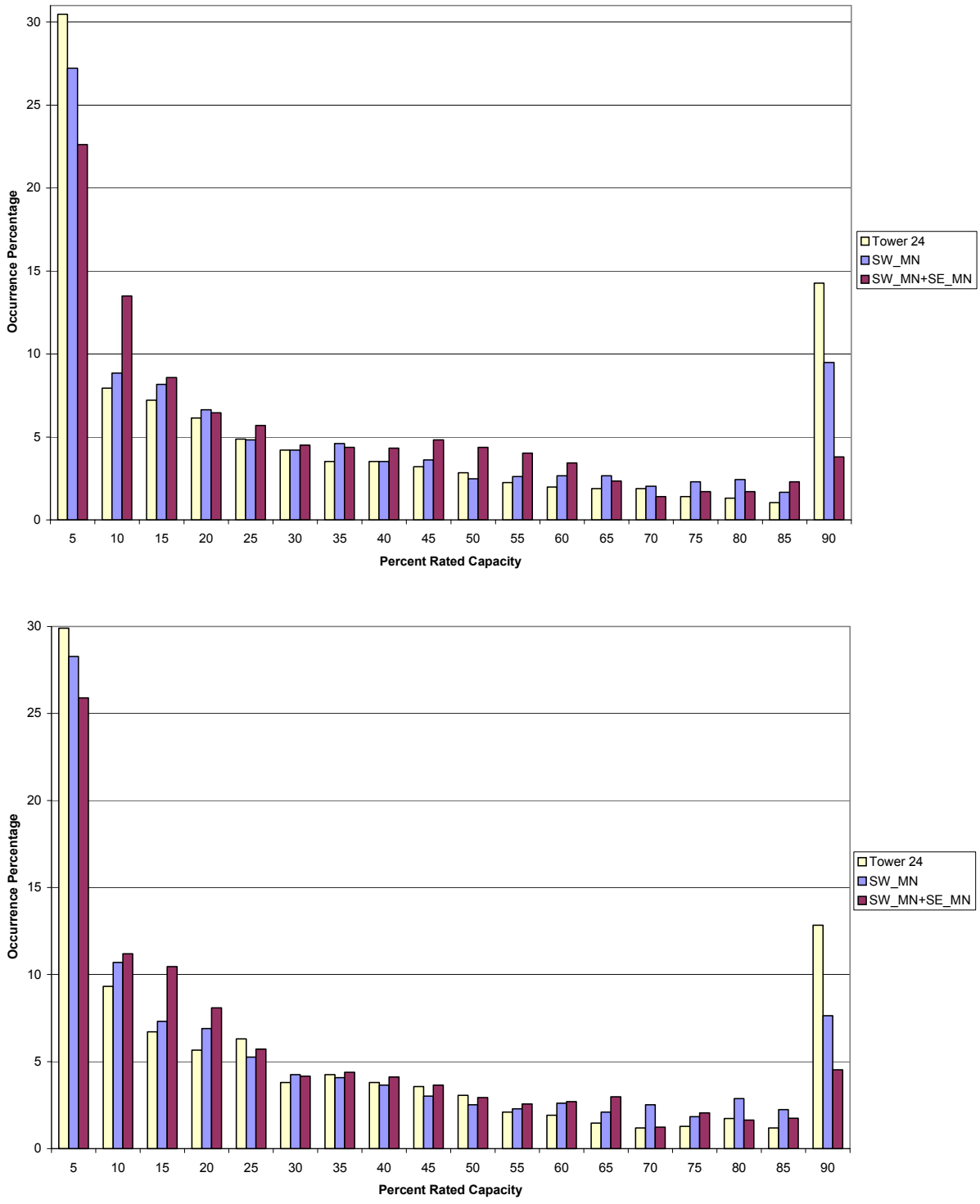

Figure 55: July and August frequency distributions of the occurrence percentage of power production (as a percent of capacity) for the SW_MN and SW_MN+SE_MN geographical dispersion experiments (Z-750).

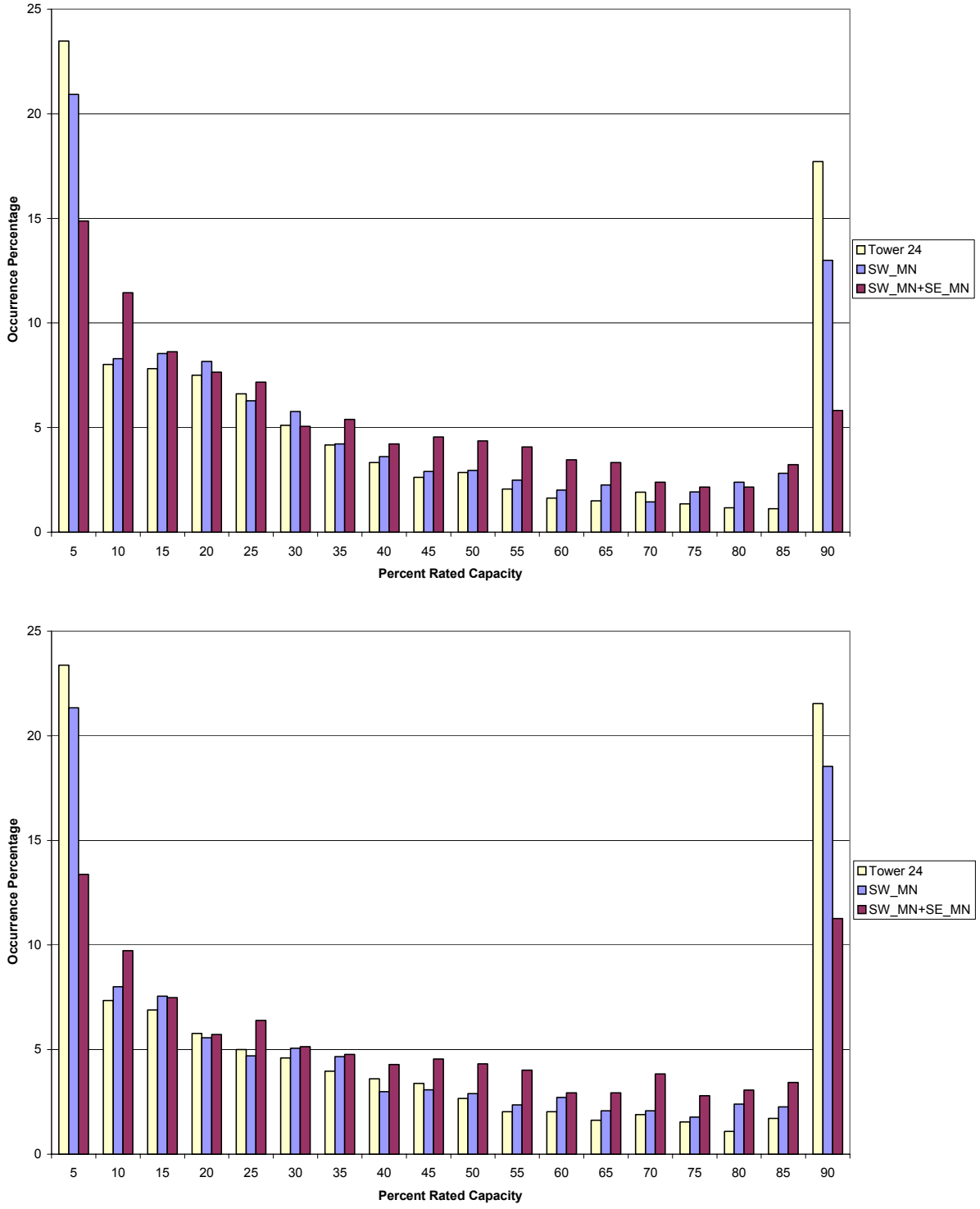

Figure 56: September and October frequency distributions of the occurrence percentage of power production (as a percent of capacity) for the SW_MN and SW_MN+SE_MN geographical dispersion experiments (Z-750).

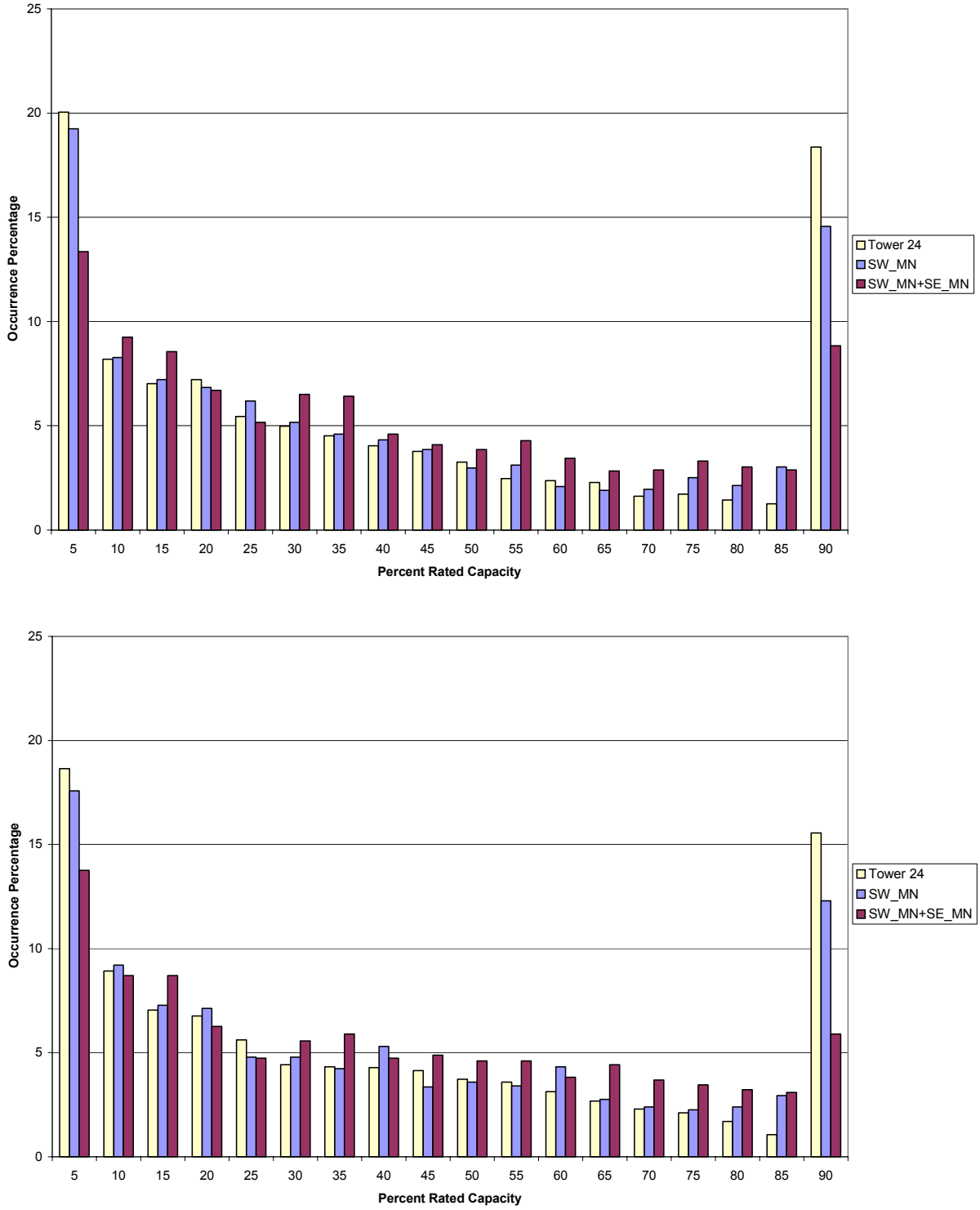

Figure 57: November and December frequency distributions of the occurrence percentage of power production (as a percent of capacity) for the SW_MN and SW_MN+SE_MN geographical dispersion experiments (Z-750).

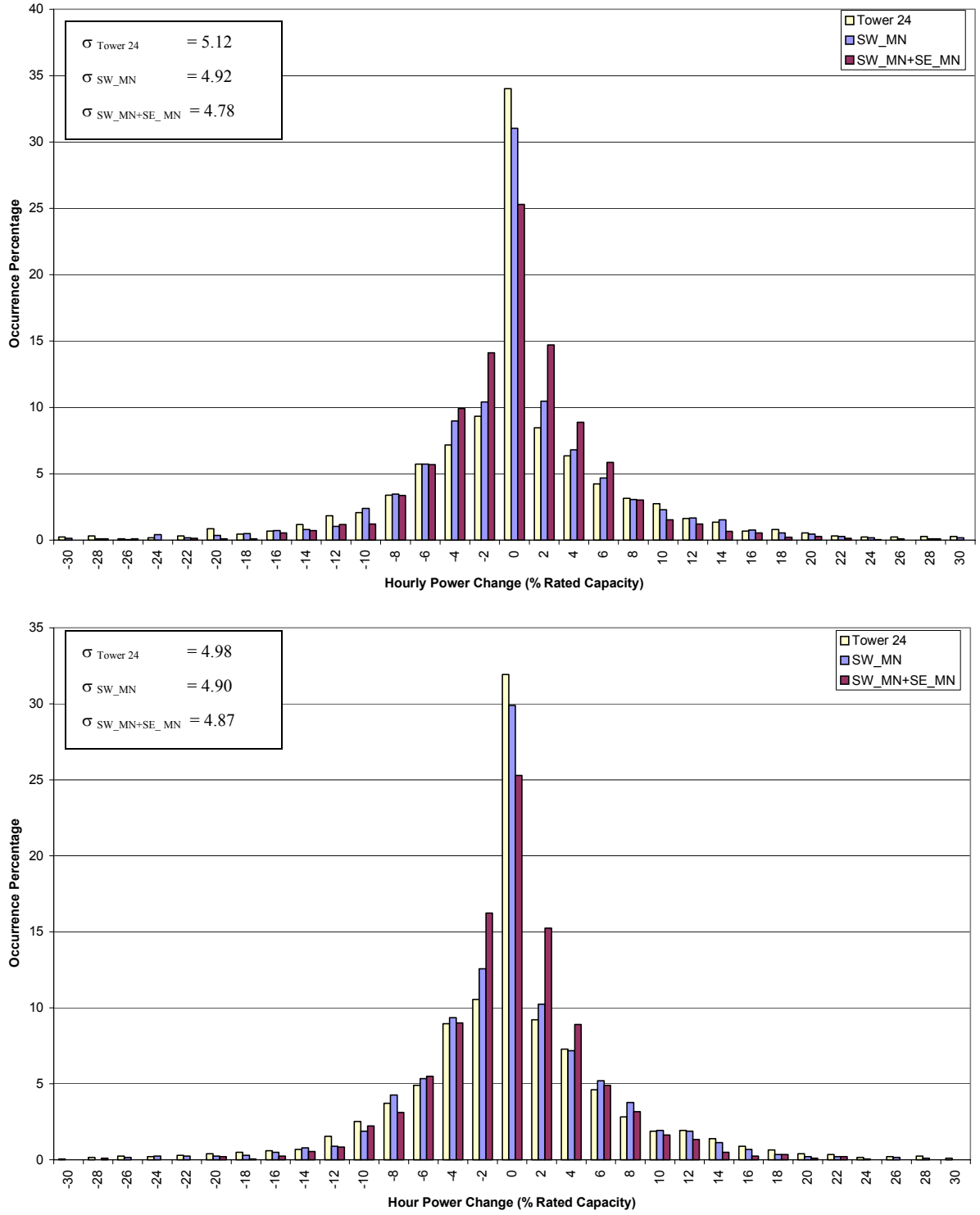

Figure 58: January and February frequency distributions of the hourly power change (as a percent of capacity) for the SW_MN and SW_MN+SE_MN geographical dispersion experiments (Z-750). Standard deviation for each scenario is shown at the upper left.

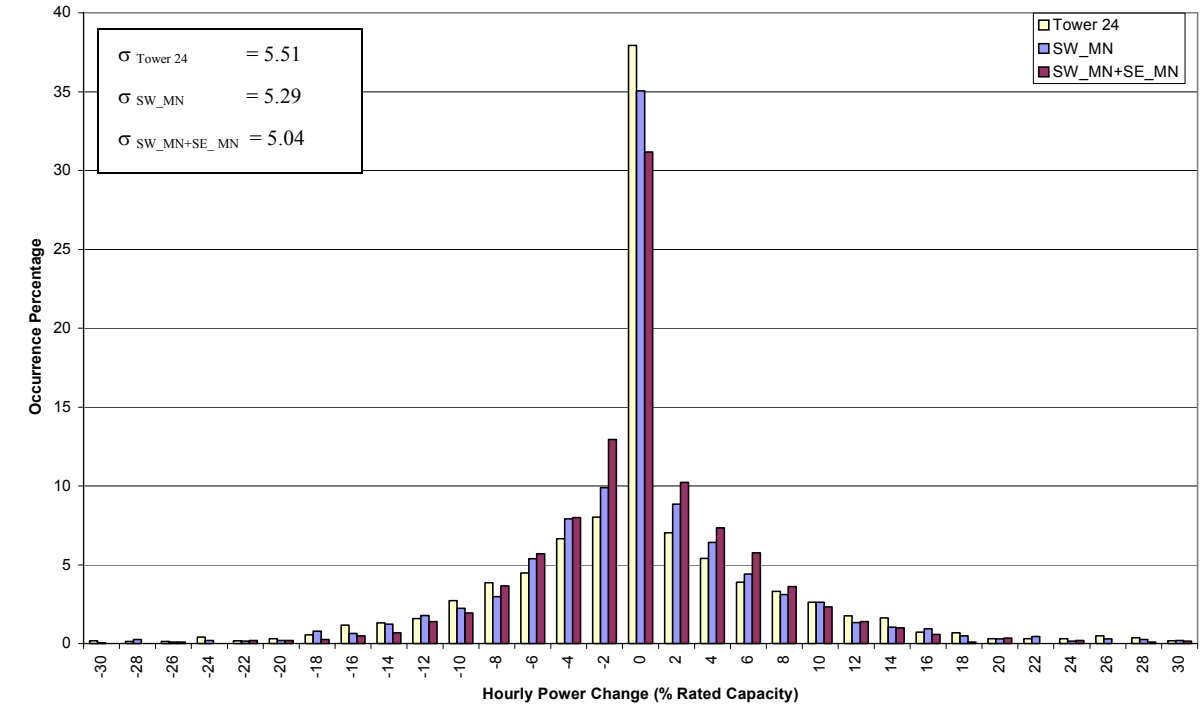

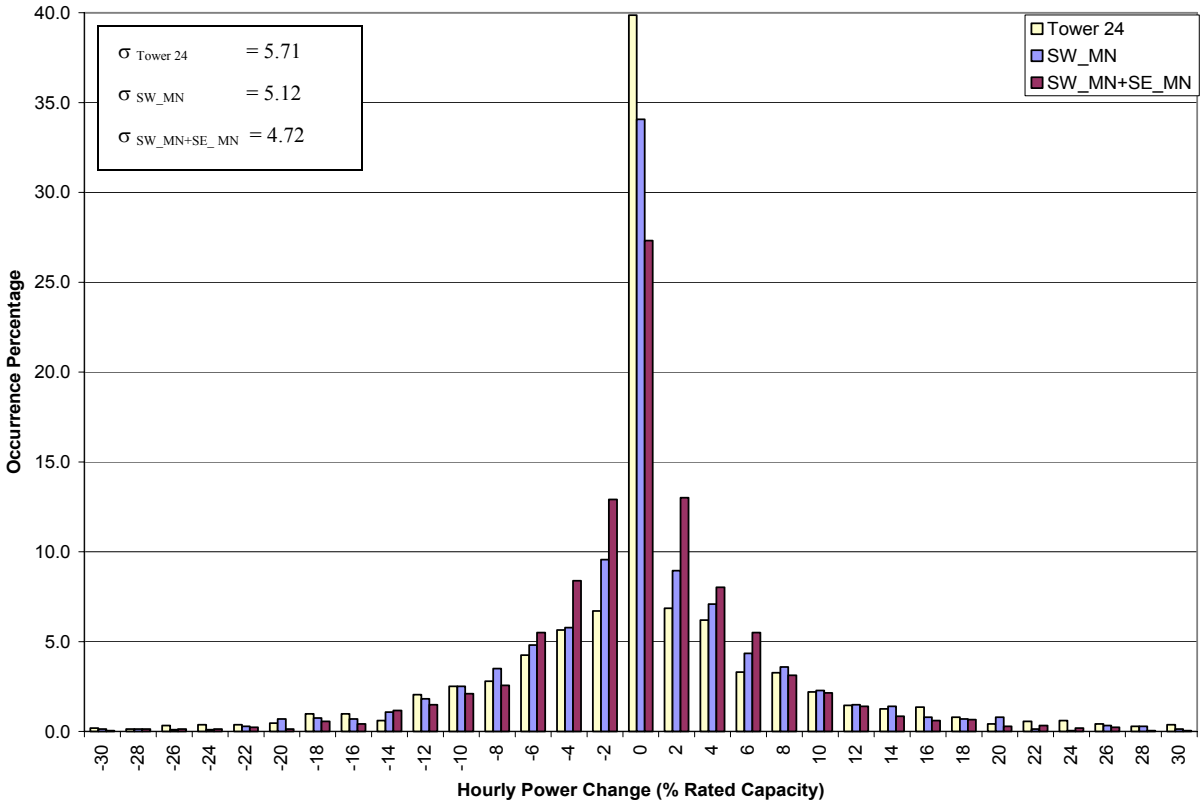

Figure 59: March and April frequency distributions of the hourly power change (as a percent of capacity) for the SW_MN and SW_MN+SE_MN geographical dispersion experiments (Z-750). Standard deviation for each scenario is shown at the upper left.

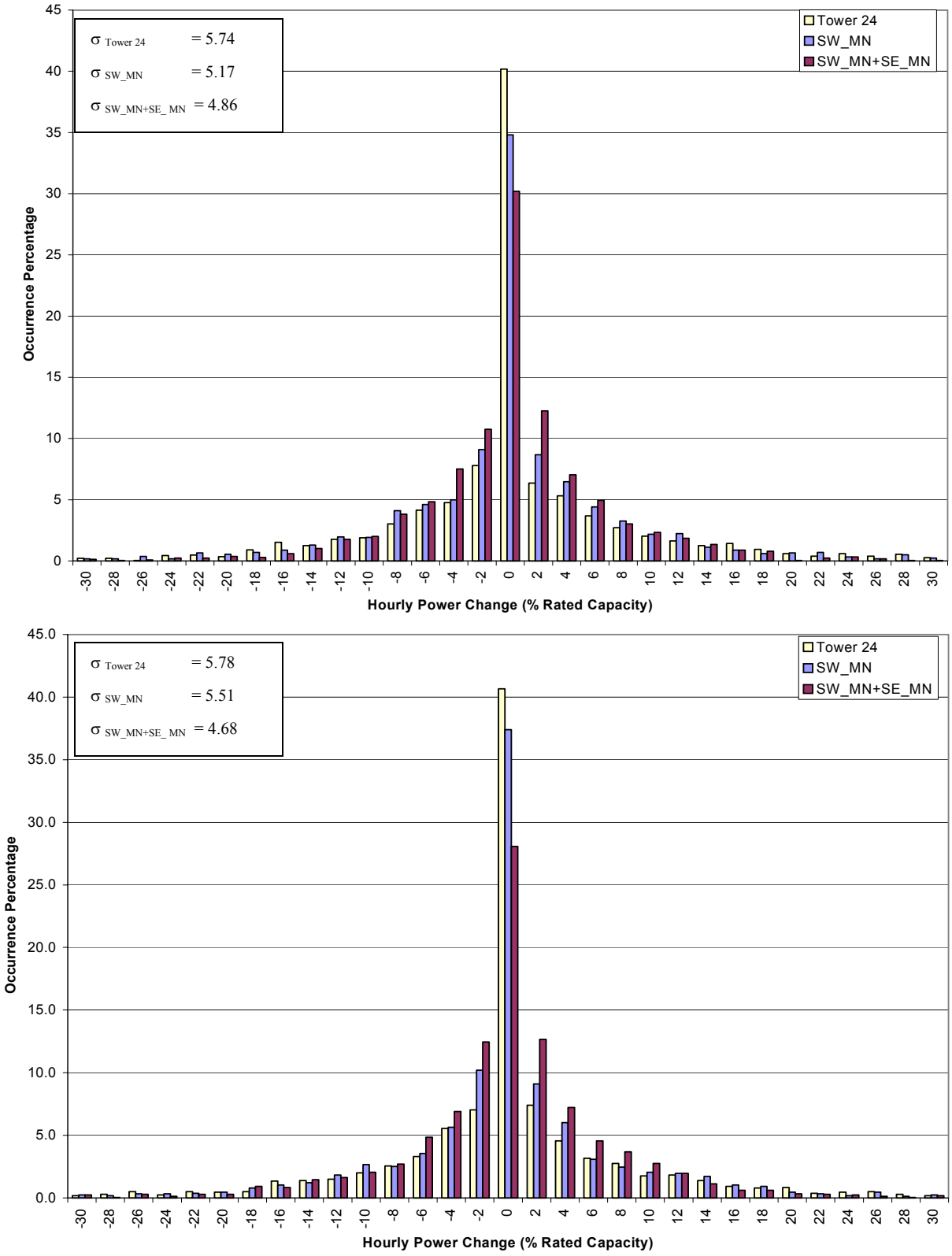

Figure 60: May and June frequency distributions of the hourly power change (as a percent of capacity) for the SW_MN and SW_MN+SE_MN geographical dispersion experiments (Z-750). Standard deviation for each scenario is shown at the upper left.

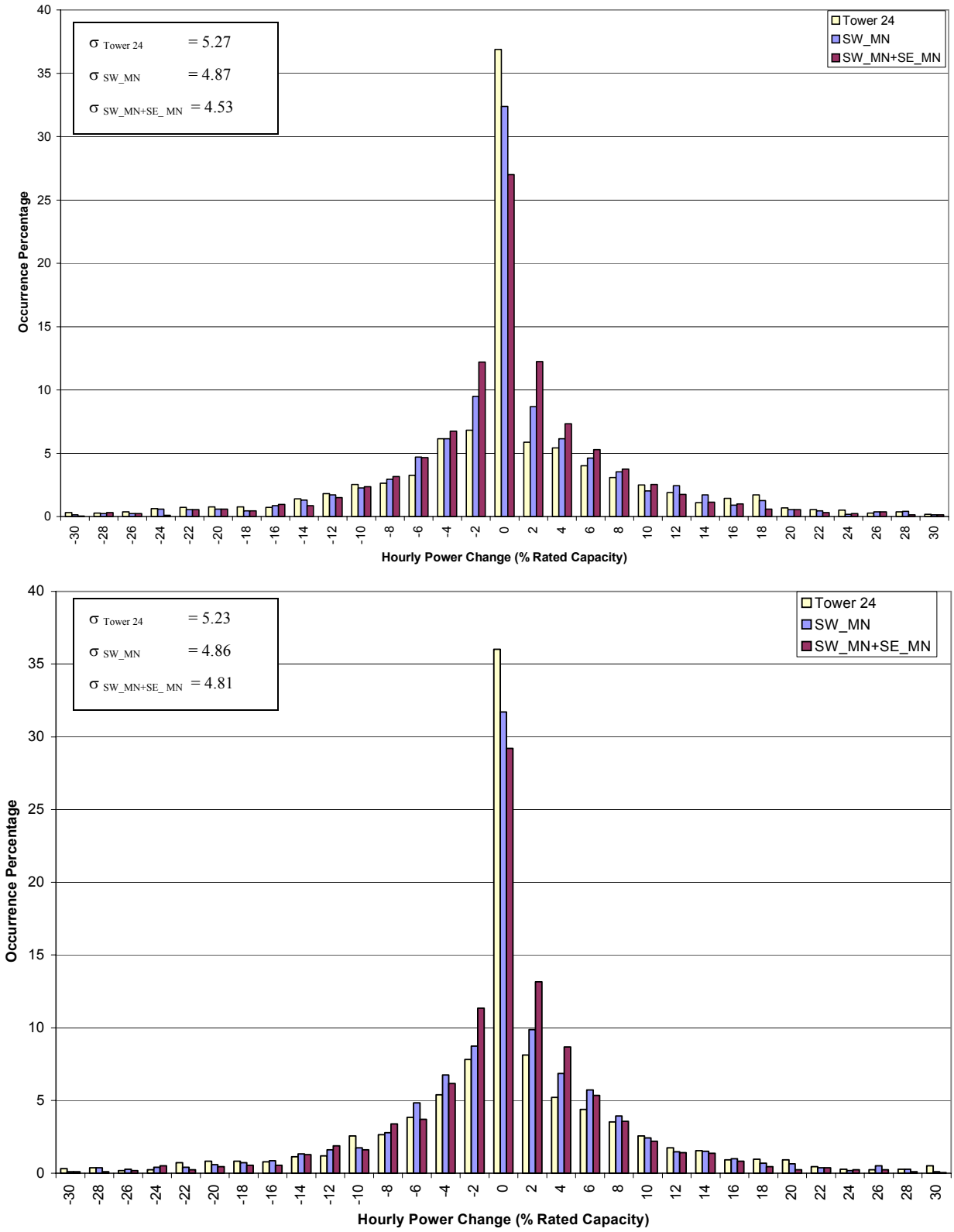

Figure 61: July and August frequency distributions of the hourly power change (as a percent of capacity) for the SW_MN and SW_MN+SE_MN geographical dispersion experiments (Z-750). Standard deviation for each scenario is shown at the upper left.

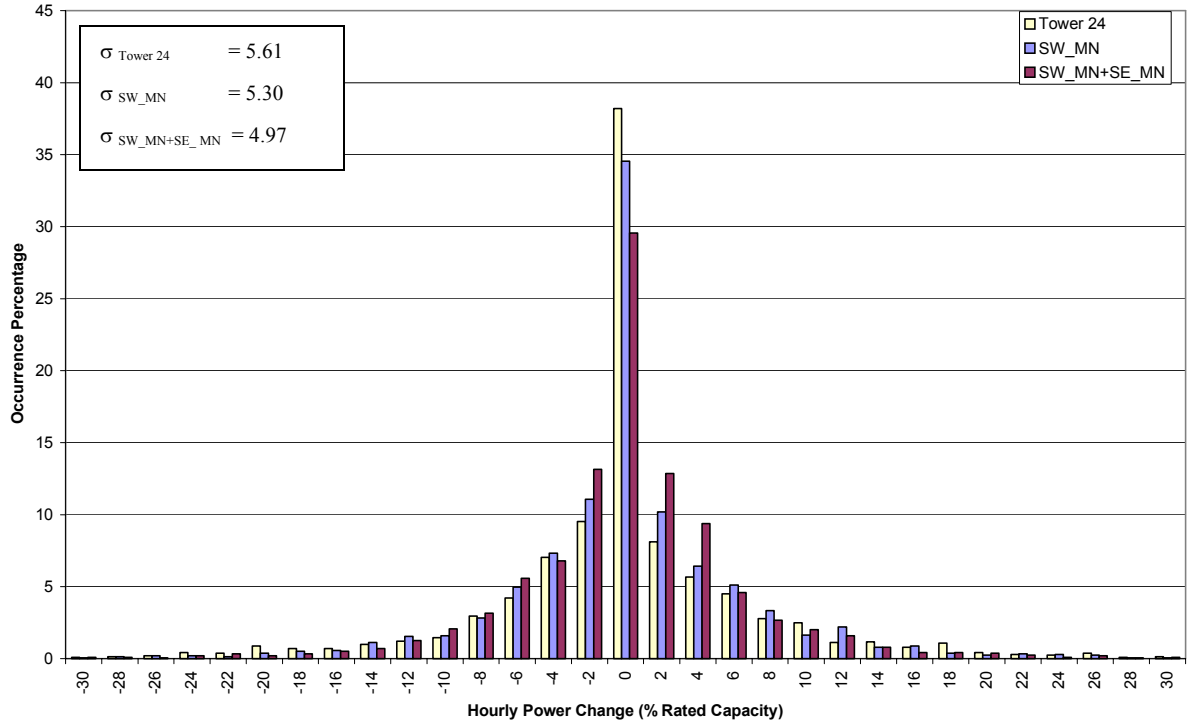

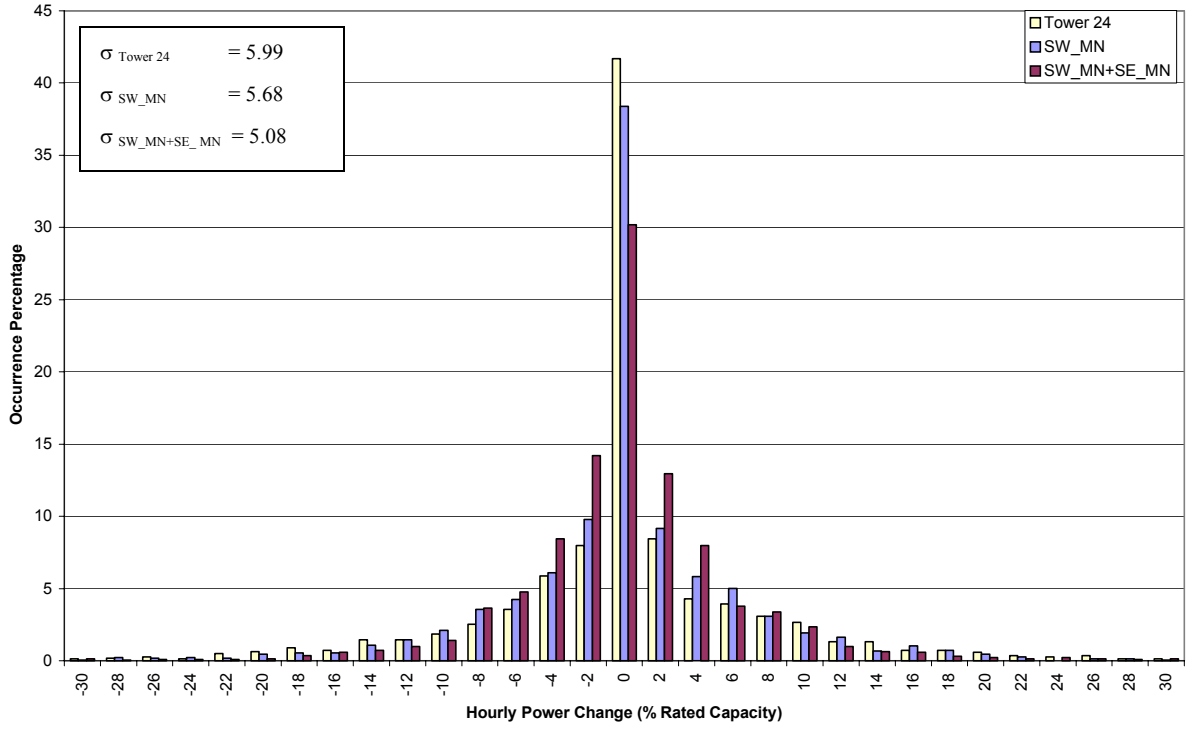

Figure 62: September and October frequency distributions of the hourly power change (as a percent of capacity) for the SW_MN and SW_MN+SE_MN geographical dispersion experiments (Z-750). Standard deviation for each scenario is shown at the upper left.

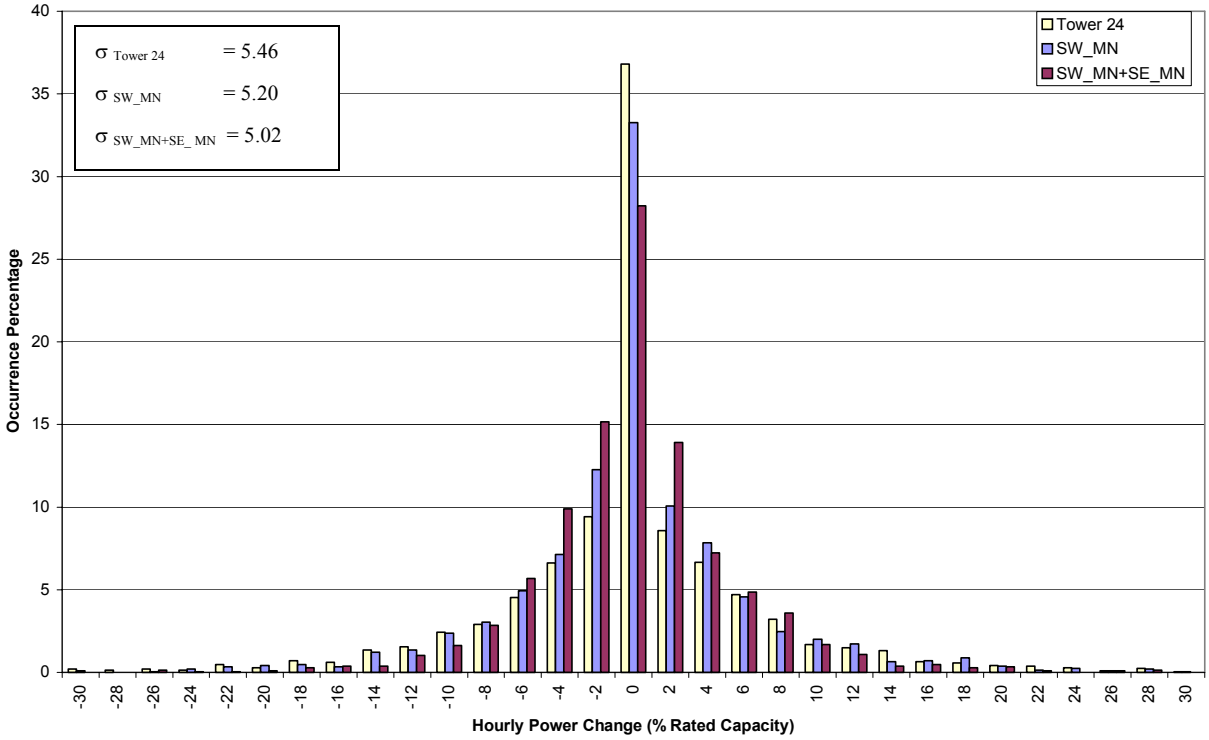

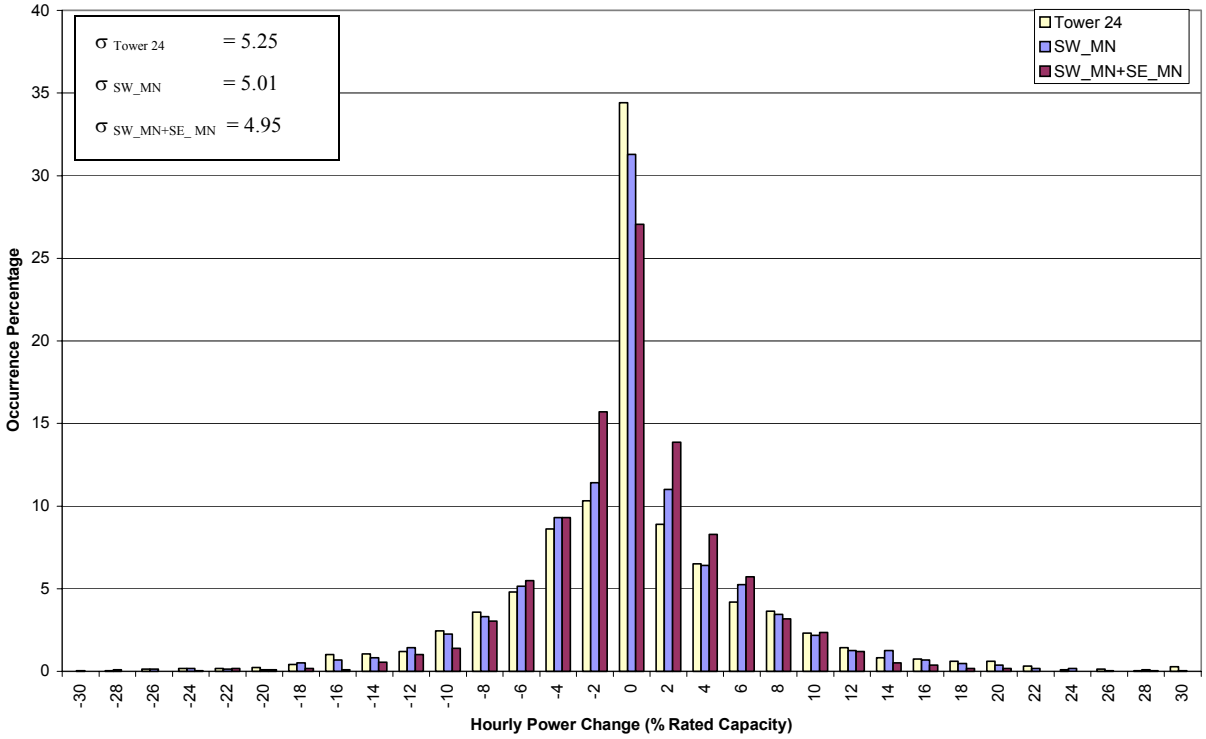

Figure 63: November and December frequency distributions of the hourly power change (as a percent of capacity) for the SW_MN and SW_MN+SE_MN geographical dispersion experiments (Z-750). Standard deviation for each scenario is shown at the upper left.

2. Validation of Modeled Winds

To assess the degree to which the MM5 numerical model simulated the actual meteorology occurring over southern Minnesota, and importantly, the temporal variability of the wind, a comparison was made between the model output and known power production data from the Delta Sector in the Lake Benton II wind farm. This exercise entailed taking an entire year of model data for 2003 and making an hour by hour comparison with site data.

2.1 Description of Multi-Scale Aspects of Modeled Wind Variability

The meteorological variability of the region and related wind resource variability may be categorized by the inherent time-scale of the phenomena. On the one to several day time scale, the passage of synoptic weather systems (cyclones and anticyclones) exert a large influence on the wind variability. Typically, attendant fronts associated with cyclone passages may impose significant wind speed variability on a time scale of several hours to one day. On the diurnal time scale, boundary layer stability influenced by solar insolation cycles control the vertical transport of momentum and wind speed variability. Related to the diurnal evolution of the atmospheric boundary layer, nocturnal low-level jets are a common phenomena over the study region, especially in the summer and early fall months. These nocturnal low-level jet episodes induce large variations in the diurnal wind resource above the shallow nocturnal inversion. On time scales of 10s of minutes to several hours, convective phenomena such and thunderstorm and thunderstorm complexes with their associated outflows have a large influence on low-level wind variability. In the time scale of seconds to 10s of seconds, boundary layer turbulence control wind speed variability. On the small time and space scales of turbulence, the numerical model employed is not capable of resolving these features.

2.2 NREL Database, Comparison Methodology, and Model Output Loss Factor Adjustment

NREL power production data was obtained for the Delta Sector of the Lake Benton II Wind Farm for 2003. Of the 4 sectors of Lake Benton II, the Delta Sector was selected due to its geographical overlap with MM5 proxy Tower 24. The Delta Sector aggregate power data was quality controlled for periods where large numbers of turbines were off-line by comparing this sector's power output trends to the 3 other quadrants of Lake Benton II. A running 10 min average was applied to the NREL database to eliminate small time scale noise. The NREL data was further reduced to 1 hr time increments to make the hourly comparison with the model data for an entire year tractable.

For the validation, MM5 Tower 24 power production was based on the meteorological conditions at hourly intervals at the 52 m hub height of the Delta Sector turbines. The MM5 wind data was not normalized to the long term RNL dataset for this validation analysis. Power curve data for the Zond-750 was applied to obtain the appropriate power production commensurate with the wind speed and density values. The MM5 Tower 24 power values were then multiplied by the number of turbines in the Delta Sector (30) such that the model-derived power could be compared to the NREL aggregate power values.

To represent various losses in the model data (transmission, collection, array, off-line turbines, etc), a 10 % loss factor was applied to all the model power values. This value was arrived at by plotting out the NREL Delta Sector power time series and evaluating the power production values during periods throughout the year when this wind farm sector was obviously on the top plateau of the power curve. The difference in power between what was actually being produced and the theoretical capacity value for the Delta Sector enabled a loss factor to be estimated (10 %). This methodology likely did not represent the full extent of the array losses but, when applied to the model power data, this 10 % adjustment produced model peak power production periods representative of those exhibited by the Delta Sector. A more conservative loss adjustment value was utilized in the wind resource temporal variability and geographic dispersion analysis presented in section 1.5.

2.3 Validation for 2003 – Monthly Comparison Time Series and Statistics

MM5 Tower 24 and Delta Sector power time series comparison plots for all the months of 2003 are presented in Figs. 52-57. The MM5 simulation demonstrates a high degree of skill in capturing meteorological variability on all the relevant time scales. The model trends (power time gradients) compare very favorably with the Delta Sector time series trends. In comparing seasonal model performance, the MM5 clearly produces a higher quality solution in the winter and transitional seasons that are dominated by synoptic-scale systems. Due to their size and intensity, these synoptic systems are better resolved by the model, and thus, the model simulates the wind resource more accurately. The much weaker summer weather systems and warm season convective episodes are much more difficult to simulate. Convection is inherently difficult to model due to its relatively short life span and often small horizontal dimension. Additionally, simulating the timing and position of convective initiation is a substantial challenge. However, even in the summer months, the model demonstrates some skill in simulating short time scale events while being less accurate on event magnitudes. As an assessment of model performance, the mean error for 7 months is less than 6 % of capacity with no months having a mean error greater than 8.9 % of capacity. The mean absolute error is less than 15% of capacity for 6 months with no months having a mean absolute error of greater than 18.9 % of capacity. In terms of time series comparative correlation, 8 months had correlation coefficients of 0.78 or greater. No operational status information was provided with the NREL power data, so it was not possible to account for errors resulting from a variable number of turbines operating correctly due to maintenance or weather related events such as icing.

1.72	ME as % of Cap
12.82	MAE as % of Cap
0.82	Correlation

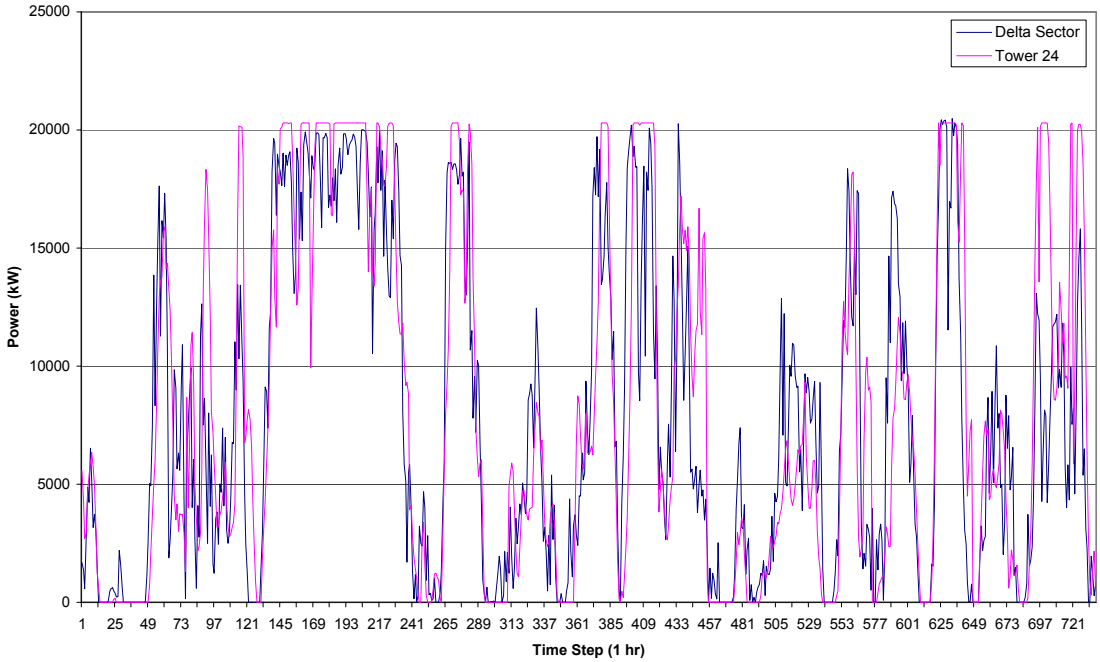

2.38	ME as % of Cap
14.23	MAE as % of Cap
0.79	Correlation

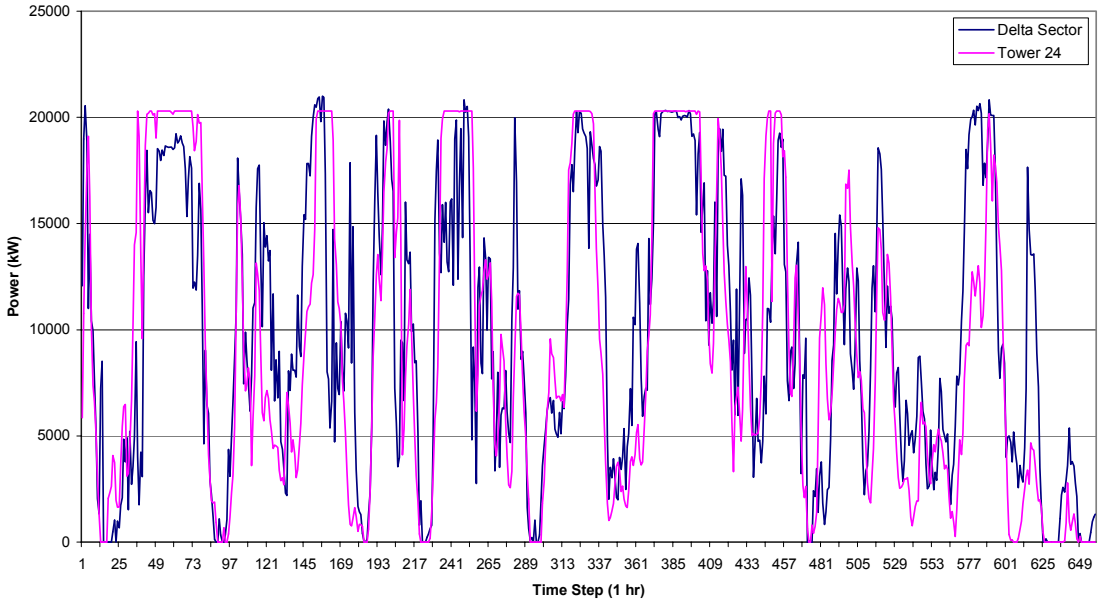

Figure 64: January (top) and February (bottom) power time series for MM5 Tower 24 and the Delta Sector. Mean error (ME), mean absolute error (MAE) and correlation coefficient are shown in the upper right box.

5.87	ME as % of Cap
14.8	MAE as % of Cap
0.81	Correlation

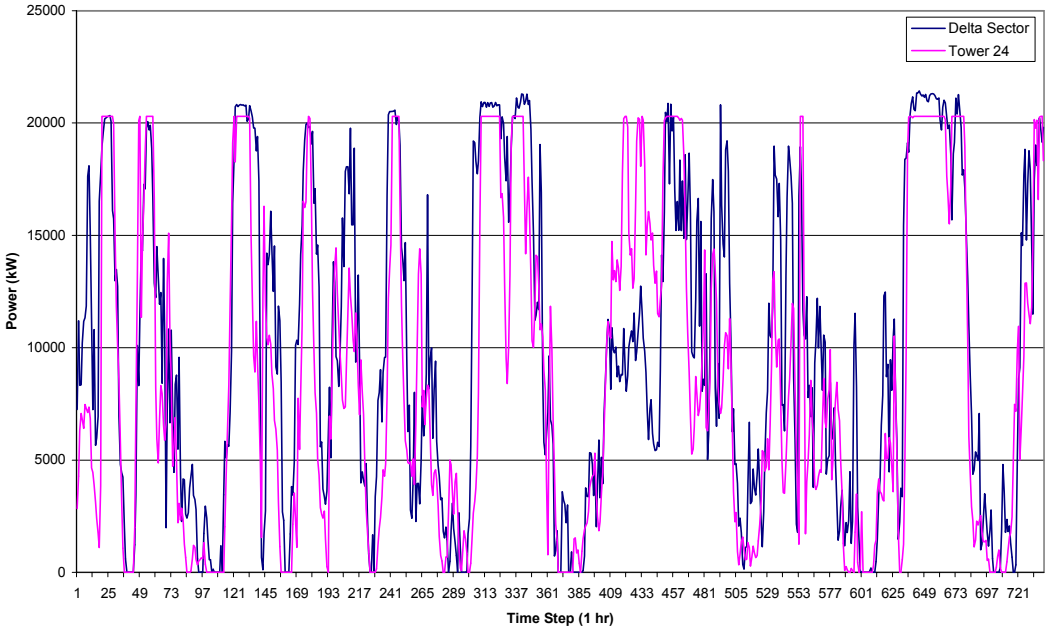

4.33	ME as % of Cap
15.62	MAE as % of Cap
0.79	Correlation

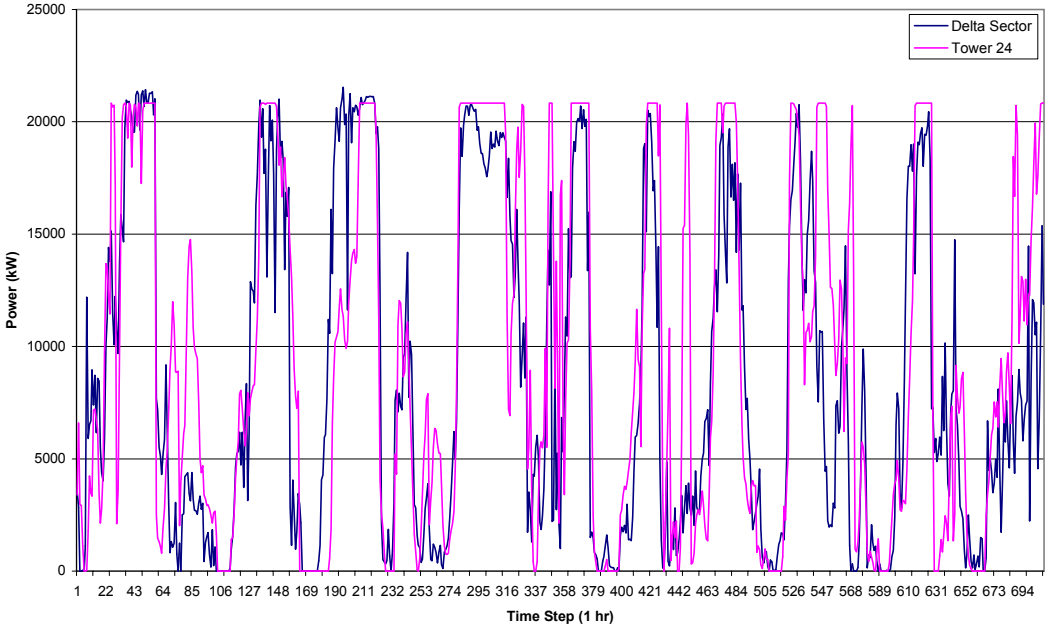

Figure 65: March (top) and April (bottom) power time series for MM5 Tower 24 and the Delta Sector. Mean error (ME), mean absolute error (MAE) and correlation coefficient are shown in the upper right box.

7.58	ME as % of Cap
15.52	MAE as % of Cap
0.80	Correlation

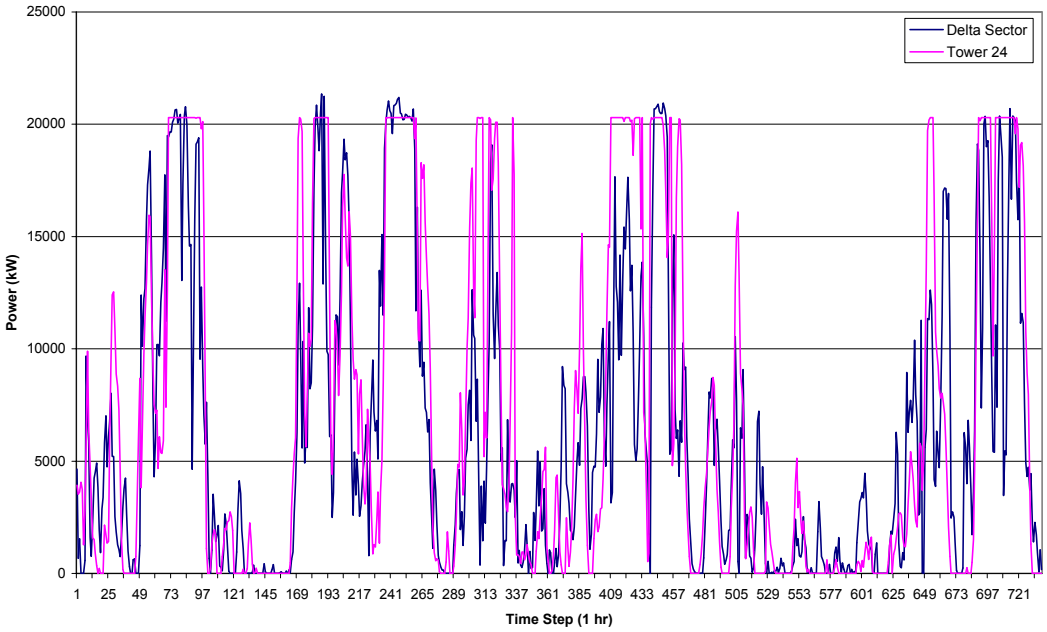

7.39	ME as % of Cap
15.03	MAE as % of Cap
0.75	Correlation

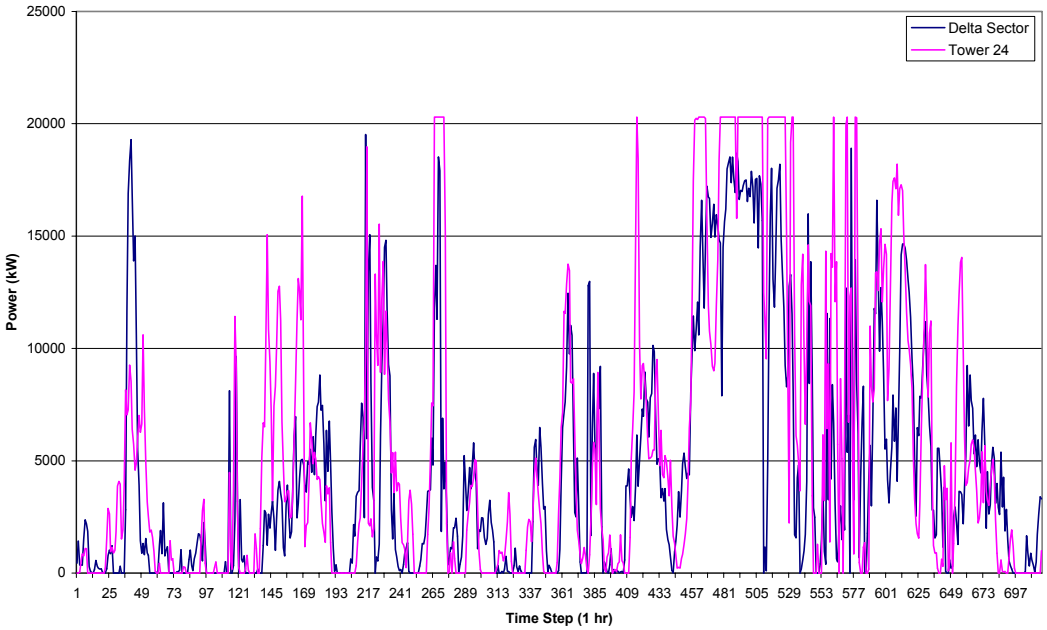

Figure 66: May (top) and June (bottom) power time series for MM5 Tower 24 and the Delta Sector. Mean error (ME), mean absolute error (MAE) and correlation coefficient are shown in the upper right box.

8.46	ME as % of Cap
17.99	MAE as % of Cap
0.67	Correlation

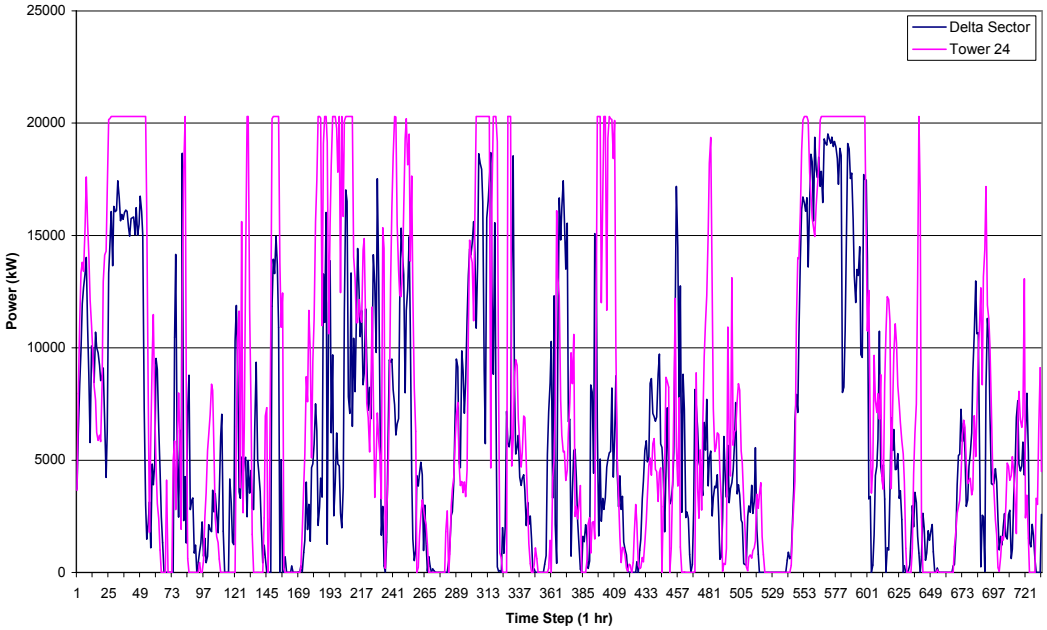

8.30	ME as % of Cap
14.63	MAE as % of Cap
0.75	Correlation

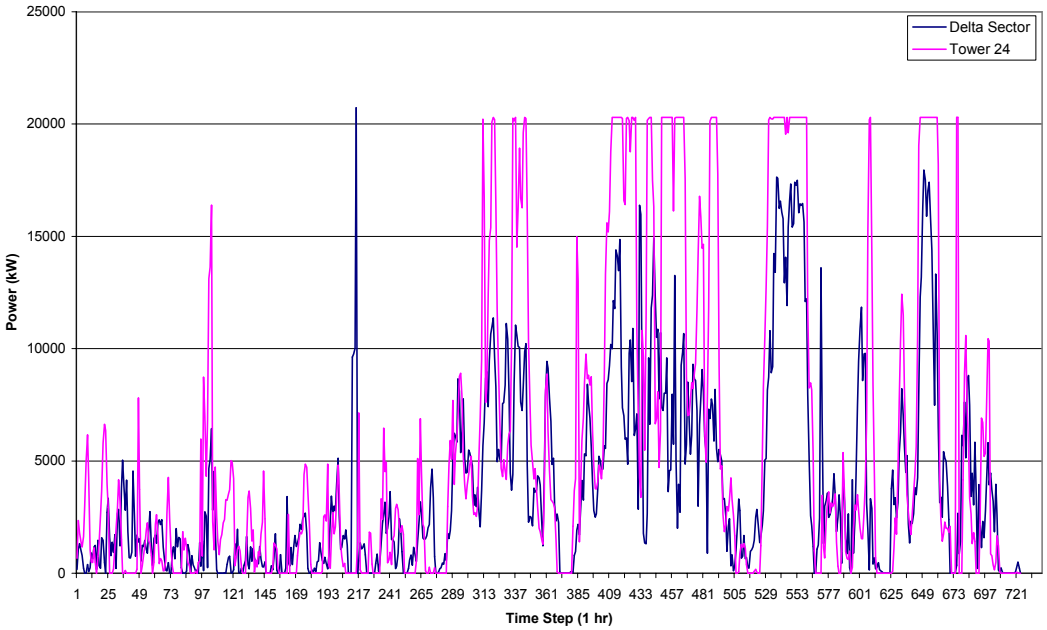

Figure 67: July (top) and August (bottom) power time series for MM5 Tower 24 and the Delta Sector. Mean error (ME), mean absolute error (MAE) and correlation coefficient are shown in the upper right box.

8.86	ME as % of Cap
18.79	MAE as % of Cap
0.68	Correlation

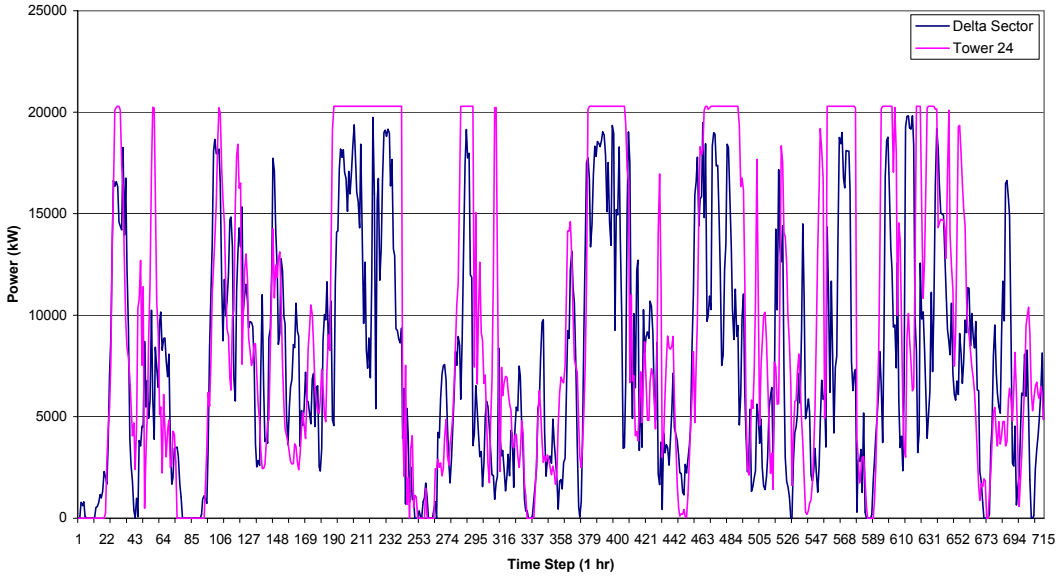

4.79	ME as % of Cap
15.85	MAE as % of Cap
0.79	Correlation

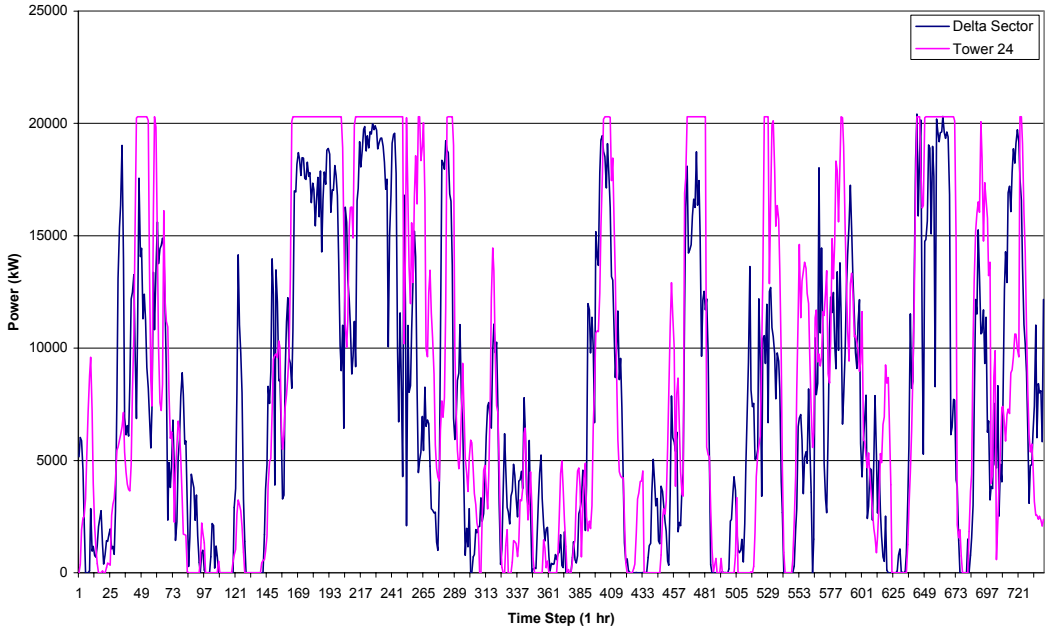

Figure 68: September (top) and October (bottom) power time series for MM5 Tower 24 and the Delta Sector. Mean error (ME), mean absolute error (MAE) and correlation coefficient are shown in the upper right box

5.56	**ME as % of Cap**
14.97	**MAE as % of Cap**
0.79	**Correlation**

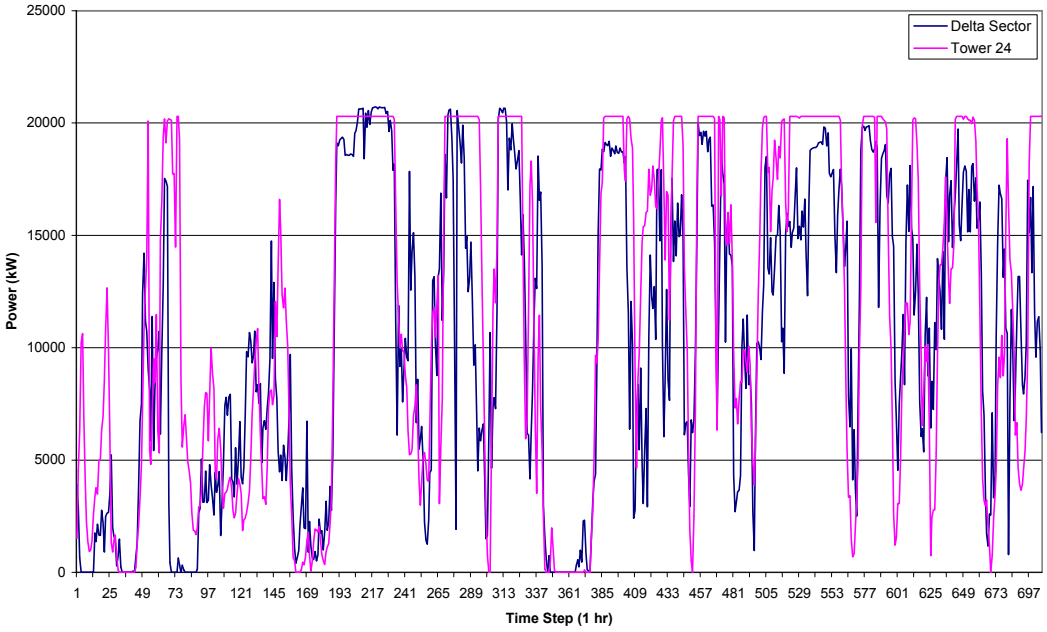

3.85	**ME as % of Cap**
14.79	**MAE as % of Cap**
0.78	**Correlation**

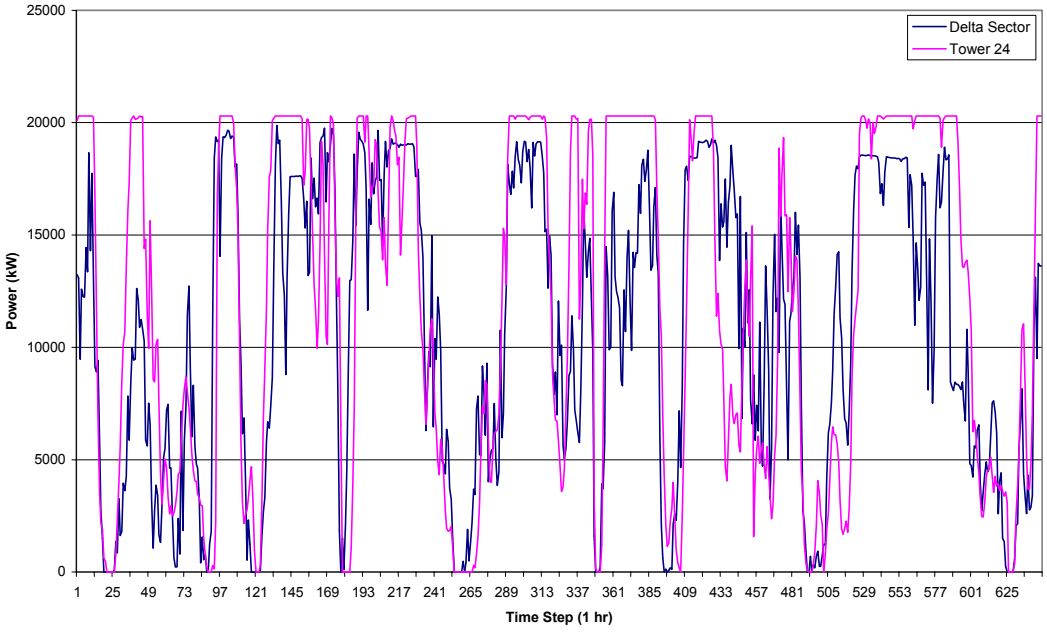

Figure 69: November (top) and December (bottom) power time series for MM5 Tower 24 and the Delta Sector. Mean error (ME), mean absolute error (MAE) and correlation coefficient are shown in the upper right box.

3. Forecasting Evaluation Experiment

3.1 The Forecast Model

The physics-based weather forecast model used in this study is the NCEP ETA model. The ETA model is one in a suite of numerical forecast models that is routinely used by the National Weather Service for making 1-3 day forecasts. The model calculates wind, temperature, pressure, humidity, and precipitation along with a host of other meteorological parameters at various heights in the atmosphere ranging from 10 m to 20 km above the surface. The model utilizes a horizontal grid spacing of 12 km. New 84-hour forecasts are made every 6 hours. These forecasts are being archived by WindLogics for use in forecasting studies. The archived data used in this study had a grid spacing of 20 km.

3.2 Computational Learning System (CLS) and Methodology

While it is possible to make wind (and power) forecasts for a particular site directly from the ETA model output, further refinements to the site-specific power forecast are made by using the ETA model output and NREL archived historical power production from the Delta Sector during 2003 to train a Computational Learning System. Recently developed Computational Learning System methods such as Support Vector Machine (SVM) relate complex patterns in forecast model outputs (such as wind, density, etc.) to wind facility target variables (such as power production). While earlier artificial intelligence approaches such as neural nets have been applied, the SVM-based approach offers distinct advantages, such as simplified optimization of training schemes, and estimation of output probability distributions. In this study, data (such as wind speed and direction, density, temperature, etc.) is extracted from the ETA model output at several heights and 4 horizontal grid points surrounding the Delta Sector. The model winds are utilized to calculate power production using the power curve for the Zond 150 turbine. The ETA model output and the 2003 Delta Sector power production data are then used to train the Computational Learning System to make more accurate power production forecasts than those derived by using the ETA model alone. This improvement in forecasting can be expected on a site-specific basis given the interplay of synoptic, mesoscale, local geographic and diurnal influences on the three-dimensional wind field. One strength of the CLS is in mitigating systematic errors inherent in the model forecast. For each month forecast, the actual production data for that month was excluded from the training. CLS forecasts are made out to 48 hours twice a day starting with the 00 UTC and 12 UTC runs of the ETA model. One caveat to the forecast accuracy results that follow involves the Delta Sector historical power dataset used for training the CLS. Wind turbine outage information for the Delta Sector was not available, so the training dataset could not be adjusted to reflect the actual number of turbines available at any one time. Inaccuracies in the training datasets constrain the potential of the CLS system to produce optimal forecasts. Another potential factor influencing the accuracy of the CLS system was the lack of adequate on-site historical wind information that could have been used in the training along with the historical power.

3.3 Forecast Accuracy Results

To evaluate the benefits of utilizing the CLS for wind farm power and energy forecasting, plots have been created for both annual and seasonal forecasting performance. For comparison, the error performance for power and energy for forecasts based on climatology and persistence are also plotted. As shown in Fig. 70, the CLS forecast demonstrates a far superior ability to prognosticate the power production and energy than either persistence or climatology. In terms of power production, the CLS forecasts have MAEs in the 11 – 15 percent range in the 6 – 33 hour forecast period, with MAEs in the 15-18

percent range thereafter to 48 hours. It is notable that even at the 48 hour point, the CLS forecast has considerable value over climatology. The waves in the power plots are due to inadequacies in the forecast methodologies to accurately represent (climatology and persistence) or forecast the timing (ETA and CLS) of transitional diurnal boundary layers. In term of energy forecast accuracy, the system demonstrates energy MAEs in the 20 – 23 percent range (as a percent of actual energy) for the 6 – 48 hour period. The growth rate of the error over this period is very gradual. It is not surprising that the CLS forecast for power and energy is far superior to climatology throughout the 48 hour period, especially in the 0-6 hr time frame, but a striking facet of the CLS forecast involves its ability to outperform persistence within just a few hours into the forecast period. In fact, by the 3 hour forecast point, the CLS forecast outperforms the persistence power forecast by 3 % of the Delta Sector's rated capacity. In terms of the accuracy of forecasted energy, the CLS system shows an improvement over persistence at the 3 hour point of 3.8 percent of actual energy production. Figure 71 shows the improvement in power forecasts for the CLS over both persistence and climatology. Thus, for the example given above, a 3 percent improvement over persistence in the power forecast (as a percent of rated capacity) at the 3 hour forecast point translates into a 20 percent improvement over persistence based on the MAE of the persistence forecast at 3 hours. As shown in Fig. 71, the relative forecast percent improvement of the CLS power forecast over persistence and climatology is large from this 3 hour point through the 48 hour evaluation period. At this 48 hour point, the CLS system showed a 40 and 27 percent improvement over persistence and climatology, respectively.

The seasonality of forecast power and energy errors is shown in Figs. 72 and 73 for the CLS, persistence and climatology. As shown in Fig. 72, the power MAE profiles are similar to the annual profile shown in Fig. 70, but with differing magnitudes. The smaller MAEs in the summer can generally be attributed to a weaker wind regime and commensurately smaller forecast error magnitudes resulting in the reduced MAEs calculated as a fraction of wind farm rated capacity. The definitive advantage of utilizing the CLS forecast over persistence and climatology is present in both summer and winter seasons. Examining forecast energy error as a fraction actual energy produced in Fig. 73 reveals that, on a season-relative basis, the winter season CLS forecasts are superior to the summer season. To understand these season-relative forecasting differences, the time and space scales of the controlling meteorology of the Upper Midwest must be addressed. The winter season wind forcing is dominated by synoptic-scale weather systems that tend to be more accurately forecast by weather prediction models because they are large in dimension (up to several 1000 km in horizontal scale) and have 3-7 day life spans. Thus, these synoptic systems are well resolved in the numerical model forecasts. In contrast, summer season weather and regional winds are often influenced by mesoscale systems that, due to their size, life span, and transient nature (like mesoscale convective systems) are more difficult to accurately simulate.

Another way to characterize the CLS power forecast performance is in the examination of the frequency distribution of binned forecast errors for multiple forecast times as shown in Fig. 74. The profile of the distributions clearly shows the relationship between forecast length and power error. The shorter the forecast period, the more accurate the power forecast. An examination of the tails of the distribution shows a diminishing error frequency for progressively shorter forecasts. Although this result was expected, the relatively small degradation of the 24 and 48 hour forecasts from the 6 hour results was noteworthy. As an example, the frequency of power forecast errors less than 30 percent of

rated capacity was 95 percent for the 6 hour forecast, but only degraded to 92 and 85 percent for the 24 and 48 hour forecasts, respectively. The trend of these results indicate that CLS forecasts beyond 48 hours into the day 3 regime may still have value.

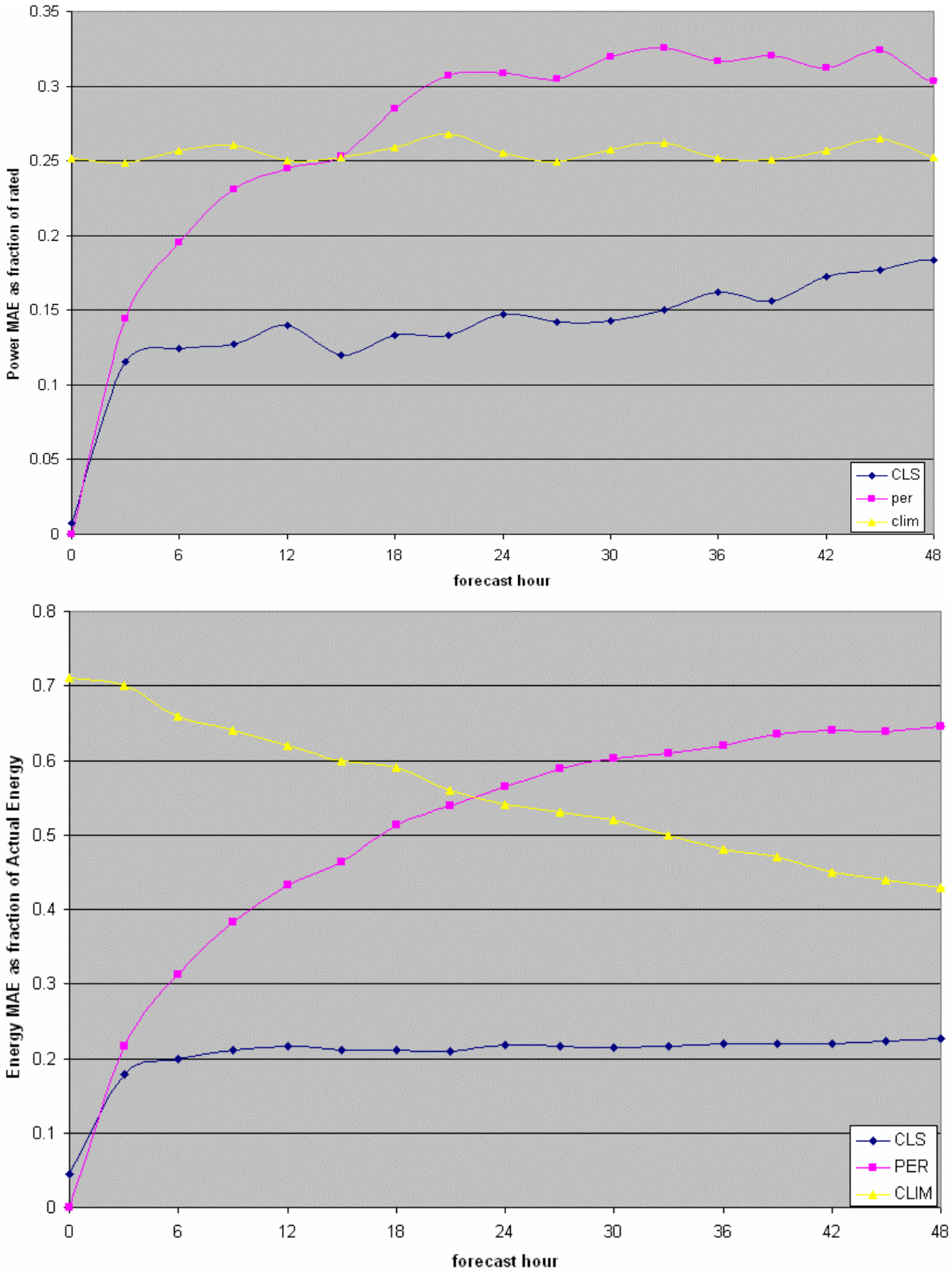

Figure 70: Power mean absolute error (top) and energy mean absolute error as a fraction of actual production (bottom) for all months for the CLS, climatology (CLIM), and persistence (PER) forecasts.

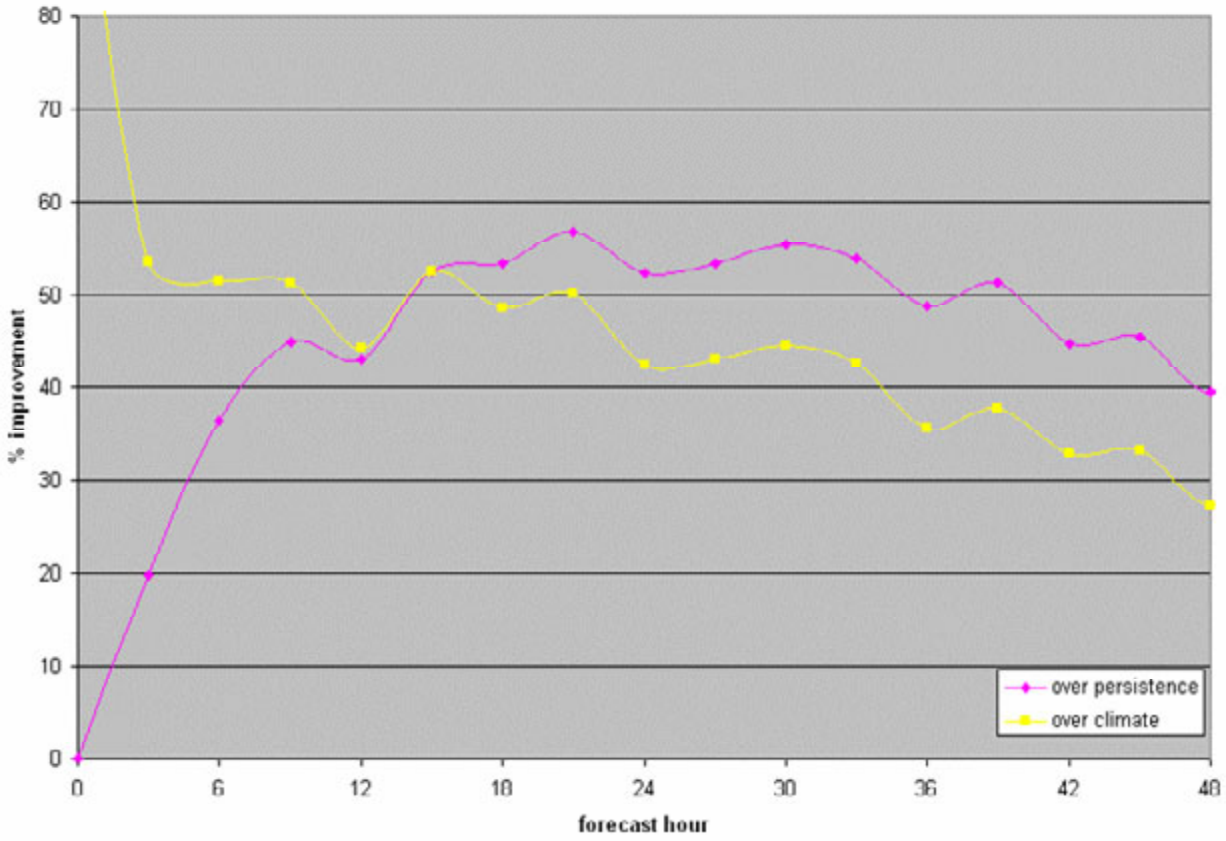

Figure 71: Forecast improvement of the CLS power forecast over climatology and persistence forecasts.

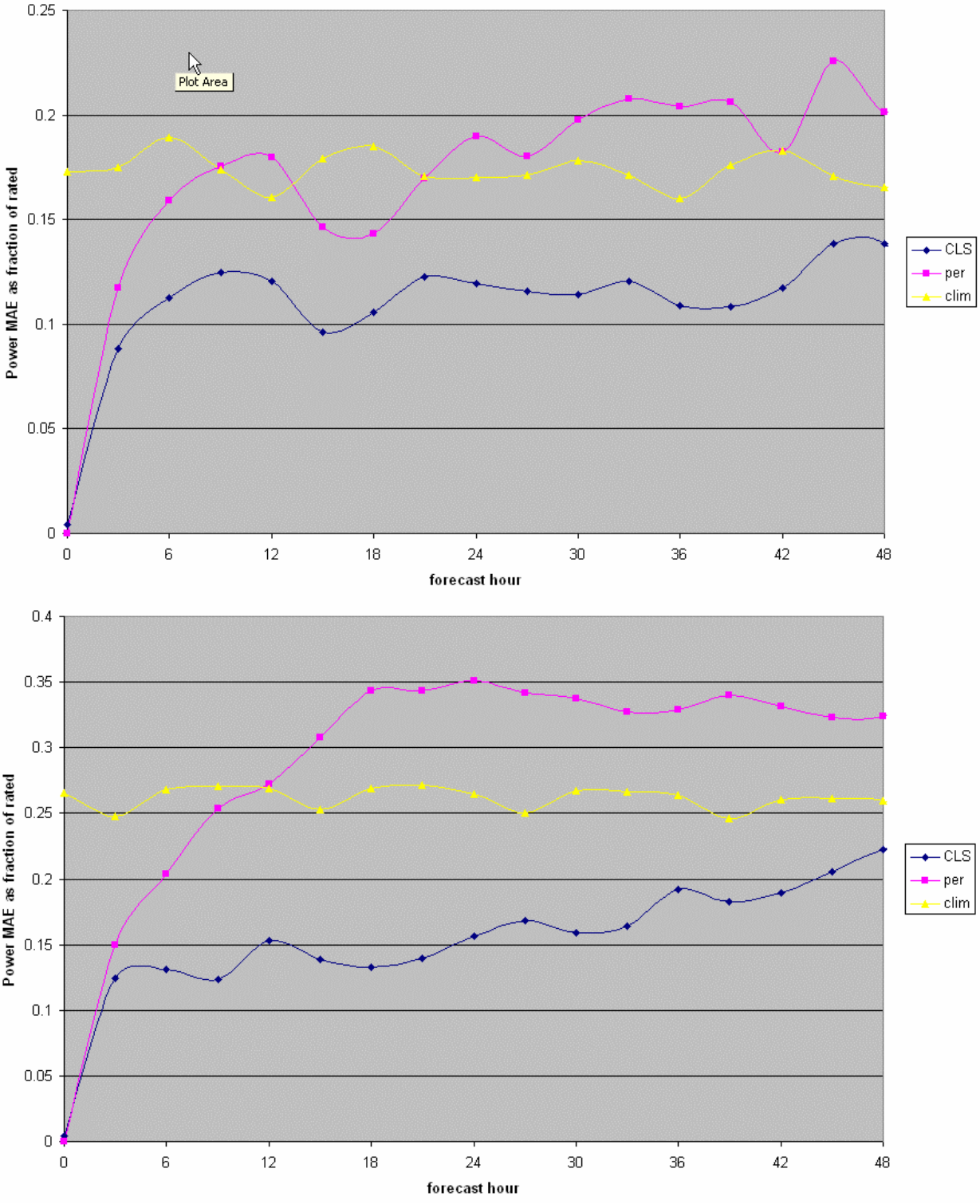

Figure 72: Summer season (top) and winter season (bottom) power mean absolute errors for all months for CLS, persistence (per) and climatology (clim) forecasts.

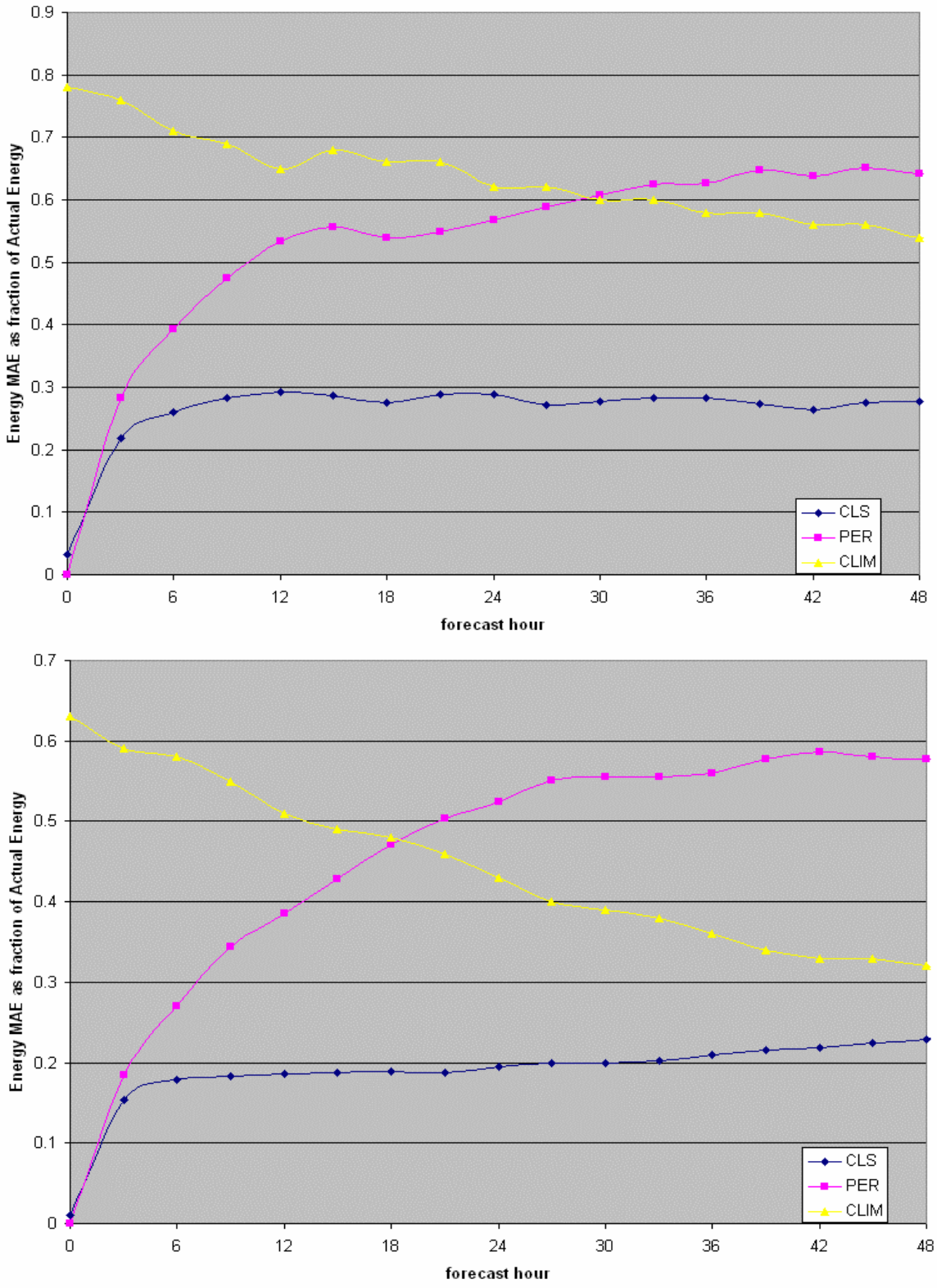

Figure 73: Summer season (top) and winter season (bottom) energy mean absolute error as a fraction of actual energy for all months for CLS, persistence (per) and climatology (clim) forecasts.

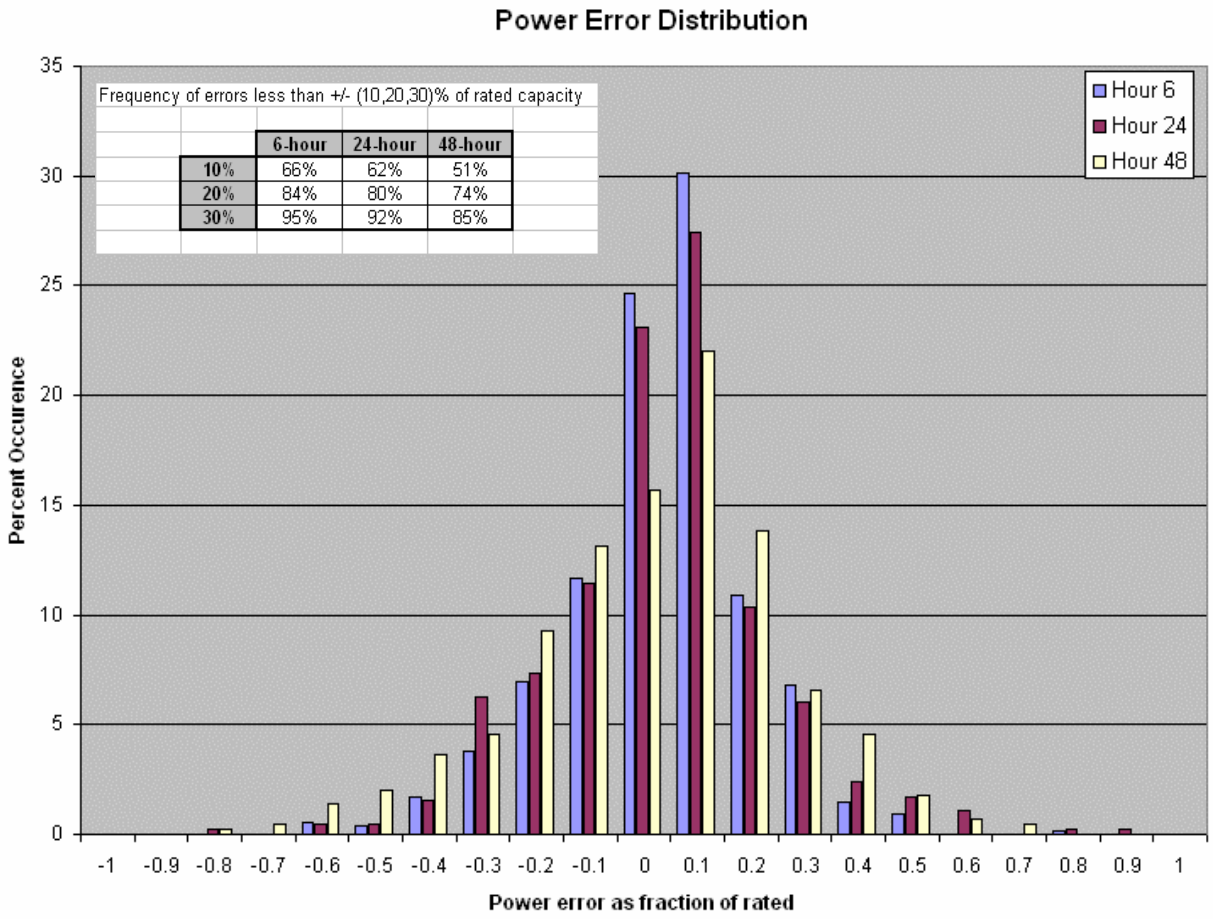

Figure 74: Frequency distribution of power error as a percent of rated capacity for 6, 24 and 48 hour forecasts. Inset table shows the frequency of power errors less than 10, 20 and 30 percent of rated capacity for the CLS 6, 24 and 48 hour forecasts.

References

Bonner, W. D., 1968: Climatology of the low level jet. *Mon. Wea. Rev.*, **96**, 833-850.

Grell, G. A., J. Dudhia, and D. R. Stauffer, 1995: A description of the fifth-generation Penn State/NCAR Mesoscale Model (MM5). NCAR Technical Note TN-398+STR, 122 pp.